DISSERTATION

Revealing the molecular nuances of TRPC6 in focal segmental glomerulosclerosis in an *in vitro* human podocyte model

Aufdeckung der molekularen Nuancen von TRPC6 bei der fokalen segmentalen Glomerulosklerose in einem In-vitro-Modell menschlicher Podozyten

zur Erlangung des akademischen Grades

Doctor of Philosophy (PhD)

vorgelegt der Medizinischen Fakultät

Charité – Universitätsmedizin Berlin

von

Lilas Batool

Erstbetreuung: Dr. Andreas Kurtz

Datum der Promotion: 30 Juni 2024

PREFACE

Parts of the results of this dissertation have recently been published in:

Batool, L., Hariharan, K., Xu, Y., Kaßmann M., Tsvetkov D., Gohlke BO., Kaden S., Gossen M., Nürnberg B., Kurtz A., & Gollasch M. An inactivating human TRPC6 channel mutation without focal segmental glomerulosclerosis. *Cell. Mol. Life Sci.* 80, 265 (2023). https://doi.org/10.1007/s00018-023-04901-w / 24 August 2023

Batool L., Storozhuk O., Raab C., Beez CM., Selig M., Harder A., & Kurtz A. Generation of two human induced pluripotent stem cell lines from a patient with Neurofibromatosis type 1 (NF1) and pathogenic NF1 gene variant c . 1466 A > G BCRTi011-A as well as a first-degree healthy relative. *Stem Cell Res*. 2023;71(August):103184. doi:10.1016/j.scr.2023.103184/ 13 August 2023

Batool L., Raab C., Beez CM., Hariharan K., Kurtz A., Gollasch M., & Rossbach B. Generation of human induced pluripotent stem cell line (BCRTi006-A) from a patient with focal segmental glomerulosclerosis disease. *Stem Cell Res*. 2023;69(March):103070. doi:10.1016/j.scr.2023.103070 / 11 March 2023

Batool L, Raab C, Beez CM, Kurtz A, Gollasch M, & Rossbach B. Generation of human induced pluripotent stem cell line (BCRTi007-A) from urinary cells of a patient with autosomal dominant polycystic kidney disease. *Stem Cell Res*. 2023;69(March):103071. doi:10.1016/j.scr.2023.103071 / 11 March 2023

TABLE OF CONTENTS

LIST OF FIGURES

LIST OF TABLES

ABBREVIATIONS

ACE	Angiotensin-converting-enzyme
ADPKD	Autosomal dominant polycystic kidney disease
AKI	Acute kidney injury
BMP	Bone morphogenetic protein
Bsd	Blasticidin
Ca^{2+}	Calcium ions
CD	Cluster of differentiation
cDNA	Complementary deoxyribonucleic acid
Cryo-EM	Cryo-electron microscopy
CH1	C-terminal helix 1
CH2	C-terminal helix 2
DAG	Diacylglycerol
DAPI	4', 6-diamidino-2-phenylindole
DMEM	Dulbecco´s Modified Eagle´s Medium
DMSO	Dimethyl sulfoxide
DNA	Deoxyribonucleic acid
DOG	1, 2-dioctanoyl-sn-glycerol
Dox	Doxycycline
E8	Essential 8
EBiSCs	European Bank for induced pluripotent Stem Cells
EDTA	Ethylenediaminetetraacetic acid
ERA-EDTA	European Renal Association- European Dialysis and Transplant Association
FACS	Fluorescence Activated Cell Sorting
FGF	Fibroblast growth factor
FGFR	Fibroblast growth factor receptor
FSGS	Focal segmental glomerulosclerosis
GBM	Glomerular basement membrane
Gd^{3+}	Gadolinium
GDNF	Glial-derived neurotrophic factor
GFP	Green fluorescent protein
GOF	Gain-of-function
GSHs	Genomic safe harbor sites

HEK	Human embryonic kidney
HIV 1	Human immunodeficiency virus 1
hiPSC	Human Induced pluripotent stem cells
ICD	Intracellular cytoplasmic domain layer
ISKDC	International study of kidney disease in children
ISN	International Society of Nephrology
La^{3+}	Lanthanum
LAMB2	Integrins and laminin-β2
LOF	Loss-of-function
MCD	Minimal change disease
MOTiF	Multi-organ tissue-flow
NF1	Neurofibromatosis type 1
NGS	Next generation sequencing
NPHS2	Podocin
OAG	1-oleoyl-2-acetyl-sn-glycerol
PFA	Paraformaldehyde
PIP2	Phosphatidylinositol 4,5-bisphosphate
PLC	Phospholipase C
PODXL	Podocalyxin
PSC	Pluripotent stem cells
PTEC	Proximal tubular epithelial cells
qPCR	Quantitative real-time PCR
RA	Retinoic acid
REGM	Renal epithelial growth medium
rhHGF	Hepatocyte growth factor
RNA	Ribonucleic acid
ROCK	Rho-associated protein kinase
rtTA	Reverse tetracycline-controlled transactivator
SEM	Scanning electron microscopy
SOCE	Store-operated calcium entry
SOX2	Sex determining region Y-box 2
SRNS	Steroid-resistant nephrotic syndrome
SSEA4	Stage-specific embryonic antigen 4
STCs	Scattered tubular cells

STR	Short tandem repeat
suPAR	Soluble urokinase Plasminogen Activator Receptor
SYNPO	Synaptopodin
TALEN	Transcription activator-like effector nuclease
TBS	Tris-buffer saline
TEM	Transmission electron microscopy
TRP	Transient receptor potential
TRPC6	Transient receptor potential cation channel 6
WT	Wild-type
YFP	Yellow fluorescent protein
ZFN	Zinc finger nuclease

ABSTRACT (English)

Focal segmental glomerulosclerosis (FSGS) is a rare disease-causing glomerular lesion in the nephron and inadvertently end stage renal disease. Pathologically, FSGS is characterized by sclerosis in some (focal) parts of the glomeruli. Podocyte injury is the earliest morphological hallmark of FSGS supporting the notion that FSGS is a podocyte disease. The physiological function of podocytes is critically dependent on the proper intracellular calcium levels; excessive or deficient Calcium influx into these cells may result in foot process effacement, apoptosis, and nephron degeneration. A key protein involved in the regulation of Calcium influx is the transient receptor potential cation 6 (TRPC6), which is expressed in podocytes. Rare mutations in the TRPC6 gene were implicated to cause FSGS with high penetrance, presumably by increasing or decreasing calcium influx.

Here I studied the effect of gain- and loss-of-function (GOF, LOF) mutations in TRCP6 on intracellular Calcium levels using novel model systems, including podocytes derived from human induced pluripotent stem cells (hiPSC). To establish an inducible human FSGS model system, I generated and phenotypically characterized three transgenic hiPSC lines with controllable overexpression of TRPC6 wild-type and FSGS-associated GOF and LOF mutations (P112Q and G757D). Furthermore, these cell lines were induced to differentiate into podocytes (iPodocytes). Initial experiments in HeLa and HEK293 reporter cell lines confirmed the impact of TRPC6 GOF and LOF mutants on Calcium influx. Although iPodocytes also showed Calcium responses consistent with GOF and LOF phenotypes, these were lower in comparison to data obtained from the reporter lines, probably due to reduced and aberrant expression of TRPC6 during podocyte differentiation. In addition, I reported a novel heterozygous TRPC6 mutation (V691Kfs*) in a large kindred with no signs of FSGS despite the presence of a largely truncated TRPC6 protein. Functional analysis showed that the V691Kfs* truncation inactivated the TRCP6 channel-specific Calcium influx consistent with a complete LOF phenotype. Our data corroborate that one defective dominant-negative TRPC6 gene copy and reduced Calcium influx through TRPC6 are not sufficient to cause FSGS.

To increase our capacity to study the effect of mutations in rare disease models other than the kidney, I have established four new hiPSC lines derived from three different patients diagnosed with FSGS, Polycystic Kidney Disease (PKD), and Neurofibromatosis

Type 1 (NF1), as well as a healthy relative, respectively. These hiPSC lines can be differentiated into both 2D and 3D nephrogenic models and relevant tubule cell types (FSGS and PKD), or neural crest derivatives (NF1) using standard differentiation protocols to analyze disease-related phenotype and pathology. The newly established hiPSC – lines are available for research through the European Bank for iPSC (EBiSC).

ZUSAMMENFASSUNG (German)

Fokale segmentale Glomerulosklerose (FSGS) ist eine seltene Erkrankung, die zu glomerulären Läsionen im Nephron und unweigerlich zum Funktionsverlust der Niere führt. Pathologisch ist die FSGS durch Sklerose in einigen (fokalen) Bereichen der Glomeruli charakterisiert. Die Podozytenschädigung ist das früheste morphologische Merkmal der FSGS. Die physiologische Funktion der Podozyten hängt entscheidend von genauen intrazellulären Ca^{2+}-Spiegeln ab; ein übermäßiger oder fehlender Ca^{2+}-Einstrom in diese Zellen könnte zu einer Tilgung der Fußprozesse, Apoptose und Abbau des Nephrons führen. Ein an der Regulierung des Ca^{2+}-Einstroms beteiligtes Protein ist das in Podozyten exprimierte Transient Receptor Potential Cation 6 (TRPC6). Seltene Mutationen im TRPC6-Gen werden mit der Entstehung von FSGS mit hoher Penetranz in Verbindung gebracht, vermutlich durch Erhöhung oder Verringerung des Kalziumeinstroms.Ich untersuchte den Einfluss von Gain- und Loss-of-Function (GOF, LOF) - Mutationen in TRCP6 auf den intrazellulären Ca^{2+}-Spiegel mithilfe von neuartigen Modellsystemen, einschließlich aus menschlichen induzierten pluripotenten Stammzellen (hiPSC) differenzierte Podozyten. Für die Etablierung des FSGS-Modellsystems wurden drei transgene hiPSC-Linien mit regulierbarer Überexpression von TRPC6-Wildtyp und FSGS-assoziierten GOF- und LOF-Mutationen (P112Q und G757D) erzeugt, charakterisiert und in Podozyten differenziert (iPodozyten). Anfängliche Experimente in HeLa- und HEK293-Reporterzelllinien bestätigten die Auswirkungen der TRPC6 GOF- und LOF-Mutanten auf den Ca^{2+}-Einstrom. Obwohl auch in iPodozyten die mit den GOF- und LOF-Phänotyp übereinstimmenden Ca^{2+}-Reaktionen gezeigt wurden, waren diese verglichen zu den Daten aus den Reporterlinien geringer, was vermutlich an einer reduzierten und abweichenden Expression von transgenem TRPC6 während der Differenzierung lag. Zusätzlich wurde eine neuartige heterozygote TRPC6-Mutation (V691Kfs*) in einer Kohorte, die trotz eines weitgehend verkürzten TRPC6-Proteins keine Anzeichen von FSGS zeigte, generiert. Die funktionelle Analyse zeigte, dass die V691Kfs*-Trunkierung den TRPC6-spezifischen Ca^{2+}-Einstrom inaktiviert, was einem vollständigen LOF-Phänotyp gleicht. Unsere Daten bestätigen, dass eine defekte dominant-negative TRPC6-Genkopie und ein verminderter Ca^{2+}-Einstrom durch TRPC6 nicht ausreichen um eine FSGS auszulösen.

Um die Auswirkungen von Mutationen in Modellen für weitere seltene Krankheiten besser untersuchen zu können, wurden vier neue hiPSC-Linien etabliert, die von drei verschiedenen Patienten mit FSGS, polyzystischer Nierenerkrankung (PKD) und Neurofibromatose Typ 1 (NF1), sowie von einem gesunden Verwandten stammen. Diese Zelllinien können mithilfe von Standardprotokollen in 2D- und 3D-Nephronmodelle und Tubuluszelltypen (FSGS und PKD) oder Neuralleisten-Derivate (NF1) für eine Analyse des Krankheitsbilds und der Pathologie differenziert werden und stehen für Forscher über die Europäische Bank für iPSC (EBiSC) zur Verfügung.

1. INTRODUCTION

1.1 Kidney certainly matters

Kidney disease has gained global attention due to the rapid increase in its prevalence, the enormous cost of treatment, the understanding of its significant contribution to the risk of cardiovascular disease, and the scientific research into effective measures to prevent its progression. More than 850 million people worldwide have some form of kidney disease, and 5-10 million people die each year from complications associated with chronic kidney disease (Facts- International Society of Nephrology (ISN). Chronic kidney disease is defined as an abnormality in the kidney structure or function that has been present for more than three months (Stevens & Levin, 2013). This condition, also known as end-stage renal disease, is characterized by persistent renal impairment ranging from minor kidney damage to total kidney failure. In 2019, chronic kidney disease caused 1.2 million deaths, ranking 18th on the list of causes of death worldwide (Naghavi et al., 2017), and is expected to be the 5th leading cause of loss of life by 2040 (Foreman et al., 2018). In addition, chronic kidney disease increases the relative risk of cardiovascular disease due to several classical factors such as hypertension, diabetes mellitus, and dyslipidemia, and also other factors such as elevated lipoprotein, phosphate, homocysteine, fibrinogen levels, and other conditions (Gansevoort et al., 2013).

Hemodialysis and kidney transplantation are the two available options to treat end-stage renal disease patients. Individual studies show that kidney transplantation results in lower mortality and better quality of life than chronic dialysis. Kidney dialysis requires highly specialized and expensive machinery. In addition, all dialysis procedures are tiring and have several side effects on patients, such as low blood pressure, muscle cramps, itchy skin, infection, blood clots, anemia, heart conditions, etc. However, the demand for donor kidneys far exceeds the available supply. Immunosuppressive medications used in transplant recipients may cause anemia, hypertension, glucose intolerance, and dyslipidemia (Tonelli et al., 2011). A major barrier to kidney transplantation continues to be the death of transplant recipients due to cardiovascular disease, cancer, and infection (Knoll, 2008). Thus, there is an increasing demand for new methods to understand the causes of kidney disease, to alleviate, cure, or prevent it. Stem cell-based models are

increasingly being used as promising new tools to study regenerative and maladaptive cellular responses involved in acute and chronic renal diseases.

1.1.1 Kidney regeneration: endogenous repair

The kidney is a major excretory organ for the elimination of metabolic waste from the body. It modulates other tissues by regulating blood pressure and blood cell composition, and modulates the bone composition by activating vitamin D. These tasks are performed by approximately one million nephrons within the kidney that filter the body's blood volume once every 1-2 hours (OSHIMA, 1963). In general, the renal corpuscle (glomerulus), which serves as the filtration unit, is typically located at one end of the nephron followed by segmented tubules that recapture vital filtrate components (Brunskill et al., 2008). Within the glomeruli, mesangial cells, endothelial cells, and podocytes are involved in multidirectional cross-talk among themselves. For example, injury to podocytes may induce mesangial cell proliferation, and injury in mesangial cells can lead to podocyte foot processes and fusion (Saleem, 2015). Injury to the endothelial cells may promote tubulointerstitial fibrosis, leading to end-stage renal disease in chronic kidney disease (Ballermann & Obeidat, 2014). The renal tubular epithelium is constantly exposed to filtrates, and thousands of living cells from healthy humans, including approximately 2000 to 7000 renal tubular epithelial cells (ca. 0.002 cells per nephron or about 2 -7 cells per 1000 nephrons) are excreted daily into the urine (Rahmoune et al., 2005). These cells need to be replenished for the normal function of nephrons. Experiments to identify the progeny of renal tubular cells showed that some revert to a proliferative state and can defend themselves against single cell loss or catastrophic insult (Vogetseder et al., 2008). In the past decade, several research groups have identified the proliferative capacity of renal tubular progenitor populations *in vitro* and *in vivo* isolated from human tubular cells when introduced into mouse models of acute kidney injury (AKI) (Angelotti et al., 2012; Bussolati et al., 2005; Lazzeri et al., 2018; Peired et al., 2021). Similarly, the presence of the cluster of differentiation 133 (CD133) protein on some renal tubular epithelial cells marks their multipotent ability to expand and self-renew and to engage in renal injury repair (Bussolati et al., 2005).

Although acute kidney injury can be treated by using renal progenitor cells, chronic kidney disease, which is characterized by rising fibrosis resulting from the primary injury to the glomerulus or tubule, cannot be treated in this way. The development of

myofibroblasts that proliferate over many years and cause nephron dysfunction, atrophy, and collapse, coincides with damage to the vasculature. This amplifies inflammation and fibrogenesis and triggers a vicious cycle of damage in the fibrotic lesions, most likely due to excessive proliferation of cells of pericytic origin (Li & Wingert, 2013). Renal fibrosis has been successfully reversed by the therapeutic administration of bone morphogenetic protein 7 (BMP-7) (Zeisberg & Kalluri, 2008), and the treatment with an angiotensin-converting-enzyme (ACE) inhibitor reversed proteinuria and the progression of chronic kidney disease in patients with nondiabetic chronic nephropathy (Ruggenenti et al., 1999). Animal studies provided evidence that ACE inhibitors caused alterations to the glomerular structure, including the repopulation of podocytes (Macconi et al., 2009).

The human kidney tends to compensate for nephron loss by hypertrophy and hyperplasia, while no new nephron formation occurs in the adults. Therefore, endogenous regeneration/recovery cannot be relied upon alone to resuscitate renal health during acute kidney injury/chronic kidney disease. Furthermore, there is a 10-fold variation in nephron number between individuals, no capacity to form new nephrons after birth, and a clear inverse relationship between nephron number and renal disease. The kidney has 30 different cell types that are involved in fluid homeostasis, secretion, and excretion (Takasato & Little, 2015). The nephrons, each of which consists of an unbranched epithelial tubule vascularized at one end (the glomerulus) to enable blood filtration, carry out the primary function of the kidney, which is to filter the blood to eliminate metabolites and nitrogenous wastes and reabsorb water. Taking all of these considerations into account, a closer examination of the molecular and cellular makeup of the kidney, as well as its embryonic development, may aid in understanding the intricacies of recreating a nephron.

1.2 Decipher the kidney origin

To fully understand the recent advances made in deciphering the molecular events that pattern the kidney field, it is important to recognize the temporal and spatial organization of the embryonic kidney and its progenitors. The following section provides an overview of kidney organogenesis from the blastocyst stage to the embryo.

1.2.1 Embryology: dawn of organogenesis

Wolpert's dictum said, "It is not birth, marriage or death, but gastrulation, which is truly the most important time in your life". Humans are trophoblastic organisms, derived

from three germ layers, endoderm, mesoderm, and ectoderm formed during the process of gastrulation as shown in Figure 1. Pluripotent progenitors gradually commit their fate to one of the three primary germ layers during gastrulation, and they begin organogenesis by forming organ primordia (Kinder et al., 2017). During gastrulation, the cells of the bilaminar disk (epiblast and hypoblast) undergo migration, invagination, and involution largely controlled by the primitive streak (Figure 1). At the primitive streak, cells start to differentiate and migrate to form a middle mesodermal layer, adjacent to where a majority of the hypoblasts dislodge to create an endodermal layer. The epiblast is formed from the ectoderm without cell movement. The endoderm forms the epithelial lining of the digestive and respiratory tracts, liver, and pancreas and the ectoderm gives rise to the epidermis of the skin, cornea, lens of the eye, and central nervous system. Lastly, the mesoderm gives rise to the circulatory system, heart, notochord, musculoskeletal system, and muscular layer of the digestive system, gonads, and most importantly the kidney. Therefore, in this introduction I will focus on mesoderm development (Tam & Beddington, 1987).

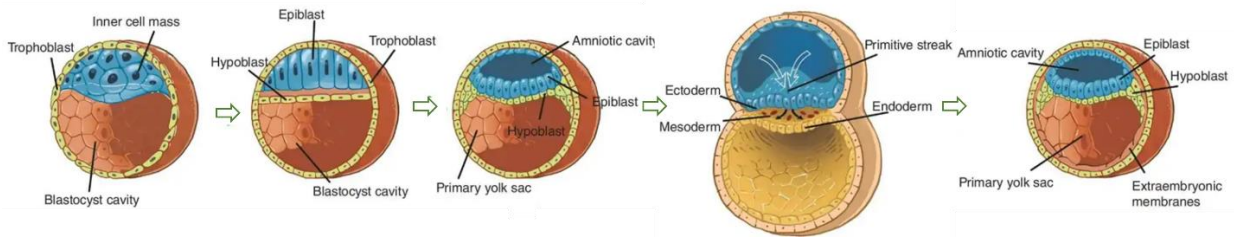

Figure 1: Embryonic development during gastrulation (adapted from https://pocketdentistry.com/growth-and-development-2/)

1.2.2 Mesoderm

The embryonic and extraembryonic mesoderm is made up of layers of mesodermal cells that are organized during gastrulation when cells move from the epiblast via the primitive streak. Fate mapping studies of the mesoderm at the gastrulation stage reveal that cells destined for the extraembryonic mesoderm are the major tissue type in the nascent mesodermal layer. (Kinder et al., 2017). Throughout the process of embryonic trunk elongation, the developing mesodermal cells divide and continuously push the newly formed daughter cells toward the anterior end. These daughter cells divide into paraxial mesoderm, lateral plate, and intermediate mesoderm (Takasato & Little, 2015). The early stages of the embryo show that the precursor cells for the cranial and cardial mesoderm arise later, during the mid-streak stage, within the mesodermal layer

(Parameswaran & Tam, 1995; Tam et al., 1997). These research findings also indicate that the different precursors of mesodermal cells exhibit clear regional distinctions (Tam & Beddington, 1987).

The trunk mesoderm in the neurula stage can be divided into four regions. (i) The central region is the chordamesoderm, forming the notochord. (ii) Flanked on both sides of the notochord is the paraxial mesoderm. Its development involves several stages including somitogenesis, and somite specification. (iii) The lateral plate mesoderm is responsible for the development of the heart, blood vessels, and the blood cells that make up the circulatory system. (iv) The intermediate mesoderm forms the urogenital system, including the kidney, gonads, and ducts (Figure 2).

The specification of the dorsal-ventral axis in these four subdivisions appears to be influenced by different levels of BMP (Michael Jones et al., 1996). During intermediate mesoderm development, a low level of BMP signaling is required for the formation of the nephric duct, together with nodal/activin expression from the lateral plate mesoderm (Fleming et al., 2013; Obara-Ishihara et al., 1999). In addition, the paraxial mesoderm appears to play a critical role in both initiating and completing the kidney formation process in the IM, as evidenced by experiments in which co-culturing lateral plate mesoderm with paraxial mesoderm results in the formation of pro-nephric tubules, a feat not achievable by any other cell type (Mauch et al., 2000). Furthermore, along the anterior-posterior axis, the decision between rostral and caudal IM fates is regulated by opposing gradients of BMP, activin, retinoic acid (RA), and fibroblast growth factor (FGF) signaling, as shown in studies using Xenopus and chick embryos (Amaya et al., 1993; Duester, 2008; Re'em-Kalma et al., 1995; Yatskievych et al., 1997).

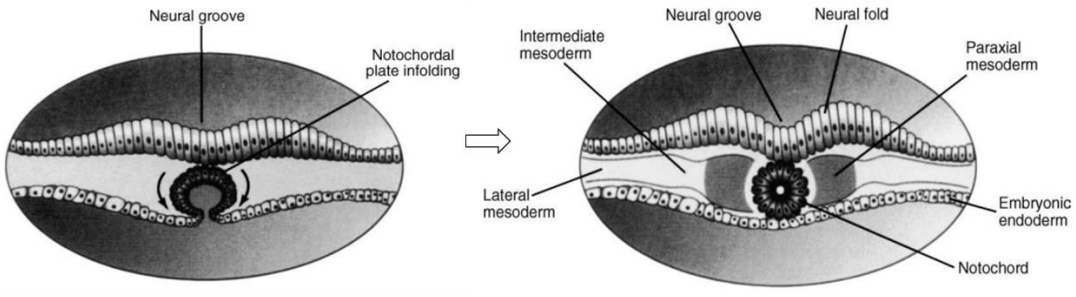

Figure 2: Fate of mesoderm derivatives. Adapted from (Moore KL et al., 2016, 10th edition)

1.2.3 Intermediate mesoderm

The intermediate mesoderm, located between the somites and the lateral plate of the mesoderm, is the source of kidney tissue (Saxon & Sariola, 1987). Several studies have characterized inductive signals and transcription factors secreted by the axial and paraxial mesoderm that regulate intermediate mesoderm differentiation (Costantini & Kopan, 2010; Dressler, 2006; James & Schultheiss, 2005; Obara-Ishihara et al., 1999). Activation of the earliest intermediate mesoderm genes, encoding the transcription factors Osr1, Lim-1, and Pax2, requires an intermediate level of BMP signaling, as a higher level leads to the formation of lateral plate mesoderm and a lower levels leads to paraxial mesoderm (James & Schultheiss, 2005). The activation of such markers is the first indication that the lateral plate mesoderm and subsequent intermediate mesoderm are differentiated from surrounding cells. *In vitro* experiments in the Xenopus embryo suggest that synergism between Pax2 and Lim-1 leads to the establishment of the pronephric primordia (Carroll & Vize, 1999). A mediolateral gradient of BMP and activin-like signaling cooperates with an anterior-posterior gradient of RA signaling to assemble *Hox* gene expression domains; cells at specific levels along these gradients will undergo nephric duct specification. This process requires the co-expression of the transcription factors *Pax2*, *Pax8*, and *Lhx1* (Bouchard et al., 2002). Detailed lineage analysis in animal models such as mice shows that the anterior part of the intermediate mesoderm contributes to the development of the Wolffian duct, while the posterior part gives rise to the metanephric mesenchyme (Taguchi et al., 2014). These specific regions are of great importance because they are exposed to a variety of spatial and temporal signals, as depicted in Figure 3 (Taguchi et al., 2014; Takasato & Little, 2015).

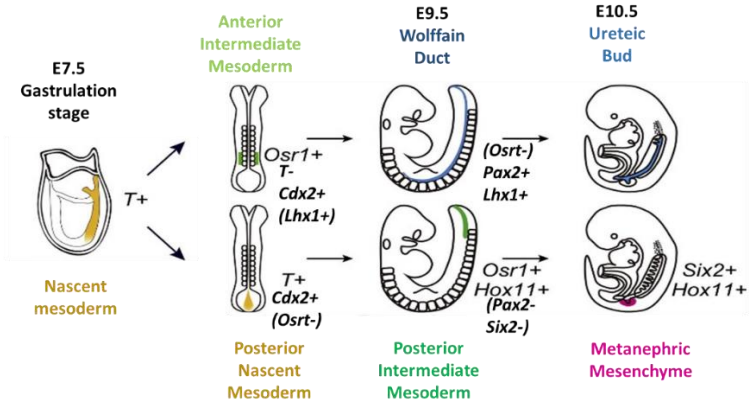

Figure 3: Distinct lineage segregation during the development and differentiation of ureteric bud and metanephric mesenchyme. Proposed by (Taguchi 2014)

1.3 Nephrogenesis

1.3.1 Nephric duct

The nephric duct represents the initial epithelial component of the urogenital system (Schultheiss et al., 2003). In mammalian embryos, the nephric duct originates from a group of mesenchymal cells known as the "duct primordia" within the intermediate mesoderm (Attia et al., 2015). Subsequently, these duct primordia elongate in a posterior (caudal) direction until they merge with the cloaca at the caudal end of the embryo. During this elongation process, a crucial transformation called “mesenchymal to epithelial transition” occurs. This transition leads to interactions between the duct and neighboring mesodermal cells, ultimately giving rise to both the mesonephros (the embryonic kidney) and the metanephros (the adult kidney). The nephric duct itself forms the collecting ducts of the kidney and the ureter, which are responsible for draining urine from the kidney. In males, it also contributes to the formation of the spermatic duct. Importantly, if the nephric duct elongation is disrupted or inhibited, neither of these vital structures can form (Soueid-Baumgarten et al., 2014). Fibroblast growth factor (FGF) signaling accompanied by glial-derived neurotrophic factor (GDNF), is essential for the nephric duct migration. Several FGF receptors and ligands are expressed in the nephric duct and surrounding tissues. Among these receptors, fibroblast growth factor receptors (FGFR) 2 and 3 are initially found to be expressed in the duct. However, at later stages of embryonic development, only FGFR2 expression can be observed. This observation suggests that FGFR2 is likely to play a more critical role in duct migration compared to FGFR3 (Attia et al., 2015).

1.3.2 Pronephros, mesonephros, and metanephros

The pronephros marks the earliest stage of kidney development, occurring at day 22 in humans, day 11 in rats, and day 8 in mice (Saxon & Sariola, 1987; Seely, 2017). During this stage, the cells of the pronephric duct migrate caudally (toward the tail end), and the anterior part of this duct induces the adjacent mesenchyme to form the pronephros. Although the pronephros itself is non-functional, the caudal part of the pronephric duct persists after regression and eventually transforms into the Wolffian duct. One of the functions of the Wolffian duct is to induce the development of the mesonephros. In fish and amphibians, the mesonephros functions as the primary kidney, but in adult mammals, it becomes non-functional. However, during mammalian embryonic

development, mesonephric nephrons are initially formed but later undergo regression. (Romagnani et al., 2013).

The metanephros, which will eventually become the permanent kidney (as shown in Figure 4), arises from two crucial tissues: the ureteric bud and the metanephric mesenchyme. At approximately 4 to 5 weeks of human gestation, metanephric development is initiated (Cullen-McEwen et al., 2015). During this process, the out-branching epithelium extends into and penetrates the metanephric blastema, a collection of mesenchymal cells that gather around the terminal part of the advancing ureteric bud. Cells in direct contact with the bud stimulate the ureteric epithelium to proliferate, elongate, and branch. Reciprocally, a mesenchymal-to-epithelial transition occurs at the tips of the ureteric bud, which induces the formation of nephrons from the mesenchymal cells. These sequential and inductive interactions between the ureteric bud and the surrounding metanephric mesenchyme are responsible for the formation of the permanent kidney (Cullen-McEwen et al., 2015; Saxon & Sariola, 1987). The ureteric bud eventually develops into the collecting duct system, which includes the ureter, renal pelvis, calyces, and collecting tubules. On the other hand, the metanephric mesenchyme differentiates into the glomeruli, the tubular segments of the nephron, and the interstitial tissue (stroma). Kidney development involves a series of branching and induction events between the ureteric bud and the adjacent metanephric mesenchyme. Each branch tip induces mesenchymal-epithelial transitions, and this process continues until the appropriate number of nephrons has formed (Saxon & Sariola, 1987) (Figure 4).

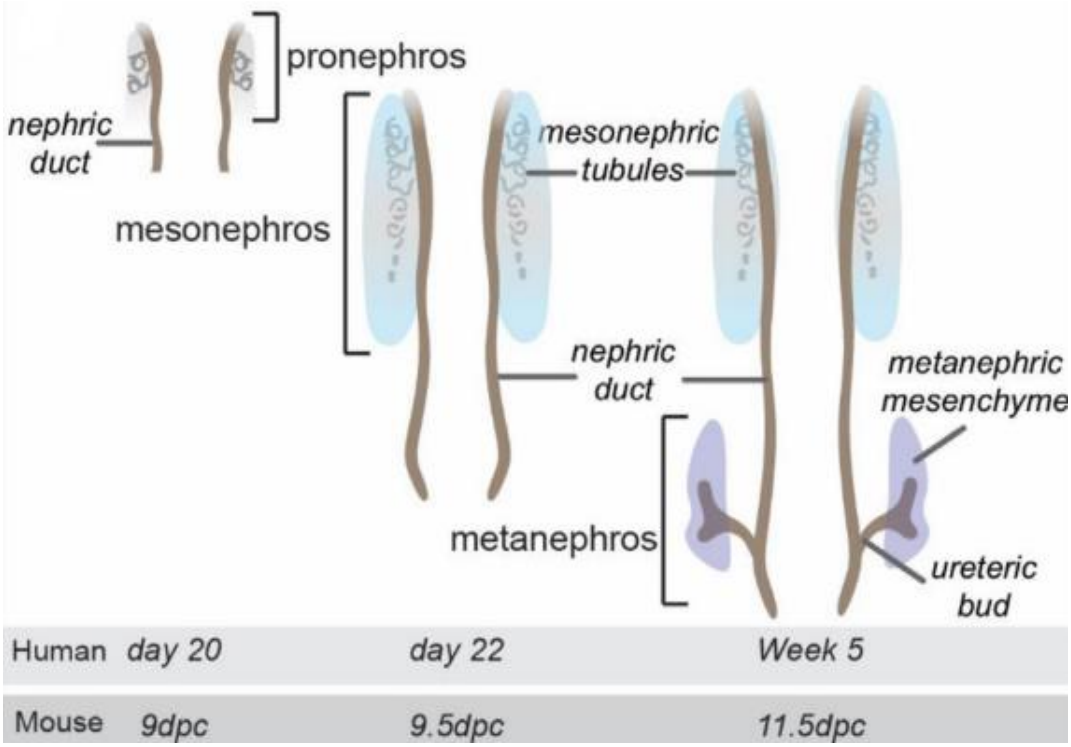

Figure 4: Pronephros, mesonephros, and metanephros development. At the nephrogenic zone, multiple rounds of branching morphogenesis and nephron induction occur. This dynamic process is responsible for the formation of nephrons, the functional units of the kidney. Adapted from (Melissa Little 2018)

1.3.3 Shaping of the nephron: renal vesicles and S-shaped body

Renal vesicles are the first polarized epithelial derivatives of the metanephric mesenchyme. During development, there are three primitive stages that form the nephrogenic body: the renal vesicle, the comma-shaped body, and the S-shaped body. Tubular structures in their early stages always emerge on the proximal side of the ureteric bud tip, and their proximal-distal axis remains aligned, with the duct tip indicating the distal end (Kopan et al., 2007). In the comma-shaped body, this proximal-distal polarity is visible, and the nascent nephrogenic bodies are the first cells to elongate, change in shape, and eventually form a "slit" structure. This slit is located at the proximal end, furthest from the ureteric bud (Saxon & Sariola, 1987).

Proliferation and differential adhesion could be the factors responsible for reshaping the comma-shaped body into an S-shaped structure that eventually connects to the ureteric bud at its distal end, with all the podocyte precursors appearing at its proximal end. (Saxon & Sariola, 1987). Molecular markers such as Pax2, WT-1, Jag1, Cdh6, and E-cadherin (as shown in Figure 5) can help to identify the epithelial precursors

responsible for the formation of three nephron segments, namely the glomerulus, proximal tubule, and distal tubule, all of which are localized within the S-shaped structure (Dressler, 2006) (Figure 5). Experimentally, it has been suggested that Wnt signaling facilitates the transformation of mesenchymal cells into epithelial cells by extending the lifespan of ß-catenin. In particular, when ß-catenin is artificially stabilized in the metanephric mesenchyme, it induces the conversion to epithelial structures (Kuure et al., 2007). Cells will express Lhx1, a marker for distal regions, while cells further away will be the first to elongate and subsequently take on identities as proximal tubule and glomerular podocyte precursors. This is consistent with the concept that a brief exposure to the morphogen leads to the formation of proximal tubule and podocyte precursors (Kopan et al., 2007).

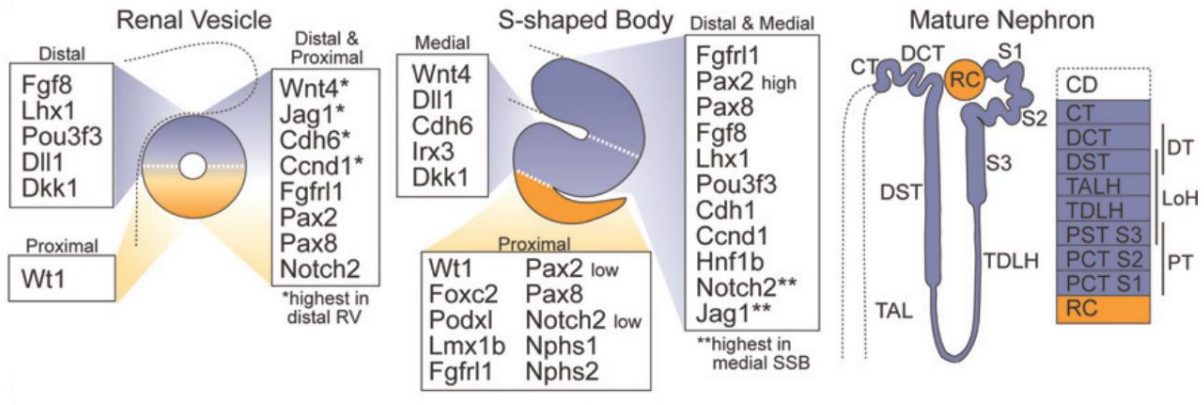

Figure 5: Expression pattern of genes during nephrogenesis. (Left) Gene expression profile in renal vesicle and S-shaped body. (Right) the mature nephron segments showing RC: renal corpuscles, DCT: distal convoluted tubule, DST: distal straight tubule, S1, S2, and S3: segments of the proximal tubule, TDLH: descending thin loop of Henle, TAL: thin ascending limb, CT: connecting tubule; CD: collecting duct. Adapted from (Melissa little, 2010)

Following the mesenchymal to epithelial transition, a variety of distinct cell populations become active in the renal vesicles, each responsible for forming different segments of the mature nephron (Saxon & Sariola, 1987) , as shown in Figure 5:

1. A population of WT+ cells gives rise to proximal structures, including the specification of the glomerular podocyte layer and a segment of proximal tubules.
2. A population of Jag1+ cells contributes to the medial portions of both proximal and distal tubules, as well as the loop of Henle.

3. Lgr5+ cells are responsible for generating the distal nephron segments, specifically the distal convoluted tubules (Barker et al., 2012; L. Chen & Al-Awqati, 2005; Desgrange & Cereghini, 2015; Kreidberg, 2010; M. Little et al., 2010).

Furthermore, each of these nephron segments can be further subdivided into specialized functional regions that play critical roles in regulating transmembrane transporters and channels for substances such as glucose, salt, and metals (Raciti et al., 2008).

1.3.4 Renal corpuscle and tubules

The renal corpuscle is a complex structure with a specialized role in producing glomerular filtrate while retaining plasma proteins in the circulation. It consists of two major components: the glomerulus, which consists of a cluster of capillaries and mesangial cells, and Bowman's capsule, a double-walled epithelial structure. Within Bowman's capsule, there is a proximal convoluted tubule. The glomerular tuft includes the glomerular capillaries, the mesangium (located within the glomerular basement membrane), and the podocytes that cover the outer surface of the membrane. The glomerular capillaries are connected to an afferent arteriole that brings blood into the glomerulus. Finally, these capillaries converge to form an efferent arteriole that carries blood away from the glomerulus. This intricate arrangement allows the renal corpuscle to play its crucial role in filtration and protein retention (Kriz & Kaissling, 2007).

The mesangial cells that lie between the glomerular capillaries regulate blood flow by their contractile activity and secrete extracellular matrix, prostaglandins, and cytokines. The outer layer of Bowman’s capsule is the outer boundary of the renal corpuscles forming a single layer of squamous epithelial cells resting on a basement membrane. The inner visceral layer of Bowman’s capsule is composed of modified epithelial cells called podocytes. These have a voluminous, smooth-surfaced cell body that floats in the urinary tract and appears to adapt in shape to the surrounding flow conditions created by the filtrate. The cells give rise to long primary processes that extend toward the endothelial cells of the capillaries, eventually splitting apart into terminal foot processes that attach to the glomerular basement membrane (GBM). The foot processes of adjacent podocytes regularly interdigitate with each other, leaving meandering slits (filtration slits) between them that are bridged by an extracellular structure, called a slit diaphragm. The fusion of the endothelium, podocytes, and basement membrane leads to

the formation of GBM. In adults, the collagen component of the GBM is derived exclusively from podocytes, whereas the laminin component is derived from both podocytes and endothelial cells. This association of glomerular capillary endothelial cells, podocytes, and GBM results in glomerular filtration barriers. The glomerular filtrate originates from the capillary lumen with its porous endothelium, followed by the GBM, and a layer of interdigitating foot processes with filtration slits in between. Charge, size, and shape determine the specific permeability of a macromolecule in the filtrate. All components of the glomerular filter are highly negatively charged. As blood circulates through the glomerulus, approximately 10 to 20 percent of the plasma proteins pass through the filtration membrane. These filtered proteins are then captured by Bowman's capsule and directed into the proximal convoluted tubule as part of the glomerular ultrafiltrate. This process is a crucial step in the formation of urine and the regulation of the fluid and solute balance in the body (Kriz & Kaissling, 2007).

The renal tubule consists of 5 components: the proximal convoluted tubule PT, the descending limb of loop of Henle, the ascending limb loop of Henle, the distal convoluted tubule, and the collecting duct. The proximal tubule is a *tour de force* of the glomerular filtrate reabsorption. It begins with a urinary pole of the renal corpuscle and ends at the transition to the descending thin limb of the loop of Henle, which defines the boundary between the outer and inner stripes. The proximal tubule consists of a single layer of cuboidal epithelial cells lined with microvilli and intermicrovilli, which play a critical role in reabsorbing approximately two-thirds of the filtered salt, water, organic solutes (mainly glucose and amino acids), bicarbonate, and phosphates from the glomerular ultrafiltrate into the peritubular capillaries. As the U-shaped loop of Henle extends deeper into the medulla, the osmolarity of the interstitial fluid surrounding the renal tubule increases. This higher osmolarity outside the tubule causes water from the descending limb to be readily absorbed into the more concentrated interstitium to achieve balance. Consequently, the tubular fluid becomes more concentrated at the bottom of the loop of Henle. As the concentrated tubular fluid rises through the ascending limb, the surrounding osmolarity outside the tubule begins to decrease again. The tubular fluid is now more concentrated than the interstitial fluid, resulting in the reabsorption of sodium instead of water. The ascending limb of the loop of Henle is also known as the diluting portion of the nephron. By the time the filtrate reaches the distal tubule, it has become hypotonic due to the significant loss of sodium. While the cells in the distal tubule are similar in structure to

those in the proximal tubule, they have fewer microvilli and mitochondria and are responsive to hormonal regulation. Aldosterone, a hormone released by the adrenal cortex in response to factors such as low blood pressure, low sodium levels, or activation of the renin-angiotensin-aldosterone system, increases sodium reabsorption and potassium secretion. In addition, calcium regulation occurs in the distal tubule through the reabsorption of calcium into the vasculature, mediated by receptors for parathyroid hormone. The distal tubule then enters the collecting duct system where water reabsorption is controlled by antidiuretic hormone. In the presence of antidiuretic hormone, aquaporin channels are inserted into the apical membrane of collecting duct cells, allowing water to be osmotically drawn into the renal calyces and pelvis for eventual urine excretion (Kriz & Kaissling, 2007; Matlin & Caplan, 2008).

In humans, nephrogenesis is typically completed by 36 weeks of gestation. Importantly, there is no conclusive evidence for the generation of new nephrons after this developmental stage. It is worth noting, however, that the renal tubule has an extraordinary capacity for regeneration. It can rapidly recover and regenerate within a few days after an episode of acute kidney injury. This regenerative capacity of the renal tubule plays a critical role in restoration of kidney function following damage to the kidney. Studies suggest that proximal tubular cells regenerate from any surviving tubular cells or that specific differentiated tubular cells (scattered tubular cells, STCs) potentially act as a reserve to re-enter in the cell cycle upon injury (Vogetseder et al., 2008). However, the lack of regenerative capacity of the nephrons after birth suggests that regeneration of the kidney is highly beneficial, albeit a challenge. In order to recapitulate nephrogenesis in vitro the following section will elaborate the pathways to generate nephron progenitors from stem cells.

1.4 Legacy of pluripotent stem cells to the birth of regenerative medicine

Since the advent of the term “stem cell” in the 19th century (Ramalho-Santos & Willenbring, 2007), the concept of a single cell’s ability to differentiate into different tissues has piqued the curiosity of both biologists and clinicians. In modern terms, stem cells are defined as undifferentiated cells that have the capacity for self-renewal and the potential to develop into different cell types (Morrison et al., 2010). However, the renewal capacity of adult stem cells is limited because they can only transform into a limited number of cell types (Dulak et al., 2015). For example, hematopoietic stem cells located in the bone

marrow can only generate blood cells. Despite this limitation and other associated challenges, human bone marrow stem cells have pioneered clinical application, dating back to 1957 (Simpson & Dazzi, 2019), when bone marrow transplantation was first performed. This procedure is now a common practice in the treatment of various blood disorders (Passweg et al., 2016). The more recent focus of stem cell research has broadened their potential in regenerative and personalized medicine, as well as in the modelling of human disease. Embryonic stem cells differentiate into all cells of an organism, but their derivation has met ethical opposition (Gough, 2011). A possible alternative was found in 2006 when Takahashi and Yamanaka published the results of their work on reprogramming differentiated fibroblasts “backwards” into pluripotent stem cells (PSCs) (Takahashi et al., 2007). One of the major advantages of induced PSCs (iPSCs) over embryonic stem cells is that they can be generated from any individual. This opens up the possibility of studying and treating genetic disorders on a personalized level. iPSCs have been instrumental in recapitulating various aspects of embryonic development *in vitro* due to their pluripotency. This includes the ability to recapitulate processes such as trophoblast formation, neural tube induction, and primitive streak formation, and extends to the generation of neurons, beating cardiomyocytes, and insulin-producing beta cells in the pancreas. The successful development of numerous differentiated cell types that closely resemble their fully specialized counterparts *in vivo* represents a major achievement in the field of stem cell research. These cells have great potential as regenerative sources for the treatment of degenerative diseases and related conditions.

1.5 Cutting-edge development of kidney cells from pluripotent stem cells (PSC)

Over the past decade, there has been a significant increase in the development of human tissue models. This progress has been achieved by various methods, such as the transdifferentiation of somatic cells using specific transcription factors or direct differentiation of PSCs using key genes or growth factors. Numerous protocols have been established to direct the differentiation of human PSCs into various cell types. The kidney, with its intricate architectural complexity comprising at least 26 specialized cell types has been a particular focus (Al-Awqati & Oliver, 2002). Initially, attempts to generate specific kidney tissues involved using mouse embryonic stem cells and exposing them to media containing serum, along with various combinations of factors such as RA, BMP4, BMP7,

activin A, leukemia inhibitory factor (LIF), and GDNF. These protocols resulted in the generation of cells expressing differentiation markers such as Pax2 (associated with renal tubules), Aquaporin-2 (found in collecting duct principal cells), Wilms tumour (WT1) (present in metanephric mesenchyme and podocytes), or Ksp-Cadherin (associated with distal nephron tubules) within embryonic stem cell-derived embryoid bodies. These findings provide evidence for renal lineage induction (Bruce et al., 2007; Kobayashi et al., 2005; Morizane et al., 2015; Nishikawa et al., 2012; Ren et al., 2010; Vigneau et al., 2007). However, it is important to note that despite these efforts to generate different renal cell types, none of these studies provided a comprehensive evaluation of the intermediate steps involved in the differentiation process.

In the meantime, several groups have established protocols to study kidney development using growth factors to influence primitive streak formation (RA, activin A, FGF2, WNT3A), apical to proximal mesodermal patterning (RA, FGF2/9, WNT3A/5A), mesoderm to lateral mesodermal patterning (BMP4, activin A, FGFs), nephric duct identity (RA, activin A), metanephric mesenchyme fate (WNTs, BMP7, FGF2/9) and survival (FGF2/ 9, BMP2/7) (Lam et al., 2014; Mae et al., 2013; Taguchi et al., 2014; Takasato et al., 2014; Xia et al., 2013). Genetic lineage tracing revealed that the cap mesenchyme expresses the Six2 transcription factors that possesses self-renewing nephron progenitors capable of giving rise to all cell types within the nephron (Kobayashi et al., 2008). Moreover, Mugford et al. (2008) confirmed the intermediate mesoderm origin of kidney cells using a temporal fate mapping approach to address that the majority of cell types within the metanephric kidney arise from $Osr1^{+}$ cells. Osr1 serves as a molecular connection between the maintenance of progenitors and the branching of ureteric epithelium. It does this by regulating the activation complex involving Pax2, Eya1, and Hox11, which in turn influences the expression of Six2 and GDNF (Mugford et al., 2008).

In addition, several other methods/protocols have been developed to induce different cell types within the nephron. For example, hiPSC-derived podocytes expressing podocin, nephrin, and synaptopodin were generated from embryoid bodies using a BMP7, activin A, and RA on gelatin-coated plates (Song et al., 2012). Similarly, podocytes were generated from hiPSCs expressing podocalyxin, podocin, and synaptopodin using a combination of the growth factors activin A, RA, BMP4, GDNF, and HGF on laminin-

coated plates (Hariharan et al., 2019). Other studies have demonstrated the generation of approximately 90% AQP1+ proximal tubule cells by treating a monolayer PSC culture with renal epithelial growth factor-containing media for 9 days (Kandasamy et al., 2015). Recent reports have provided insights into the stepwise induction of the ureteric bud and/or metanephric mesenchyme through a systematic approach, starting with the induction of the primitive streak and progressing to intermediate mesoderm pacification (Hariharan et al., 2019; Lam et al., 2014; Taguchi et al., 2014; Takasato et al., 2014; Xia et al., 2013). These studies performed thorough characterization of the cell types obtained at each stage; focusing on obtaining PAX2+ GATA3+ LHX1+ ureteric bud cells (Xia et al., 2013), SIX2+ PAX2+GDNF+ HOX11+ WT1+ metanephric mesenchymal cells (Taguchi et al., 2014), and SIX2, LHX1, OSR1, PAX2, WT1, CDH1, HOXB7+, JAG1 cells (Hariharan et al., 2019). Researchers have achieved the generation of ureteric bud and metanephric mesenchyme within specific time frames, such as between 14 and 18 days (Takasato et al., 2014), 8 days (Lam et al., 2014), and even as quickly as 4 days (Hariharan et al., 2019). In addition, these studies have demonstrated the potential of specific cell populations to give rise to tubule structures, highlighting the progress in nephron differentiation protocols.

Kidney organogenesis from PSC was reported by Takasato et al. (2014) after 18 days of PSC differentiation, ECAD+ ureteric epithelium developed surrounded by clumps of SIX2+ WT1+ PAX2+ metanephric mesenchymal cells or JAG1+ CDH6+ renal vesicles (Takasato & Little, 2015). Tubule-like structures positive for loctus lectin (a proximal tubule marker) were observed by Lam et al. (2014) on day 7 of SIX2 cap mesenchyme cell cultures, treated with the Wnt pathway activator CHIR99021. Similarly, a slightly different experiment was performed by Taguchi et al. (2014) using PSC from embryoid bodies to obtain SIX2+ WT1+ SALL1+ PAX2+ metanephric mesenchymal cells after 8.5 days in mouse embryonic stem cells and 14 days in hiPSCs, which can give rise to tubules and podocytes when induced in mouse embryonic spinal cord. Another protocol by Hariharan et al. (2019) demonstrated the fastest way to generate nephron progenitors in which 4-day exposure to activin A, BMP4, and RA generates intermediate mesoderm, ureteric bud, and metanephric mesenchyme, which become the basis for the generation of nascent renal vesicle stage nephron progenitors. At this stage, the renal progenitors are directed towards terminal differentiation to produce podocytes and mesangial cells, along with proximal and distal tubular epithelial cells, collecting duct cells and the all-

encompassing nephron organoid. It is this type of fundamental study that leads to the organ-typical structures that reflect embryonic kidney development from PSC.

1.6 Disease modeling and regenerative medicine

Kidney disease is a diverse group of disorders, not a single disease in terms of underlying etiology, pathology, onset, or prognosis. Congenital anomalies occur in approximately 1 in 1000 births and account for 50% of cases of renal failure in childhood (M. H. Little, 2021). However, genetic factors contributing to kidney disease without obvious structural anomalies are increasingly being identified. There are specific categories of kidney diseases in which the clinical manifestations predominantly affect the kidneys. For example, autosomal dominant tubulointerstitial kidney disease caused by uromodulin (UMOD) mutations is a condition in which the molecular defect is restricted to the cells of the ascending loop of Henle (Lam et al., 2014; Zhong et al., 2017). Glomerulopathies, such as inherited forms of nephrotic syndrome with podocyte specific defects, tauopathies such as focal segmental glomerulosclerosis (FSGS) (Mallipattu & He, 2016), and nephrogenic diabetes insipidus involve proteins expressed in specific segments of the glomerulus and tubules. On the other hand, certain inherited kidney diseases show symptoms in multiple organs. One example is autosomal dominant polycystic kidney disease (ADPKD), in which cysts can develop not only in the kidneys but also in other organs outside of the renal system (Matlin & Caplan, 2008). This highlights the diversity and complexity of kidney disease, each with its own unique characteristics.

Extensive research efforts have been directed towards the development of disease models for inherited kidney diseases to identify abnormal pathways and potential therapeutic targets (Molinari & Sayer, 2020). hiPSCs derived from patients with genetic disorders have emerged as valuable tools for creating *in vitro* patient-specific disease models, facilitating the study of the underlying pathophysiology of these genetic diseases (Miyoshi et al., 2020). Similarly, hiPSCs are compatible with genome editing technologies such as zinc finger nuclease (ZFN) technology (Geurts et al., 2009), transcription activator-like effector nuclease (TALEN) (Tesson et al., 2011), clustered regularly interspaced short palindromic repeat (CRISPR)/Cas (Gasiunas et al., 2012; H. Wang et al., 2013), and Tet-on 3G systems (Bertero et al., 2016; Pawlowski et al., 2017a; Randolph et al., 2017). These technologies allow the precise introduction of candidate

gene mutations into hiPSCs, thereby facilitating the rapid and straightforward generation of humanized and patient-specific disease models. This advancement paves the way for the development of precision medicine approaches aimed at tailoring treatments to individual patients with inherited kidney diseases. One such modification is discussed in the following chapters.

1.7 Focal segmental glomerulosclerosis (FSGS)

FSGS is a major cause of end-stage renal disease worldwide. It was first identified in the 20th century as a histopathologic pattern of glomerular injury associated with nephrotic syndrome (Weening & Jennette, 2012). The initial description can be attributed to the German pathologist Theodor Fahr in 1925, when it was referred to as "lipid nephrosis with degeneration" (Cameron, 2003a). It was not until 1957, that another pathologist named Arnold Rich, defined the histological characteristics of FSGS in nephrotic children. He showed that the lesions associated with FSGS were either localized or most prominent in the glomeruli near the renal medulla (Rich et al., 1957). Although FSGS was occasionally mentioned in adults (MCGOVERN, 1964), it was not until a decade later, in the late 1960s, that Jack Churg and colleagues from the International Study of Kidney Disease in Children (ISKDC) officially classified FSGS as a distinct renal glomerulopathy based on renal biopsies performed between 1966 and 1969 (Churg et al., 1970; Habib, 1973). Notably, the incidence of FSGS seems to have increased in the last few decades. (Kitiyakara et al., 2004). However, the true incidence of FSGS is unknown, as many patients probably remain undiagnosed, either because they present late with advanced renal failure, because their symptoms are unclear and a glomerular disease is not suspected, or because the cause of end-stage renal disease, if known, is not reported. FSGS can occur at any age, and occurs in approximately 7-10% of children and 20-30% of adults with nephrotic syndrome (Shabaka et al., 2020). FSGS has an annual incidence rates of 0.2 to 0.8/100,000 in adults per year (McGrogan et al., 2011). In Germany, the incidence of nephrotic syndrome is 1.2–1.65/100 000 in children under 18 years per year, while 0.1/100,000 has been reported for FSGS in children under 18 years of age (Franke et al., 2018). Data from the European Renal Association - European Dialysis and Transplant Association (ERA-EDTA) registry report the number of unresolved end-stage renal disease cases is as high as 27% (Kramer et al., 2021). When FSGS is associated with high proteinuria, 50% of patients progress to end-stage renal

disease within 3 to 8 years, making FSGS accountable for 4% of all end-stage renal disease cases (D'Agati, 2008). Even after kidney transplantation for FSGS, the relapse rate is 40% (Hickson et al., 2009).

1.7.1 Clinical presentation and progression

FSGS is characterized by a distinct pattern of histological injury in which sclerosis, or scarring, occurs in "some" part (segmental) of at least one glomerulus (focal) as seen by light microscopy. This means that not all glomeruli are affected, and the scarring is limited to specific segments within those glomeruli (Figure 6B and D). In electron microscopy, FSGS is associated with varying degrees of effacement (flattening or loss of structure) of the podocyte foot processes (Figure 6C andE). These podocyte foot processes are essential for the normal function of the glomerular filtration barrier, and their effacement is a hallmark of glomerular injury in FSGS as shown in Figure 6E (Sambharia et al., 2022). In addition, FSGS is further characterized by the presence of hyalinosis and the formation of adhesions or synechiae within the affected glomeruli. These adhesions or synechiae can lead to segmental obliteration of glomerular capillaries, contributing to the scarring and dysfunction observed in FSGS (Gipson & Gipson, 2019). The focal origin of FSGS in the juxtamedullary glomeruli progresses to global sclerosis without segmental lesions, making it indistinguishable from other forms of chronic kidney diseases in which non-specific global glomerulosclerosis, interstitial fibrosis, and tubular atrophy predominate (Sambharia et al., 2022). The collapsing form of FSGS is characterized by severe hypertension, a very poor response to corticosteroids, massive proteinuria, and a much faster rate of progression to end-stage renal disease (Shabaka et al., 2020).

Clinically, FSGS patients show varying degrees of proteinuria and, in some cases, changes in kidney function. In cases where nephrotic syndrome is present, proteinuria is typically severe, with protein excretion exceeding 3.5 grams in 24 hours. This often results in low serum albumin levels (<35 grams per liter or <3.5 grams per deciliter) (Glassock et al., 2015), whereas some individuals with FSGS may be asymptomatic and are found to have proteinuria with or without noticeable changes in kidney function (Sambharia et al., 2022). Infants and children with relatively preserved glomerular filtration rate who present with nephrotic syndrome (characterized by proteinuria, edema, and hypoalbuminemia) may not undergo kidney biopsy unless corticosteroid treatment fails to induce remission.

Thus, some children with steroid-sensitive nephrotic syndrome may have unrecognized FSGS, although most clinicians believe that patients who have durable remission with corticosteroids are likely to have minimal change disease. In contrast, adults with varying degrees of proteinuria or nephrotic syndrome are often recommended for a kidney biopsy before treatment decisions are made. This is because FSGS is more commonly seen in adults in this clinical context. In the literature, the terms steroid-resistant nephrotic syndrome (SRNS) and FSGS are sometimes used interchangeably. This is because a significant proportion of children with relapsing-remitting or steroid-resistant nephrotic syndrome are found on biopsy to have FSGS as the underlying histopathological diagnosis (Lee et al., 2021; Reidy & Kaskel, 2007).

Only in the past 10 years has it been recognized that FSGS has a remarkable ethnic predominance. This is especially true in adult nephrotics, with almost two-thirds of African-American adults with nephrotic syndrome having FSGS. This is also true for one third or more of African-American nephrotic children (Haas et al., 1995). However, all these reports are from the United States, and it is not clear whether these findings apply worldwide (Cameron, 2003b).

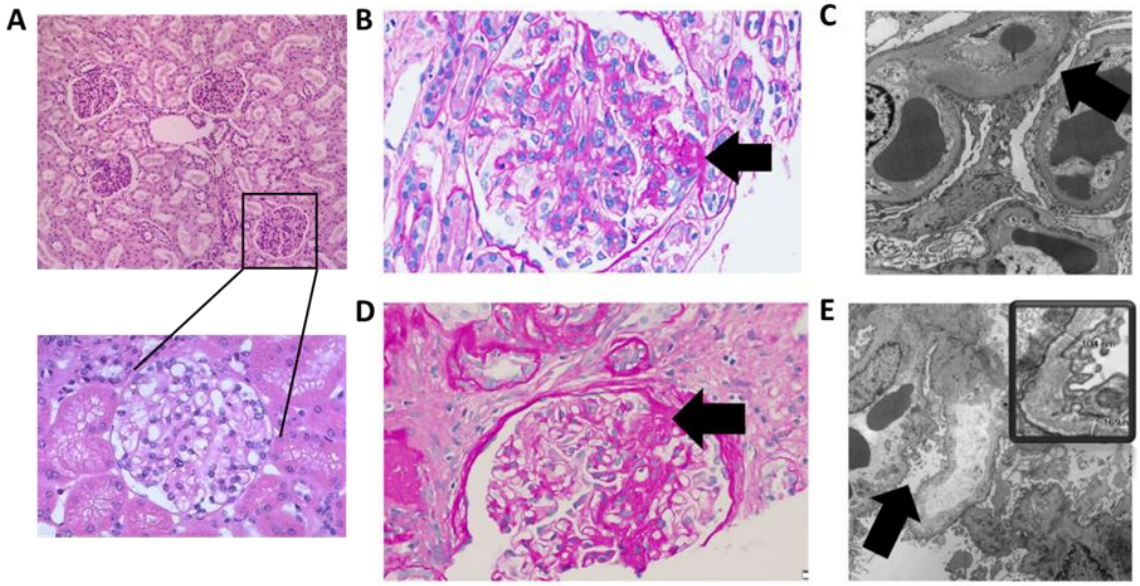

Figure 6: Histology of focal segmental glomerulosclerosis (FSGS). (A) Normal glomerulus. **(B)** Renal sample of a patient with autosomal dominant FSGS showing glomerulus with an area of segmental sclerosis under light microscopy (PAS stain, 40X objective). **(C)** Electron microscopy image (10,000X direct magnification) show a glomerulus with diffuse podocyte epithelial foot process effacement (arrow). **(D)** Renal sample of a patient with X-linked FSGS under light microscopy (PAS stain, 40X objective) shows a glomerulus with an area of segmental sclerosis (arrow). **(E)** Electron microscopy (10,000X direct magnification) shows focal podocyte epithelial foot process effacement (arrow). Adapted from (Sambaria et al., 2022)

1.7.2 Pathogenesis of FSGS

The glomerular filtration barrier is composed of three primary components: the podocyte, the glomerular basement membrane, and the capillary endothelial cells (as shown in Figure 7). Any injury or damage to this filtration barrier can result in proteinuria, and the presence of excess protein in the urine, and may contribute to the development of FSGS. A specialized tight junction “slit diaphragm” plays a vital role in preventing the loss of proteins from the bloodstream into the urinary tract. Dysfunction or disruption of this barrier, as seen in FSGS and other glomerular diseases, can lead to the leakage of proteins into the urine (Asanuma & Mundel, 2003a).

A key factor in the pathogenesis of FSGS is the damage and loss of podocytes (Asanuma & Mundel, 2003b; Kriz, 2003). Podocyte damage can occur by four main mechanisms:

1. Alteration to the slit diaphragm: Alterations in the components of the slit diaphragm or disruptions in its structural integrity can contribute to podocyte damage.
2. Dysregulation of the actin cytoskeleton: Abnormalities in the actin cytoskeleton within podocytes can lead to their dysfunction and damage.
3. Alteration of the glomerular basement membrane: Alterations in the glomerular basement membrane and its interactions with podocytes can also be detrimental.
4. Alteration of podocyte surface charge: Any changes in the negative surface charge of podocytes may affect their function and integrity (Asanuma & Mundel, 2003b; Kwoh et al., 2006).

Damage to podocytes can lead to apoptosis and a reduction podocyte number. Importantly, podocytes are terminally differentiated cells with limited capacity to proliferation in response to damage (Fogo, 2003). The initial insult to podocytes triggers a cascade of events, including the release of cytokines, mechanical stress, further loss of polarity, and the eventual development of sclerotic scarring within the glomerulus. Together, these processes contribute to the pathogenesis of FSGS (Fogo, 2003; Kwoh et al., 2006).

On the basis of the pathogenesis of FSGS, the disease has been divided into three subtypes.

1.7.2.1 Primary FSGS

Primary (idiopathic) FSGS has been associated with the presence of circulatory permeability factors/cytokines that cause foot process effacement and proteinuria. These include corticotrophin-like cytokine factor 1, anti-CD40 Ab, apoA1b, and soluble urokinase plasminogen activator receptor (suPAR). Primary FSGS may respond to corticosteroids, immunomodulatory agents, plasmapheresis, or immunoadsorption and is prone to relapse after transplantation (Lim et al., 2016). Variants of primary FSGS include cellular and collapsing forms, FSGS with mesangial hypercellularity, and glomerular lesions (Stokes et al., 2006).

1.7.2.2 Secondary FSGS

In secondary forms of FSGS, most cases are maladaptive and result from a mismatch between glomerular load and glomerular capacity. Conditions associated with a reduced renal mass include low nephron endowment at birth; renal anomalies such as reflux nephropathy; hypoplastic kidney, which may be overwhelmed by an increase in total kidney glomerular filtration rate in conditions such as overweight, obesity, high protein intake, or androgen abuse; and acute kidney injury. Any chronic glomerular or tubular disease can reduce overall nephron function and result in maladaptive FSGS that is superimposed on the primary disorder (Shabaka et al., 2020). Other types of secondary FSGS include inflammation, toxins, intra-renal hemodynamic changes, viruses, and drug-associated FSGS, which are the initiators of podocyte injury and cause glomerulosclerosis (De Vriese et al., 2018).

1.7.2.3 Genetic FSGS

Over the past two decades, human genetic studies have revealed that FSGS is primarily a podocytopathy including more than 20 mutated genes that have been linked to the pathogenesis of FSGS (Schell & Huber, 2012). These mutated genes are mainly associated with the following categories:

a) SD-associated molecules: nephrin (Kestilä et al., 1998), podocin (Boute, 2000), CD2AP (J. H. Kim et al., 2003), and transient receptor potential cation channel 6 (TRPC6)(Winn et al., 2005).

b) Podocyte cytoskeleton-related molecules: α-actinin-4 (Michaud et al., 2006), inverted formin 2 (E. J. Brown et al., 2010; Subramanian et al., 2016) (INF2), and

anillin (ANLN) (Gbadegesin et al., 2014), ARHGDIA (Gee et al., 2013), and ARHGAP24 (Akilesh et al., 2011).

c) Mutations in podocyte transcription factors: LMX1B (H. Chen et al., 1998) and WT-1 (Pelletier et al., 1991) causing nail-patella syndrome (Hall et al., 2015; Kreidberg, 2010) and Denys-Drash/Frasier syndrome (Pelletier et al., 1991), respectively.

d) Mutations in adhesion and extracellular matrix molecules: integrins and laminin-β2 (LAMB2) (Matejas et al., 2010; Zenker et al., 2005).

Patients with genetic forms of FSGS have an autosomal dominant and autosomal recessive pattern of inheritance (Table 1). Based on exome sequencing studies, mutations in TRPC6 account for 62.8% of the cases in families with FSGS with likely causal rare variant genotypes (M. Wang et al., 2019).

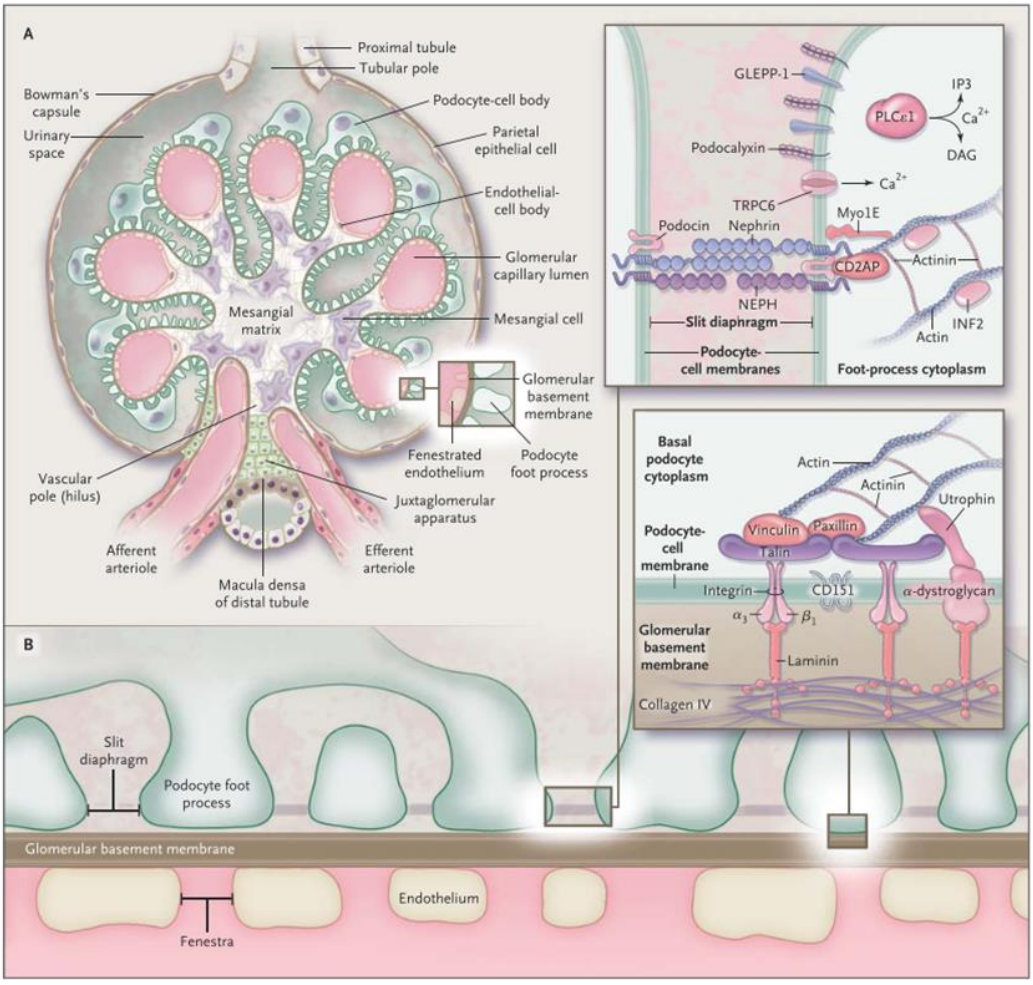

Figure 7: Normal glomerulus and glomerular filtration barrier. Adapted by (Agati et al., 2011)

1.7.3 The causative gene of FSGS: transient receptor potential cation channel 6 (TRPC6) as a determinant of podocyte injury

The causative gene underlying FSGS is the transient receptor potential cation channel (TRPC6), which belongs to the transient receptor potential (TRP) superfamily of cation-selective ion channels. TRP channel superfamily consists of TRPC (canonical), TRPV (vanilliod), TRPM (melastatin). TRPP (polycystin), TRPA (ankyrin), TRPML (mucolipin), and TRPN (no mechanoreceptor potential C, only ofund in invertebrates and zebrafish) subfamilies. (Venkatachalam & Montell, 2007) While TRP channels are normally permeable to both monovalent (Na^+, K^+, Cs^+) and divalent (Ca^{2+}, Mg^{2+}) cations, it is thought that TRP-dependent Ca^{2+} influx and subsequent $[Ca^{2+}]_i$ elevations are responsible for the majority of the physiological roles of TRP channels. All TRP channels are tetramers assembled around the central pore with each subunit containing six transmembrane domains and intracellular amino- and carboxyl-termini (Khayyat et al., 2020; Venkatachalam & Montell, 2007). The TRPC subfamily (TRPC1-7) comprises a group of calcium-permeable cation channels that play a significant role in increasing intracellular calcium ion (Ca2+) levels following the activation of G protein-coupled receptors (GPCRs) and receptor tyrosine kinases (Montell, 2005). TRPC channels could be further subdivided into TRPC1, TRPC3/6/7, and TRPC4/5 groups based on the sequence homology and the ability to form functional heteromers. These TRPC channels can assemble as homo- or heterotetramers and can interact with a variety of other proteins (Clapham, 2003). Expression of several TRPC channels, namely TRPC1, TRPC3, TRPC5, and TRPC6, has been reported in the renal tissue (Goel et al., 2006). Specifically, TRPC1 and TRPC3 are found in the proximal tubule and collecting duct, TRPC3, TRPC5, and TRPC6 are present in the podocytes of the glomerulus (Greka & Mundel, 2011).

TRPC6 was first identified in the mouse brain (Boulay et al., 1997), and later in the human placenta (Hofmann et al., 1999). This channel is widely expressed in numerous tissues, including different regions of the lung, brain, placenta, and kidney, and is found in many species (Dietrich & Gudermann, 2014). The human *TRPC6* gene is located on chromosome 11q21-q22 and consists of 13 exons encoding 931 amino acids. The TRPC6 channel is a tetramer consisting of an intracellular NH2 and COOH terminus facing the cytosol and six transmembrane domains (TM), of which TM 5 and 6 are

required for the pore formation of the ion channel (Figure 8). They show high functional variation in their selectivity for cation permeability (Montell, 2005; Montell et al., 2002). At the N-terminus there is a series of 4 ankyrin repeats and 9 linker helices, followed by a highly conserved 25-residue TRP domain, which is further attached to the C-terminus and comprises of a proline-rich domain called TRP box 2. The ankyrin repeats and TRP box 2 domains are responsible for protein interactions. C-terminal calmodulin and inositol 1,4,5-trisphosphate receptor binding region (CIRB region) bind to phosphoinositide (Kiselyov et al., 1999). These binding domains have been localized in both the N and C-terminus of the TRPC6 channel (M. X. Zhu, 2005).

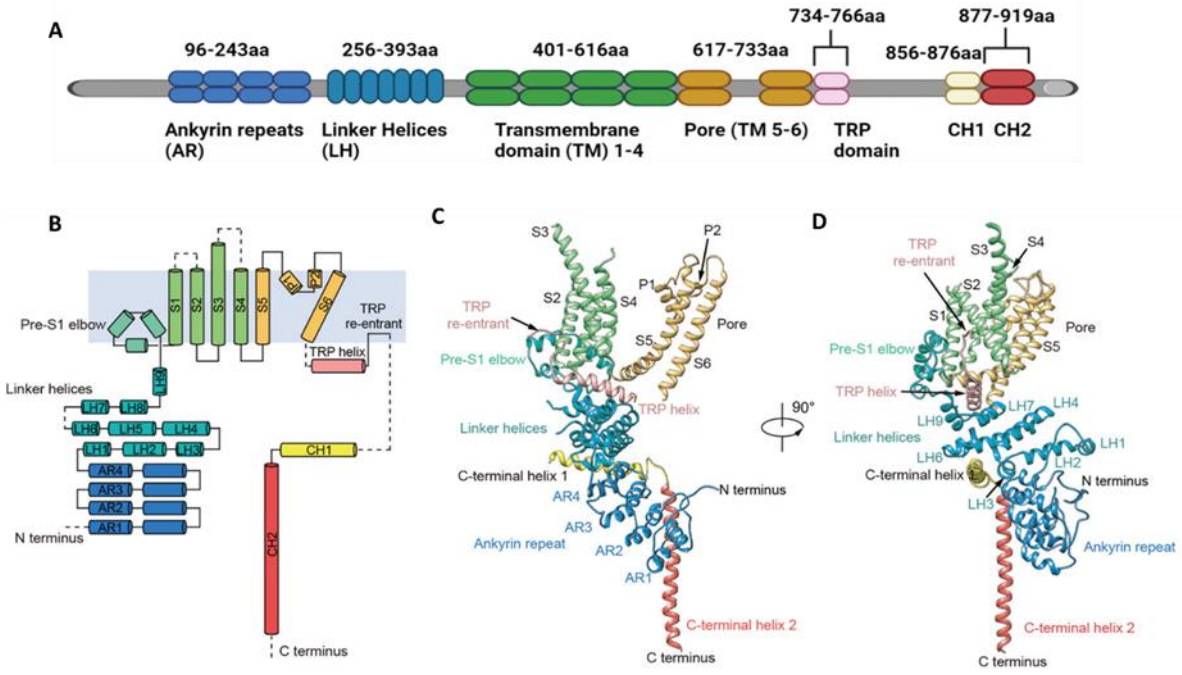

Figure 8: Tetrameric structural illustration of a single TRPC6 subunit. **(A)** Linear layout of TRPC6 domains. **(B)** Configuration of TRPC6 domain. Alpha helices are shown as cylinders. Dashes show flexible regions from model building. **(C, D)** Ribbon diagrams depict two perspectives of a single TRPC6 subunit using the same color scheme as shown in A and B. These diagrams provide a visual representation of the protein's three-dimensional structure, highlighting its various structural elements and their spatial relationships. (Adapted from Tang et al. 2018)

To date, TRPC3 (Eun et al., 2009), TRPC5 (Greka & Mundel, 2011; D. Tian et al., 2010), and TRPC6 (Hofstra et al., 2013; Ilatovskaya & Staruschenko, 2015; Krall et al., 2010; Reiser et al., 2005; Schlöndorff et al., 2009) channels have been functionally and pharmacologically implicated in calcium entry in podocytes. A functional TRPC6 tetramer is activated by the second messenger diacylglycerol (DAG), which is metabolized as a result of the hydrolysis of phosphatidylinositol 4,5-bisphosphate (PIP2) mediated by phospholipase C (PLC) upon stimulation of G protein-coupled receptors (Hofmann et al.,

1999) (Figure 9). Another function for TRPC6 as an important mediator of store-operated calcium entry (SOCE) is associated with TRPC1 (Redondo et al., 2008), type II IP3 receptors (Bréchard et al., 2008; Redondo et al., 2008), as well as with STIM and Orai1 (Bréchard et al., 2008; Jardin et al., 2020) to conduct SOCE in human platelets and the acute myeloid leukemia cell line HL-60. In addition, several natural and synthetic molecules have been characterized as activators or inhibitors of TRPC6. Among the activators, the DAG analog, 1-oleoyl-2-acetyl-sn-glycerol (OAG) has been used to study exclusive cation influx through TRPC6. Regarding TRPC6 blockers, TRPC6 channels are inhibited by ions such as lanthanum (La3+) or gadolinium (Gd3+), as in other TRP channels. Other known antagonists are SAR7334 (Maier et al., 2015), Sh045 (Zheng et al., 2022) and 2-aminoethoxydiphenyl borate (2- APB), or 1-[ß-(3-(4-methoxyphenyl) propoxy)-4-methoxyphenethyl]-1H-imidazole hydrochloride (SKF- 96365) (Dietrich & Gudermann, 2014).

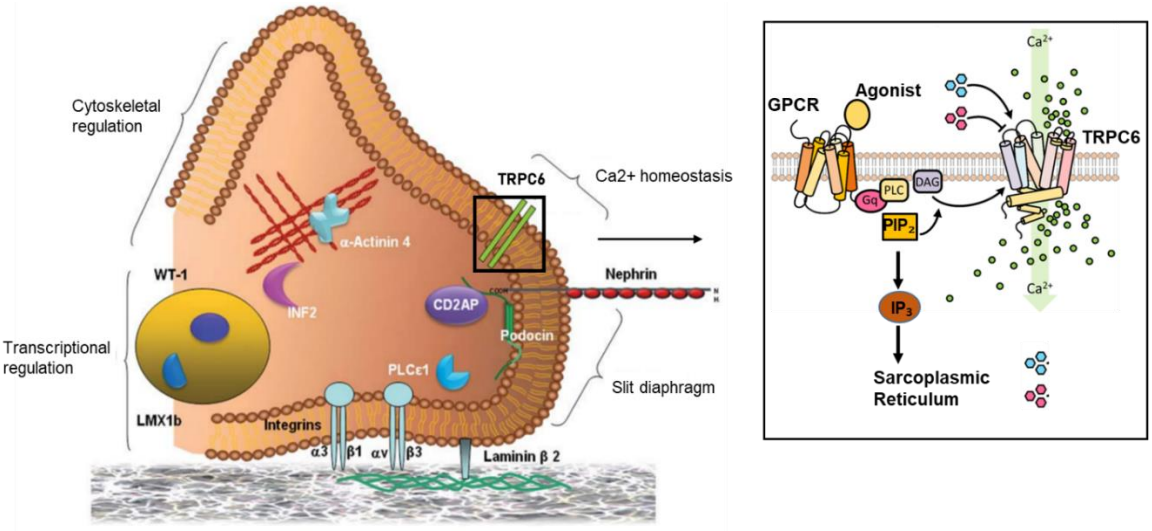

Figure 9: Overview of identified players in genetic forms of FSGS. **(Right)** Location of TRPC6 on the podocyte. **(Left)** Activation mechanism of TRPC6 channel upon G protein-coupled receptors stimulation. Adapted from (Christoph Schell et al., 2012 & Clapham et al., 2003)

A large body of data has emerged implicating TRPC6 as a key player in podocyte depletion (Ilatovskaya & Staruschenko, 2015). TRPC6 is widely expressed in renal tissues, including mesangial cells, endothelial cells, tubulointerstitial vascular and epithelial cells, and renal blood vessels (Englisch et al., 2022). Located on the podocyte membrane, TRPC6 is integrated into a signaling complex that interacts with podocin, nephrin, α-actinin-4, and a few other proteins critical for podocyte function (Huber et al., 2006; Möller et al., 2007; Reiser et al., 2005, 2006). One such example is a mutant of

podocin (P118L) which fails to activate TRPC6 channels and impairs the function of the slit diaphragm protein complex, exacerbating proteinuria, podocyte loss, and subsequently glomerulosclerosis (Ilatovskaya & Staruschenko, 2015). It has also been reported that podocin acts as a switch that determines the preferred mode of TRPC6 activation; podocin knockdown markedly increased stretch-evoked activation of TRPC6, but nearly abolished TRPC6 activation induced by a DAG analog (Anderson et al., 2013).

1.7.4 Mutations in the TRPC6 gene

Mutations in the TRPC6 gene follow an autosomal dominant pattern of inheritance (Hindi & Reiser, 2011). These mutations have been identified in families of diverse ethnic backgrounds and are responsible for a significant proportion of inherited cases of FSGS (Reiser et al., 2005; Winn et al., 2005). In a study conducted by Reiser et al. (2005), 71 families was examined with familial FSGS and found that five of them carried TRPC6 mutations, representing an approximate frequency of 7%. Interestingly, the age at which kidney disease manifested in these patients varied widely, ranging from 16 to 61 years. This raises the question of why kidney disease occurs later in life in some individuals with TRPC6 mutations. Several possible explanations include compensatory mechanisms involving other TRPC proteins, the gradual accumulation of subtle changes that eventually lead to irreversible changes in cell behavior, and the influence of additional renal insults over time (Hindi & Reiser, 2011). This situation is similar to the adult-onset and dominantly inherited form of FSGS caused by mutations in the widely expressed protein α-actinin-4 (Kaplan et al., 2000).

Most of the identified *TRPC6* mutations identified are missense mutations (Büscher et al., 2012; Gigante et al., 2011; Heeringa, Ller, et al., 2009; Hofstra et al., 2013; Joshi et al., 2015; Mir et al., 2012; Obeidová et al., 2012; Ogino et al., 2016; Reiser et al., 2005; Riehle et al., 2016; Santín et al., 2009; Winn et al., 2005; Zhang et al., 2013), which, based on functional studies, are categorized as gain-of-function (GOF; R68W, G109S, N110H, P112Q, M132T, Q134P, N143S, R175Q, H218L, S270T, A404V, Q889K, R895C, and E897K) or loss-of-function (LOF; N125S, L395A, G757D, L780P, and R985L) mutants (Table 2). Notably, both GOF and LOF mutations in the TRPC6 channel are thought to cause the FSGS phenotype (Mottl et al., 2013; Riehle et al., 2016). The mutations are mapped to the terminal domains of the TRPC6 protein. Ten N-terminal missense mutations (G109S, N110H, P112Q, M132T, N125S, N143S, R175Q, H218L,

S270T, and A404V) located in or near ankyrin repeats and an adjacent lipid/trafficking domain result in a hyperactive channel. The ankyrin domains are responsible for the self-association of TRPC homomers (Lepage et al., 2009), whereas the lipid-binding domain binds DAG and is involved in the translocation of the channel to the plasma membrane (Van Rossum et al., 2008). Most of the GOF mutations of the TRPC6 are located in the intracellular cytosolic domain architecture of TRPC6 (Guo et al., 2022). The L780P mutation is located near the EWKFAR motif, a highly conserved proline-rich motif, while four other mutations (K874X, Q889K, R895C, and E897K) map to a predicted coiled-coil domain at the C-terminus (Dietrich et al., 2010). One mutation (G757D), located in the TRP domain next to the L780P mutation, hampers a compact structure of the tetrameric channel, affecting overall activity, which is in line with TRPC6 G757D being a dominant negative mutant resulting in decreased calcium influx in podocytes. (Batool et al., 2023)

1.7.5 Animal models to study FSGS

Animal models recapitulating autosomal dominant forms of FSGS have not been reported because they do not induce glomerular pathology. Transgenic overexpression of either wild-type or mutant *TRPC6* (P111Q and E896K GOF) in podocytes causes only modest albuminuria and mild histological changes with incomplete penetrance in mice (Krall et al., 2010). Human disease-causing mutations in *TRPC6* (B. J. Brown et al., 2022), *ACTN4* (Yao et al., 2004), and *INF2* (Subramanian et al., 2016) are unable to induce a renal phenotype when present in heterozygous mice. Although homozygous *Actn4* or *Inf*2 mutant mice show increased sensitivity to damage (H. Sun et al., 2021; Yao et al., 2004), this is not observed in homozygous mutant TRPC6 (E896K GOF) mice which show no susceptibility to puromycin aminonucleoside nephrosis (B. J. Brown et al., 2022). The reason for the lack of a renal phenotype in the TRPC6 knock-in/out animals remains unclear. Reports of differences in TRPC6 mRNA expression between mouse strains (Kunert-Keil et al., 2006) and strain-specific susceptibility to kidney and glomerular injury are well known. Uncertainty exists as to whether TRPC6 mutations require a genetic or environmental trigger to induce glomerular disease in mice, or whether mice are inherently unsuitable for modeling TRPC6-mediated human FSGS.

1.7.6 Cellular models to study FSGS

Winn et al. (2005) identified the first TRPC6 mutation (P112Q), located at the N-terminal intracellular tail, in a large family from New Zealand. To determine the effect of

the P112Q mutation on TRPC6 function, they performed experiments in human embryonic kidney 293 (HEK 293) cells, transfected with mutant (TRPC6 P112Q) or wild-type (WT) TRPC6. HEK 293 cells bear little or no resemblance to those of mature renal cell lineages. Therefore, the lack of TRPC6 expression in HEK cells is likely to have little effect on whether the protein is expressed in mature kidney tissue (Winn et al., 2005). Similarly, several other groups have reported mutations in TRPC6 as mentioned in the above section, and performed their experiments in HEK or HeLa cells.

Since the advent of hiPSC generation in 2006, their potential applications in disease modeling, drug discovery research, and regenerative medicine have been based on their remarkable ability to self-renew and differentiate into all cell types. What makes hiPSCs particularly valuable is their ability to be derived from individuals while preserving their unique genetic makeup, allowing for the study of diseases in patients with sporadic forms or those with complex conditions of unknown genetic origin, such as type 1 diabetes (Maehr et al., 2009) and liver cancer (Bekker, 2021). hiPSCs can be generated from a patient's somatic cells, including fibroblasts, blood cells, or urinary cells (Loh et al., 2009; Takahashi et al., 2007; T. Zhou et al., 2012). There are a number of established strategies to introduce reprogramming factors (Yamanaka factors; Oct4, Sox2, c-Myc, and Klf4) into somatic cells by integrative viral (retrovirus (Varas et al., 2009) and lentiviral (Sommer et al., 2009)) or non-viral (plasmid with transposons like Piggybac (Woltjen et al., 2009)) or by non-integrative viral (adenovirus (W. Zhou & Freed, 2009)) and Sendai viral (Rossbach et al., 2016)) or non-viral (episomal vectors (Mulder et al., 2020)) transfer systems. However, to date, no such experiments have been performed/reported using hiPSCs to study the pathophysiology of FSGS *in vitro.*

1.7.7 Conditional modulation of kidney progenitor cell fate

As our understanding of cell phenotypes and differentiation has advanced, the potential for manipulating cells to create personalized cell products for regenerative medicine has grown significantly. In this context, various gene delivery strategies have been explored to achieve uniform expression of transgenes. One such strategy is the use of the tetracycline-controlled transcriptional activation system, often referred to as the Tet system. The Tet system is a molecular tool that allows precise control of gene expression in cells. It can be used to regulate key signaling pathways involved in cell differentiation and function. By using the Tet system, researchers can ensure that specific genes are

turned on or off in a controlled manner, enabling a more accurate and functional assessment of the engineered cells for their intended therapeutic applications in regenerative medicine.

Due to their low transfection efficiency and promoter-dependent suppression of differentiation, hiPSCs are one of the most difficult cell types to genetically modulate and alter. A systematic effort has been reported to optimize gene expression in human PSCs by targeting all components of the Tet-ON system required for the inducible expression of transcription factors at genomic safe harbor sites (GSHs) (Sadelain et al., 2012). The system is based on a dual vector Tet system that targets each of the two elements of the Tet-On system to the different GSH sites, i.e., AAVSI and ROSA26 (Pawlowski et al., 2017a). It overcomes the limitations of viral-mediated transgene delivery and promotes homogenous transgene expression compared to targeting strategies that result in mosaic expression patterns over time. In addition, this platform has been used to program various cell types such as neurons, myocytes, and oligodendrocytes (Pawlowski et al., 2017a). In this thesis, this innovative gene delivery approach was tested to deliver the TRPC6 gene to modulate cell fate in hiPSC-derived podocytes.

1.8 Aim

The ultimate aim of this project was to understand the causative relationship between TRPC6 mutations and FSGS-related changes in podocytes. Specifically, it was to be determined whether gain- and loss-of-function mutations in TRPC6 (increased or decreased intracellular Calcium levels) cause both FSGS and podocyte damage. It is viewed that sustained hyperactivation of TRPC6 channels results in Calcium overload leading to foot process effacement and ultimately podocyte loss. The decrease in podocyte population is further exacerbated due to their limited capacity for regeneration. It was also noted that the magnitude of TRPC6 potentiation correlates with the severity of disease progression. In addition the immediate closure of the TRPC6 channel results in podocyte hypertrophy and foot process effacement, leading to the same phenotype that is podocyte loss and thereby contributing to the development of FSGS. The prevailing hypothesis that calcium imbalance in either direction is causative is controversial, and I have provided tools to help resolving this dispute with the obtained data. These tools include the generation of a set of cell lines with regulatable expression of gain- and loss-of-function TRPC6 mutant protein and/or wild-type protein to study their relative effects on intracellular calcium level. The next step was to generate hiPSC lines with regulatable expression of TRPC6 mutants and hiPSC line from a patient with characterized gain- and loss-of-function TRPC6 mutations. Further, iPSC-derived podocytes carrying TRPC6 mutations were functionally and morphologically characterized to study intracellular Calcium imbalance. Lastly, a novel microfluidics-based model of the podocyte basal membrane was tested for proof-of-concept studies on the podocyte damage and repair.

This study aimed to solve a specific problem in the role of intracellular Calcium imbalance on the pathology of podocytes, and FSGS expressively.

Table 1: FSGS genes

Gene	Protein	Gene locus	Inheritance	Phenotype
Slit diaphragm protein				
TRPC6	TRPC6	11q22.	Autosomal Dominant	Adult/ childhood FSGS
NPHS1	Nephrin	19q13.1	Autosomal Recessive	CNS, SRNS, childhood FSGS
NPHS2	Podocin	1q25	Autosomal Recessive	CNS, SRNS, FSGS
CD2AP	CD2 associated protein	6p12	Autosomal Recessive/Domi-nant	Childhood and adult FSGS
CRB2	Crumbs family member 2	9q33	Autosomal Recessive	SRNS, childhood FSGS
MAGI2	Membrane-associated guanylate kinase	7q21	Autosomal Recessive	CNS
Actin cytoskeleton protein				
INF2	Inverted formin 2	14q32.33	Autosomal Dominant	Adult onset FSGS, Charcot–Marie–Tooth disease E
MYO1E	Myosin 1E	15q22.2	Autosomal Recessive	Early onset FSGS
ACTN4	Alpha-actinin 4	19q13.1	Autosomal Dominant	Adult onset FSGS
ARHGDIA	Arhgdia	17q25.3	Autosomal Recessive	CNS, SRNS
ARHGAP2	Rho GTPase-activating protein 24	4q21	Autosomal Dominant	Adolescent onset FSGS
ANLN	Anillin	7p14	Autosomal Dominant	Childhood/ adult FSGS
PLEC1	Phospholipase C epsilon 1	10q23.33	Autosomal Recessive	childhood FSGS
Nuclear protein				
PAX2	Paired box 2 nuclear	10q24	Autosomal Dominant	FSGS

Gene	Protein	Gene locus	Inheritance	Phenotype
	transcription factor			
WT1	Wilms tumor protein 1	11p13	Autosomal Dominant	FSGS
Glomerular basement membrane				
LMX1B	LIM homeobox nuclear transcription factor 1B	9q31.1	Autosomal Dominant	Isolated FSGS
LAMB2	Laminin subunit beta 2	3p21	Autosomal Recessive	CNS
COL4A3/4/5	α3/4/5 type 4 collagen	2q36-37/ 2q35-37/ Xq22	Autosomal Recessive/Dominant/X linked	Alport syndrome, isolated FSGS
High-risk FSGS				
APOL1	Apolipoprotein L1	22q12.3	Autosomal Dominant	FSGS, collapsing FSGS
Non-glomerular causes				
UMOD	Uromodulin	16p12	Autosomal Dominant	ADTKD, FSGS
CLCN5	Chloride channel 5	Xp11	X linked	Dent disease, FSGS
CC2D2A	Coiled-coil and C2 domains-containing protein 2A	4p15	Autosomal Recessive	Nephronophthisis, FSGS
MYH9	Nonmuscle myosin heavy chain IIA	22q12	Autosomal Dominant	Macrothrombocytopenia, deafness, SRNS, FSGS
OCRL	Inositol polyphosphate 5-phosphatase	Xq26	X linked	Dent disease, Lowe syndrome, FSGS

Table 2: Mutations identified in the *TRPC6* gene

***TRPC6* mutation**	**Published time**	**Effect on ion channel function**	**Ethnicity**	**Phenotype**	**References**
P112Q	2005	Increased current amplitude	Caucasian	AD FSGS	(Winn et al., 2005)
N143S	2005	Not evaluated	African American	AD FSGS	(Reiser et al., 2005)
	2009	Increased current amplitude	Caucasian	AD FSGS	(Heeringa, Möller, et al., 2009)
S270T	2005	Increase intracellular calcium	Colombian	AD FSGS	(Reiser et al., 2005)
K874X	2005	Not evaluated	Polish	AD FSGS	(Reiser et al., 2005)
R895C	2005	Increased current amplitude	Mexican	AD FSGS	(Reiser et al., 2005)
	2011	Not evaluated	Caucasian	AD collapsing FSGS	(Liakopoulos et al., 2011)
	2017	Not evaluated	Caucasian	AD FSGS	(Sayer & Iqbal, 2017)
	2017	Not evaluated	Caucasian	AD FSGS	(Tan et al., 2018)
	2020	Not evaluated	Japanese	C1q nephropathy	(Nagano et al., 2020)
E897K	2005	Increased current amplitude	Irish and German	AD FSGS	(Reiser et al., 2005)
Q889K	2008	Increased current amplitude	Chinese	AD FSGS	(B. Zhu et al., 2009)
M132T	2009	Increased current amplitude	Caucasian	AD FSGS	(Heeringa, Möller, et al., 2009)
G109S	2009	Probably damaging	Caucasian	FSGS	(Santín et al., 2009)

***TRPC6* mutation**	**Published time**	**Effect on ion channel function**	**Ethnicity**	**Phenotype**	**References**
N125S	2009	Probably damaging	Caucasian	Sporadic FSGS	(Santín et al., 2009)
	2011	Decreased intracellular calcium	Caucasian	MCD	(Gigante et al., 2011)
	2011	Decreased intracellular calcium	Caucasian	IgAN with MPGN-like pattern	(Gigante et al., 2011)
L780P	2009	Possibly damaging	Caucasian	Sporadic FSGS	(Santín et al., 2009)
89fsX8	2010	Not evaluated	Caucasian	FAGA	(Sadowski et al., 2015)
G757D	2010	Decreased current amplitude	Caucasian	FSGS	(Riehle et al., 2016)
L395A	2011	Decreased current amplitude	Turkish	Sporadic FSGS	(Mir et al., 2012)
R360H	2011	Not evaluated	Caucasian	FSGS	(Büscher et al., 2012)
H218L	2011	Increase intracellular calcium	Caucasian	Sporadic FSGS	(Gigante et al., 2011)
R895L	2011	Increase intracellular calcium	Caucasian	Sporadic collapsing FSGS	(Gigante et al., 2011)
D873fsX878	2013	Not evaluated	Korean	MCD	(Mottl et al., 2013)
R175W	2014	Not evaluated	Dutch	AD FSGS	(Hofstra et al., 2013)
A404V	2014	Increase intracellular calcium	Caucasian	MN	(Hofstra et al., 2014)
P15S	2014	Not evaluated	Caucasian	MN	(Hofstra et al., 2014)
R68W	2015	Increase intracellular calcium	Singaporean	FSGS	(Z. J. Sun et al., 2015)

***TRPC6* mutation**	**Published time**	**Effect on ion channel function**	**Ethnicity**	**Phenotype**	**References**
R175W	2017	Not evaluated	Chinese	FSGS	(F. Wang et al., 2017)
D130V	2018	Not evaluated	Iranian	FSGS	(Gheissari et al., 2018)
G162R	2018	Not evaluated	Iranian	FSGS	(Gheissari et al., 2018)
	2020	Not evaluated	Japanese	AD FSGS	(Nagano et al., 2020)
G109D	2020	Increase intracellular calcium	Japanese	MGA	(Nagano et al., 2020)
G875V	2020	Not evaluated	Japanese	AD FSGS	(Nagano et al., 2020)
H145R	2020	Not evaluated	Japanese	FSGS	(Nagano et al., 2020)

2 MATERIALS

Table 3: List of reagents

Buffers for Immunocytochemistry staining	**Manufacturer/Supplier**
BD Perm/Wash™	BD Biosciences, Franklin Lakes (USA)
BD Cytofix™	Biochrom AG, Berlin (Germany
Donkey Serum	Sigma Aldrich, St. Gallen (Switzerland)
Reagents	**Manufacturer/Supplier**
PBS (Dulbecco's Phosphate Buffered Saline) with or without Mg2+/Ca2+	Gibco®, Life Technologies GmbH, Darmstadt (Germany)
4', 6-diamidino-2-phenylindole (DAPI)	Life Tecnologies GmbH, Darmstadt (Germany)
Glutamax	Gibco®, Life Technologies GmbH, Darmstadt (Germany)
HEPES Buffer	Lonza (Switzerland)
Dimethyl sulfoxide (DMSO)	Sigma Aldrich, St. Gallen (Switzerland)
Agarose Standard	Life Tecnologies GmbH, Darmstadt (Germany)
HyperLadder™ 1kb	Bioline ©
Doxycycline monohydrate, 97%	Acros OrganicsTM, Thermo Fischer Scientific Inc
Ethanol	Carl Roth GmbH + Co. KG
Ethidium Bromide solution	Invitrogen, Thermo Fischer Scientific Inc.
Gel Loading Dye, Purple (6X)	New England Biolabs, Inc
Gel Red	Biotium, Inc. (USA)
ENZYMES	**Manufacturer/Supplier**

StemPro® Accutase®	Gibco®, Life Technologies GmbH, Darmstadt (Germany)
Trypsin/EDTA, 0.05 %/0.02 %	Biochrom AG, Berlin (Germany)
TrypLE™ Select Enzyme (1X)	Thermo Fisher Scientific, Dreieich (Germany)
KpnI-HF ® restriction enzyme	New England Biolabs, Inc.
BsrGI-HF® restriction enzyme	New England Biolabs, Inc.
EcoRI-HF® restriction enzyme	New England Biolabs, Inc
CULTURE DISHES	**Manufacturer/Supplier**
BD Falcon™ 96-well Multiwell Plate, flat bottom	BD Biosciences, Heidelberg (Germany)
BD Falcon™ 24-well Multiwell Plate	BD Biosciences, Heidelberg (Germany)
BD Falcon™ 12-well Multiwell Plate	BD Biosciences, Heidelberg (Germany)
BD Falcon™ 6-well Multiwell Plate	BD Biosciences, Heidelberg (Germany)
Falcon tubes	BD Biosciences, Heidelberg (Germany)
CellCarrier® 96-well Multiwell Plate	Perkin Elmer, Waltham (USA)
AggreWell™ 800 Microwell plates	Stemcell Technologies (Germany)
MEDIA	**Manufacturer/Supplier**
mTeSR™-1	StemCell™ Technologies, Grenoble (France)
Essential 8™ medium	Gibco™, Thermo Fischer Scientific Inc. Darmstadt (Germany)
DMEM, high glucose, GlutaMAX™ Supplement	Gibco™, Thermo Fischer Scientific Inc. Darmstadt (Germany)
Knockout™ DMEM/F-12 (1X)	Gibco™, Thermo Fischer Scientific Inc. Darmstadt (Germany)
REBM (Basal medium+ Bullet kit)	Lonza (Switzerland)

StemDiff APEL	StemCell™ Technologies, Grenoble (France)
OptiMEM	Life Technologies GmbH, Darmstadt (Germany)
RPMI 1640 Medium, GlutaMAX™	Gibco™, Thermo Fischer Scientific Inc. Darmstadt (Germany)
DMEM/F12	Gibco®, Life Technologies GmbH, Darmstadt (Germany)
LB medium	Carl Roth GmbH + Co. KG
LB agar	Carl Roth GmbH + Co. KG
BambankerTM serum-free freezing	Nippongenetics, Düren, (Germany)

SUPPLEMENTS	**Manufacturer/Supplier**
B-27 minus Insulin (50x)	Gibco®, Life Technologies GmbH, Darmstadt (Germany)
B-27 supplement without vitamin A (50x)	Gibco®, Life Technologies GmbH, Darmstadt (Germany)
Fetal calf serum	Biochrom AG, Berlin (Germany)
CHIR99021	Sigma-Aldrich, Merck KGaA
IWR-2	Invitrogen,
β -2-Mercaptoethanol	Invitrogen™, Life Technologies GmbH, Darmstadt (Germany)
Glutamax	Invitrogen™, Life Technologies GmbH, Darmstadt (Germany)
Insulin-Transferrin-Selenium	Sigma Aldrich, St. Gallen (Switzerland)
Pen Strep 10000 Units/ml	Gibco®, Life Technologies GmbH, Darmstadt (Germany)

ActivinA	PeproTech, Hamburg (Germany)
rhBMP4	PeproTech, Hamburg (Germany)
rh GDNF	PeproTech, Hamburg (Germany)
rhHGF	PeproTech, Hamburg (Germany)
rhbFGF/FGF2	PeproTech, Hamburg (Germany)
Retinoic Acid	Stemgent (USA)
Y27632-ROCK inhibitor	Wako Chemicals Inc. (USA)
Puromycin	InvivoGen ©
Blasticidin	InvivoGen ©
MEM non-essential amino acids	Gibco®, Life Technologies GmbH, Darmstadt (Germany)
One Shot™ TOP10F´ Chemically Competent *E. coli*	Thermo Fischer Scientific Inc. Darmstadt (Germany)

KITS	**Manufacturer/Supplier**
Rneasy®Micro/Mini Kit (Qiagen) CrimsonTaqTMMasterMixKit	Qiagen®, Hilden (Germany)
DNA extraction kit	Thermo Fischer Scientific Inc. Darmstadt (Germany)
SYBR® Green-ROX, PCR Master Mix	Applied Biosystems®, Life Technologies GmbH, Darmstadt (Germany)
Lipofectamine™ 2000 Transfection Reagent	Invitrogen, Thermo Fischer Scientific Inc Darmstadt (Germany)
Lipofectamine™ 3000 Transfection Reagent	Invitrogen, Thermo Fischer Scientific Inc Darmstadt (Germany
Q5® High-Fidelity 2X Master Mix	New England Biolabs, Inc.
NucleoSpin™ Gel and PCR Clean-up Kit	Macherey-Nagel GmbH & Co. KG Darmstadt (Germany)

NucleoBond™ Xtra Midi Plus	Macherey-Nagel GmbH & Co. KG Darmstadt (Germany)
NucleoSpin Tissue, a Mini kit for DNA from cells and tissue	Macherey-Nagel GmbH & Co. KG Darmstadt (Germany)
LIVE/DEAD™ Fixable Aqua Dead Cell Stain Kit, for 405 nm excitation	Invitrogen, Thermo Fischer Scientific Inc Darmstadt (Germany)

SOFTWARE	**Manufacturer/Supplier**
Columbus Image Data System	Perkin Elmer, Waltham (USA)
FlowJo Version 8.8.2	Tree Star, Inc., Ashland (USA)
GraphPad Prism	GraphPad Software, California (USA)

Table 4: List of antibodies used for immunofluorescence and flow cytometry

Name	Species	Description	Company	Cat. Nr
PODXL	Mouse monoclonal	Podocyte membrane	R&D System	MAB1658
SYNPO	Mouse monoclonal	Podocyte-actin binding protein	Progen	69254
WT1	Rabbit polyclonal	metanephric mesoderm	Santa Cruz	Sc-393498
NPHS2	Rabbit polyclonal	Podocyte membrane	Abcam	ab50339
SIX2	Mouse monoclonal	Embryonic cap mesenchyme	Abnova (tebubio)	H00010736-M01
PAX2	Rabbit polyclonal	Intermediate mesoderm	Invitrogen	71-6000
HOXB7	Mouse monoclonal		R&D System	MAB8040
AQP1	Rabbit polyclonal	Proximal tubule	Proteintech	20333-1-AP
Na+/+K ATPase	Rabbit Polyclonal	Proximal tubule	Abcam	ab76020
SGLT2	Mouse monoclonal	Proximal tubule	Abcam	ab58298
OCT4	Rabbit polyclonal	Pluripotency	Cellsignaling Technology	2840S
LIM1	Mouse monoclonal	Intermediate mesoderm	Novus Biologicals	NBP2-01926
Brachyury (T)	Rabbit polyclonal	Definitive mesoderm	Santa Cruz	SC-20109
JAG	Rabbit polyclonal	Medial Renal Vesicle	Abcam	Ab7771
FOXD1	Rabbit polyclonal	Metanephric mesenchyme	Thermo Fisher Scientific	PA5-35145
cTNT	Mouse monoclonal	Cardiomyocyte	Abcam	Ab8295

Table 5: List of sequence variants for each TRPC6 mutant and primer sequence for XLone plasmid

Plasmid	**Sequence variant 5' → 3'**
TRPC6-WT-YFP	Sequence from (Addgene#21084)
TRPC6-P112Q-YFP	CTTTTTGGATGCAGCTGAATATGGTAATATTC AAGTGGTGCGGAAGATGTTAGAAGA
TRPC6-G757D-YFP	TCTGGTTTTCCTACTTTGAGGAGGACAGAACA CTTCCTGTACCCTTCAATCT
TRPC6-V691KFS*	TTCTGGGCTATATTTGGACTTTCTGAAGTGAA ATCAAAGGTGA
Sequencing	
Primer name	**Sequence 5' → 3'**
TRPC6_P112Q_seq_fwd	TGATCGCTCCACAAGCCTATC
TRPC6_G757D_seq_fwd	CTACTCCTACTACATTGGTGC
M13-rev	CCCAGTCACGACGTTGTAAAACG
TRPC6_seq_rv	CTGCCAACTGTAGGGCATTCT

Table 6: List of primer sequences used for pUC-AAVS1-TRPC6 vector

Primer name	**Sequence 5‘→3‘**
Cloning	
TRPC6-SpeI-fw	CGCCACTAGTATGAGCCAGAGCCCGGC
TRPC6-EcoRI-rv	TCACGAATTCTCTATTGGTTTCCTCT
eGFP-EcoRI-fw	CACCGAATTCGTGAGCAAGGGCGAGGA
eGFP-KpnI-rv	ATTCGGTACCTACTTGTACAGCTCGTCCATGC
Sequencing	
TRPC6-WT-seq-fwd	GTGATCGCTCCACAAGCCTAT
TRPC6-112-seq-fwd	TGATCGCTCCACAAGCCTATC
TRPC6-757-seq-fwd	CTACTCCTACTACATTGGTGC
SV40-pA-R-156-175-seq	GAAATTTGTGATGCTATTGC
PUC-M13-F-seq	CCCAGTCACGACGTTGTAAAACG
PUC-M13-R-seq	AGCGGATAACAATTTCACACAGG
Genotyping	
Primer binding sire	**Sequence 5‘→3‘**
hAAVSI-genome (5’)	CTGTTTCCCCTTCCCAGGCAGGTCC
hAAVSI-genome (3’)	TGCAGGGGAACGGGGCTCAGTCTGA
hAAVSI-genome (5’)	CTGTTTCCCCTTCCCAGGCAGGTCC
Puro-N-ter Rv	TCGTCGCGGGTGGCGAGGCGCACCG
TRPC6-GFP-C terminal	GTGATCGCTCCACAAGCCTAT
hAAVSI-genome (3’)	TGCAGGGGAACGGGGCTCAGTCTGA
TRPC6-GFP-C terminal	GTGATCGCTCCACAAGCCTAT
pUC-AAVS1- vector BB (3')	ATGCTTCCGGCTCGTATGTT

Table 7: List of plasmids

Plasmid name	Origin	Description/experiment
htrpC6-YFP	Addgene. #21084	pcDNA3.1 vector with TRPC6 (wild-type or mutant)-YFP
XLone-GFP	Addgene. #96930	pUC57/All-in-one-Tet(Tet-on3G) inducible PiggyBac system
pPB transposase	Gossen' lab stock	PiggyBac transposase/HeLa-HEK293 Tet-on 3G
pAAV_TRE-TRPC6-EGFP	Modified from Pawlowski et al. 2017b	Tet-On TRPC6 unit flanked with AAVS1 locus homology arms/ hiPSC conditional differentiation
pZFN-AAVS1-L-ELD	(Pawlowski et al., 2017b)	AAVS1 locus ZFN left/ hiPSC conditional differentiation
pZFN-AAVS1-R_KKR	(Pawlowski et al., 2017b)	AAVS1 locus ZFN right/ hiPSC conditional differentiation
ROSA26-guideA_Cas9n	(Pawlowski et al., 2017b)	Cas9 nuclease guide A/ rtTA3 rescue in ROSA 26
ROSA26-guideB_Cas9n	(Pawlowski et al., 2017b)	Cas9 nuclease guide A/ rtTA3 rescue in ROSA 26

Table 8: List of pluripotency markers

Markers	Target	Size of band	Forward/Reverse primer (5′-3′)
Trilineage markers	Brachury (T)	2360bp	AATTGGTCCAGCCTTGGA/ CGTTGCTCACAGACCACA
	MIXL1	67bp	CTGTTCCCCTCTCTCTGAAGA/ GGCAGAAAAGATGTGTTCCTCC
	GSC	89bp	AACGCGGAGAAGTGGAACAAG/ CTGTCCGAGTCCAAATCGC
	SOX17	94bp	GTGGACCGCACGGAATTTG/ GGAGATTCACACCGGAGTCA
	NEUROD1	2081bp	GCCCCAGGGTTATGAGACTATCACT/
	Nestin	1807bp	CCGACAGAGCCCAGATGTAGTTCTT
Stem cell marker	NANOG	237bp	GGCGCACCTCAAGATGTC/ CCTGAAAGCTGAGGGAAGTC AAGGTCCCGGTCAAGAAACAG/ CTTCTGCGTCACACCATTGC
House-Keeping Genes (qPCR)	GAPDH	393bp	TTGCCATCAATGACCCCTTCA/ CGCCCCACTTGATTTTGGA

3 METHODS

3.1 Cell culture and maintenance

3.1.1 HeLa and HEK cells 293

HeLa and HEK 293 cells were grown in dulbecco's modified eagle Mmedium glutaMAX™ (DMEM) supplemented with 10% fetal calf serum (FCS), and 100 U/mL penicillin-streptomycin (P/S) in the presence of 5% CO_2 at 37°C. Medium was changed every alternate day and cells were typically passaged with TrypLE Select once or twice a week at a ratio of 1:10.

3.1.2 hiPSC

For hiPSCs culture, two different media were used: WISCi004-A was cultured in Essential 8™ medium (E8 medium) and CAMi014-A was cultured in mTeSR-1 medium on Geltrex-coated plates. Cultures were fed daily. Cells were passaged with 0.5 mM ethylene-diamine-tetraacetic acid (EDTA) every 4-6 days. Briefly, cells were washed once and incubated with 0.5 mM EDTA solution for 5 min at 37°C. The dissociation reagent was then removed, and the cell clumps were resuspended and mechanically disrupted with a culture medium. The resulting cell clumps were plated at a ratio of 1:6, 1:10, or 1:20, depending on the number of cells required for an experiment.

For certain experiments, such as podocyte and cardiomyocyte differentiation or flow cytometry analysis, hiPSCs were preferentially seeded as single cells for seeding quantification. For this procedure, the enzyme Accutase® was added to the cells and incubated at 37°C for 5 min. Accutase® was neutralized with twice the volume of the medium and the cell suspension was centrifuged at 300xg for 5 min. The resulting pellet was resuspended in a medium containing 10 µM ROCK inhibitor. Cells seeded at specific densities were maintained in ROCK inhibitor for 24 h to prevent cell death and assist in cell attachment.

3.1.3 Cryopreservation of cells

The procedure for freezing HeLa and HEK293 is identified as that of the passaging of these cells until the final step of resuspension. Briefly, the cells were incubated with TrypLE express, neutralized, and the resulting pellet was resuspended in a homemade freezing medium (10% DMSO and 50% FBS). To be more precise, $1x10^6$ cells were

resuspended in 400 µl culture medium, and for further cryopreservation, the cells were transferred to pre-cooled cryovials containing 500 µl FBS and 100 µl DMSO.

For freezing hiPSCs, the procedure is identical until the final step of resuspending the cell clumps. Briefly, after incubation with 0.5mM EDTA, the dissociation medium was removed, and the cell clumps were resuspended in 1ml cold bambanker^{TM} freezing medium and transferred to a cryovial.

All cryovials were transferred to a freezing container for overnight storage at -80°Cand transferred to liquid nitrogen the following day for long-term storage.

3.1.4 List of hiPSCs utilized

Table 9: List of iPS cell lines

Cell line	SOURCE	Vector	Factors	Reference
WISCi004-A (IMR90-4	Lung fibroblast (female)	Lentivirus	OCT4, SOX2,NANOG, LIN28	Yu Junying et al. 2007
CAMi014-A	Arm fibroblast (male)	Sendai Virus	OCT4, SOX3, KLF4, CMYC	Rashid ST et al., 2010
BCRTi006-A	Urinary cells	Episomal	OCT4, SOX2, KLF4, L-MYC, LIN28	Batool et al., 2023
BCRTi007-A	Urinary cells	Episomal	OCT4, SOX2, KLF4, L-MYC, LIN28	Batool et al., 2023
BCRTi010-A	PBMCs	Episomal	OCT4, SOX2, KLF4, L-MYC, LIN28	Batool et al., 2023
BCRTi011-A	PBMCs	Episomal	OCT4, SOX2, KLF4, L-MYC, LIN28	Batool et al., 2023

3.2 Stem cell differentiation

3.2.1 Media

The basal medium used for the differentiation of hiPSCs during the experiment was a xeno-free, serum-free defined APEL medium.

3.2.2 Extracellular matrices

Tissue culture multiwell plates used for iPS cultivation were pre-coated with geltrex™ matrix 1:10 in knockout DMEM for 2 h at room temperature (RT), 30 min in an incubator, or overnight 4°C. Another matrix used for podocyte differentiation was rhLaminin521 (10µg/ml) dissolved in PBS containing calcium and magnesium.

3.2.3 Growth factors

Table 10: List of growth factors

CATEGORY	SYMBOL	GROWTH FACTOR	CONCENTRATION USED	VOLUME FOR 10ML APEL
Mesoderm factors	A	Activin A (2ng/µl Stock)	10ng/ml	50µl
	B4	BMP4 (2ng/µl Stock)	30ng/ml	150µl
	RA	Retanoic acid	1µM	1µl
Nephrogenesis factors	G	GDNF (5ng/µl)	150ng/ml	300µl
Podocyte factor	H	HGF (10ng/µl)	50ng/ml	50µl

3.2.4 hiPSC differentiation into podocytes

Confluent hiPSC lines were differentiated into podocytes according to the protocol of Hariharan et al. (Hariharan et al., 2019). Briefly, 70-80% confluent cells were dissociated with Accutase® and seeded at 10,000 cells/cm^2 on geltrex-coated plates in mTeSR medium supplemented with 10µM Y27632-ROCK inhibitor for 24 h. After 24 h, the medium was removed and fresh mTESR-1 was added for 2 days. On the third day after single cell seeding (day 0), the cultured cells were ready for differentiation. The protocol is divided into three stages; stage I is for the induction of intermediate mesoderm (day 0-3), 10ng/ml activin A, 30 ng/ml recombinant human (rh) bone morphogenetic protein 4 (BMP-4) with 1 µM all-trans-retinoic acid (RA) and 5% protien-free hybridoma medium (PFHM-II) was added to STEMdiff™ APEL2™ medium.For stage II induction of metanephric mesenchymal cells (day 4-7), 150 ng/ml glial derived nephrotic factor (GDNF), and 5% PFHM-II were added to the same medium. In the course of differentiation, the medium was changed alternatively every 48 h. For terminal

differentiation into podocytes, the resulting iTRPC6-EGFP cells were harvested on day 8 and reseeded at the density of 8000 cells/cm^2 on Laminin521 with 50 ng/ml recombinant human (rh) hepatocyte growth factor (rhHGF) as an induction factor. The cells were cultured for 6 days to observe huge arborized cells with foot processes and mostly bi-nucleated cells. Differentiation was monitored by marker expression analysis on day 4, day 8, and day 14 for podocytes.

3.2.5 hiPSC differentiation into proximal tubular epithelial cells (PTEC)

To induce differentiation and expansion of PTEC, the protocol of Hariharan et al. (Hariharan et al., 2019) was employed. Briefly, day 8 cells were harvested and seeded on laminin521-coated 6 well plates at the density of 15000 cells/cm^2 in renal epithelial growth medium (REGM). After 6 days of culture, a highly confluent, heterogeneous mass of tubular epithelial cells in multiple layers was visualized under a microscope. The proximal tubule epithelial cells are characterized by brush border epithelial cells that are highly absorptive.

3.2.6 hiPSC differentiation into cardiomyocytes

For cardiomyocyte differentiation, hiPSC cells were seeded as single cells at 80% confluence at a density of 10,000-20,000 cells/cm2 and 10 µM ROCK inhibitor. The next day, the medium was replaced with m-TeSR-1 medium without ROCK inhibitor. The medium was changed daily for for two to three days until the cells reached 70-80% confluence and were ready for differentiation. Cardiomyocyte differentiation was induced based on a published protocol (Lian et al., 2013) which was optimized by the BIH Stem cell core facility. Briefly, mesodermal differentiation was induced by the addition of cardiac priming medium (Table 11) to induce Wnt signaling for two days. Cardiac lineage was then induced by adding a cardiac induction medium (Table 11) to inhibit Wnt signaling for two days. This was followed by daily medium changes with the basal medium were subsequently performed for two days. Finally, on day 6, the cells were kept in a cardiomyocyte maintenance medium (Table 11). At this stage, cells were quantitatively checked for beating cells every 24-48 h, with early beating observed between days 7-14. The media formulations are listed in Table 11. Cell seeding density and CHIR99021 concentration were titrated for each cell line.

Table 11: Cell culture media formulations

Media	Composition
Basal medium	RPMI-1640 and B27 minus insulin supplement (1x)
Cardiac priming medium	Basal medium + 6μM CHIR 99021
Cardiac induction medium	Basal medium + IWP-2
cardiomyocyte maintenance medium	RPMI 1640 plus B-27 supplement (1x)

3.2.7 Embryoid body formation and trilineage differentiation

Harvested hiPSC were seeded into AggreWell plates 800 (StemCell Technologies) in E8 medium supplemented with ROCK Inhibitor (10μM). Embryoid bodies formed within 24 h and were transferred to ultra-low attachment plates (Corning) in knockout DMEM medium (Invitrogen) supplemented with 20% knockout serumreplacer (Invitrogen), 1,25 mM glutaMax™, 1% (v/v) NEAA, 0,2% (v/v) beta-mercaptoethanol and P/S (100 U/mL/100 μg/mL) for 10 days. The expression of germ layer-specific genes was analyzed by RT-PCR.

3.3 Cell culture in multi-organ tissue flow (MOTiF) biochip

MOTiF biochips were purchased from microfluidic ChipShop GmbH (Jena, Germany). The chip contains two chambers, each with an integrated membrane consisting of an 11 μm thick porous polyethylene terephthalate (PET) membrane with a pore diameter of 8 μm, which serves as a culture area. This membrane horizontally separates the upper and lower microfluidic flow channels allowing exchange and perfusion of medium. The biochip membrane was functionalized with laminin521 as an extracellular matrix protein on both channels to allow anchorage of the interfacing cell types. Cell culture was performed under sterile cell culture conditions and the chips were maintained in the incubator at 5% CO_2, 70% humidity, and 37°C. iPodocytes were seeded on a chip in a lower flow chamber with a density of 8000 cells/cm^2 and endothelial cell layers were cultured with a density of 1.3 × 105 cells/ cm2 on the upper chamber of the membrane. After seeding the cells on the respective channels, the medium was manually supplied on each side of the biochip.

3.4 Genetic Engineering

3.4.1 Site-directed mutagenesis using Tet-On 3G system

Plasmid DNA encoding wild-type and two different TRPC6 mutants with C-terminally fused YFP (WT, P112Q, and G757D) was a generous gift from Prof. Dr. Bernd Nuernberg (Department of Pharmacology, Experimental Therapy and Toxicology, Universitätklinikum Tübingen). The plasmid I received contained CMV promoter that drives transient expression of the transgene. However, I needed a temporal and user control expression, so to receive an inducible expression of the different TRCP6 mutants, site-directed mutagenesis was performed by using a Tet-On 3G system (Randolph et al., 2017). This system uses a doxycycline-binding transactivator protein and a promoter to regulate gene expression. The expression level of the gene of interest under the pTRE3G promoter was regulated by changes in doxycycline (Dox) concentration. The TRPC6-YFP gene sequence was amplified using nucleotide primers (Table 5) designed from the original plasmid (addgene #21084). PCR amplification was performed using Q5 high fidelity 2X master mix (New England Biolabs) using three-step thermocycling protocol 98°C for 30 seconds (1x cycle), 98°C for 10 seconds, 59°C for 30 seconds, 72°C for 30 seconds (30x cycle) and 72°C for 2 minutes (1x cycle). After amplification, recipient Tet-ON-all-in-one vectors (XLone-GFP plasmid: Addgene #96930) were digested with restriction enzymes *KpnI* and *BsrGI* (New England BioLabs) and amplified TRPC6-YFP genes were ligated using quick ligation™ kit (New England BioLabs) into the multiple cloning sites (MCS) of the Tet-On-all-in-one vector. The ligation product was transformed into *E. coli* Top 10 F (ThermoFisher Scientific) competent cells. Plasmid DNAs from different clones were isolated and sequenced. For transfection, large-scale DNA preparation was performed using Nucleobond Xtra Maxi Kits (Macherey-Nagel). All procedures were performed according to the manufacturer's instructions. All plasmids were sequenced by Sanger sequencing by microsynth seqlab, Germany.

3.4.2 Gene targeting constructs and molecular cloning using dual genomic safe harbor (GSH) targeting strategy

The hiPSC line CAMi014-A (also referred to as A1ATD1 iPS derived from male arm fibroblasts) cell line was kindly provided by the Kotter lab, Cambridge. These cells constitutively express the rtTA3G protein under the control of the CAG promoter, which

is integrated into the *ROSA26* safe harbor locus (Bertero et al., 2016; Pawlowski et al., 2017a).

The inducible TRPC6 pAAV_TRE-TRPC6-EGFP targeting vector was constructed by the ligation (Quick Ligation™ Kit, New England BioLabs) of the *TRPC6* gene sequence (PCR-amplified from the original plasmid addgene #21084) and the EGFP gene sequence (PCR-amplified from pAAV_TRE-EGFP) into the EcoRI/SpeI sites of the pAAV_TRE-EGFP plasmid. The vector was constructed for each TRPC6 wild-type and mutants (pAAV_TRE-WT-EGFP, pAAV_TRE-P112Q-EGFP, and pAAV_TRE-G757D-EGFP). The pAAV_TRE-TRPC6-EGFP plasmids were transformed into *E. coli* Top 10 F (ThermoFisher Scientific) competent cells. Plasmid DNAs from multiple clones were isolated and sequenced. For transfection, large-scale DNA preparation was performed using Nucleobond Xtra Maxi Kits (Macherey-Nagel). All procedures were performed according to the manufacturer's instructions. All plasmids were sequenced by Sanger sequencing through microsynth seqlab, Germany.

To integrate the Tet-ON-TRPC6-EGFP transgene into the AAVS1 locus, already ROSA26 targeted CAMi014 cell lines were seeded ($0.15x10^6$ cells/well) under feeder-free culture conditions in mTeSR-1 (Stemcell Technologies) medium on Geltrex (Life Technologies) coated 6-well plates and transfected 48h after passaging. Transfection was performed in Opti-MEM (Gibco) supplemented with Lipofectamine3000 (Invitrogen) according to the manufacturer's protocol. A total of 2 µg of plasmid DNA consisting of (i) 0.5 µg pZFN-AAVS1-L-ELD, (ii) 0.5 µg pZFN-AAVS1-R_KKR, and (iii) 1 µg PUC-AAV_TRE-TRPC6-EGFP was used per reaction. The DNA-lipid complexes were added dropwise to the cells and incubated for 24 h. The next day, the medium was replaced with mTESR1 medium. After 24 h, 1 µg/ml puromycin (Sigma-Aldrich) was added to the culture medium. Selection was continued for at least three days until all cells in the non-transfected controls were dead. The presence of the transgene was visualized in the wells with doxycycline (0.5µg/ml). Individual colonies were picked and expanded for the following 7-10 days of selection and were analyzed by genotyping.

To genotype the cells, genomic DNA was isolated from one well of a 6-well plate for each monoclonal cell line using NucleoSpin® TissueGenomic (ThermoFisher Scientific). The genotyping strategy followed was published by Pawlowski et al.

(Pawlowski et al., 2017b). Primers and the adapted PCR strategy are summarized in Tables 6 and 7.

3.5 Detection of protein by immunocytochemistry

3.5.1 Flow cytometry analysis and fluorescence-activated cell sorting

Cells were detached to a single cell suspension using trypsin/EDTA (PAN Biotech) and stained with LIVE/DEAD™ Fixable Blue for 30 min. For the analysis of GFP expression, cells were treated with Dox 24 h prior to FACS analysis. For labeling intracellular antigens, cells were permeabilized by incubation with phosflow perm buffer II for 15 min. Cells were incubated with primary antibodies (Table 4) diluted in ice-cold DPBS with 2% (vol/vol) fetal calf serum (FACS) for 30 min. Cells were incubated with appropriate secondary antibodies (donkey anti-mouse IgG Alexa 647 or donkey anti-donkey IgG Alexa 488) if they were not conjugated with a fluorophore. Data were collected using MACSQuant VYB flow cytometer (Miltenyi Biotec GmbH, Version 2) and analyzed using FlowJo software (FLOWJO LCC).

For fluorescence-activated cell sorting, the AriaII "Calliope" flow cytometer (BD Biosciences) was used by collecting only the cell population with the highest YFP expression. In both analyses, FACS gating was based on non-transfected and untreated cells as a control.

3.5.2 Immunofluorescence staining of cells

Cultured cells were washed with phosphate-buffered saline (PBS) and then fixed with Cytofix (BD Bioscience) for 10 min. Cells were then permeabilized with BD Perm/wash for 15 min and then washed twice with PBS and blocked with 10% secondary antibody host specific serum diluted in washing buffer for 30 min at room temperature, and stained with primary antibodies (Table 4) incubated at 4°C overnight. Cells were washed three times and incubated with fluorescence-labeled secondary antibodies in a wash buffer at room temperature for 1 h. Cells were then washed twice with PBS and fluorescent dye 4′, 6-diamidino-2-phenylindole (DAPI; Sigma-Aldrich, D-8417) was used to stain the nuclei. Images were obtained using the Operetta high-content imaging system (Perkin Elmer) and Opera Phenix high-content imaging system (Perkin Elmer) and analyzed using the Columbus software (Perkin Elmer). All experiments were performed in 3 technical replicates and 3 biological replicates.

3.6 Characterization of differentiated cells

3.6.1 Gene expression analysis

Relative gene expression analysis was performed by quantitative real-time PCR (qPCR) and RNA-Seq analysis.

3.6.1.1 RNA isolation

RNA isolation from cell lysate was performed using the RNeasy mini kit (Qiagen), according to the manufacturer's instructions. Briefly, cells were first washed with PBS at RT and RLT lysis buffer to which β-mercaptoethanol was added at the rate of 10µm per ml of RLT buffer before use. Cells were scraped using a cell scraper and collected in 1.5ml eppendorf tubes, followed by vortexing for 1 min to ensure proper cell lysis. Ethanol was then added to the top of the lysate. The lysate was transferred to RNeasy silica membrane columns and further lysis was performed according to the manufacturer's instructions. RNase-free water (21 µl) was used to elute RNA into RNase-free tubes, from which 1µl was used for RNA quantification using a nanodrop spectrophotometer (NanoDropTechnologies, Wilmington, DE, USA).

3.6.1.2 Quantitative real-time PCR (qPCR)

A totalvolume of isolated RNA was used to generate cDNA using TaqMan™ Reverse Transcription Reagents (ThermoFisher Scientific). The components of the reagents kit was mixed with cDNA as listed in Table 12 and the thermocycling conditions as shown in Table 13. SYBR Green PCR Master Mix (Applied Biosystems) was used for qPCR. For each primer, an additional negative control (without cDNA) and GAPDH (housekeeping gene) were used as a positive control. Samples were run on the QuantStudio™ 6 flex real-time PCR system. All samples were analyzed in 3 technical replicates and normalized to the housekeeping gene GAPDH. Results were analyzed using the ΔΔCt method.

Table 12: TaqMan™ Reverse Transcription Reagents

Component	1x sample
RNA+H2O	9.625µl
10x buffer	2.5 µl
MgCl2	5.5 µl
Random Hexamers	1.25 µl
dNTPs	5 µl
RNase inhibitor	0.5 µl
Reverse transcriptase	0.625 µl
Total	25µl

Table 13: Thermocycling conditions

Step	Temperature	Time	Cycles
Initial melting	50 °C	2 min	
Melting	95 °C	10 min	40
Primer annealing	95 °C	15s	
Elongation	60 °C	1 min	
Cooling	4 °C	∞	

3.6.1.3 RNA-Seq library preparation and NGS

For Illumina NovaSeq6000 RNA sequencing, RNA-Seq library preparation, cDNA libraries were prepared from Poly-A-tail enriched RNA from 3 biological replicates from day 14 of the podocyte differentiation protocol using TruSeq mRNA sample prep kit v.2 (Illumina). Sequence alignment and RNA-seq analysis: Bcl to fastq conversion was performed using Illumina software (Illumina). Fastq files were aligned and converted to z-score values using the standard STAR-DeSeq2 pipeline. Briefly, the fastq data were mapped to human genome hg38 using the STAR aligner (star2.7.9) with the 'quantMode transcriptomeSAM gene counts' setting. The STAR index file was generated using gene model ensembl104. The gene counts were normalized using the DSeq2 package (v1.34) from the bioconductor. Sample-specific z-scores were then collated in R 4.1.2 and visualized with pheatmap_1.0.12.

Table 14: Details of RNA sequenced samples on day 14

Sample name	Sample ID
P1715_RNA_01_Wild-type	WT-1
P1715_RNA_02_GOF	G-2
P1715_RNA_03_LOF	L-3
P1715_RNA_04-undiff iPSC	C-4
P1715_RNA_05 Wild-type	WT-5
P1715_RNA_06_GOF	G-6
P1715_RNA_07_LOF	L-7
P1715_RNA_08_undiff iPSC	C-8
P1715_RNA_09 Wild-type	WT-9
P1715_RNA_10 GOF	G-10
P1715_RNA_11_LOF	L-11
P1715_RNA_12_undiff iPSC	C12

3.6.2 Albumin assay

To determine cell permeability, differentiated (day 14) hiPSC-derived podocytes were cultured as described by Krithika et al. (Hariharan et al., 2019), and after differentiation, the culture medium was replaced with serum-free media with/without FITC labeled albumin (0.5mg/ml, Abcam) and cultured at 37 °C for 1 h. The cells were treated with Hoechst 33342 to stain nuclei and live imaging was performed using Phoenix to check the albumin uptake. The cells were then fixed in 4% paraformaldehyde (PFA). Each condition reaction was performed in triplicate.

3.6.3 Calcium imaging of podocyte

For calcium imaging, the hiPSC cells obtained at the end of day 8 were replated on laminin521-coated cover slides 13mm for podocyte differentiation, and on day 14 huge arborized cells with foot processes and mostly bi-nucleated attached to the coverslipes surface were observed. The cells were treated with Dox on day 12 to observe the podocytes expressing GFP. These coverslips were washed with PBS and incubated in

Fura 2 AM (2µM) for 30 min at 37°C in the dark. For recording, the slides were placed in a recording chamber continuously perfused with bath solution (Hepes-buffered physiological saline solution (Hepes-PSS) that has the composition of (mM): 134 NaCl, 6 KCl, 1 $MgCl_2$, 2 $CaCl_2$, 10 glucose and 10 HEPES (pH 7.4, NaOH). The entire process was recorded for 15 min during which the bath solution was applied for 3 min followed by 5 min of carbachol/DOG (100µM, Sigma-Aldrich/Biomol GmbH) and switching back to bath solution for 7 min. The effect of SAR7334 (TOCRIS, 100µM) was also observed in the recordings. To check the activity of the channel blocker on TRPC6 in podocytes, the cells were placed in bath solution for 1.5 min followed by 10 min of SAR7334, followed by 5 min of a mixture of Carbachol/DOG with SAR7334, and then switched back to bath solution for 5 min, for a total of 22 min of recording. Fura 2 fluorescence was alternately excited at 340 and 385 nm using a FuraLED light source (Cairn Research). Images were captured every 100 ms with 10 ms exposure using an OptiMOS camera (QImaging). Regions of interest corresponding to individual cells expressing giving GFP were selected manually from the acquired images using Fiji. Calcium signals were extracted and analyzed using a custom Python script.

3.6.4 Immunoblotting

Cells were washed with ice-cold PBS and then lysed with RIPA buffer (Sigma) containing 1X protease inhibitor (Roche). The cell lysate was harvested, sonicated (2 min), and centrifuged at 16000g for 20 min. Protein content in the resulting supernatant was quantified by bradford assay (Pierce TM BCA Protein Assay Kit, ThermoFisher Scientific) according to the manufacturer's protocol. Each sample was prepared by mixing 10µg of protein, 2x Laemimli buffer (BioRad), and 100mM DTT (ThermoFisher) to make a total of 30µl. Samples were heated at 70 °C for 10 min and loaded onto a pre-cast 10-well Bolt 12% Bis-Tris mini protein gel (Invitrogen). The PageRuler 10−180 kDa (ThermoFisher Scientific) was used as a protein size marker. Electrophoresis was performed in 1X NUPAGE MOPS SDS running buffer (Invitrogen), followed by transfer to 0.45 µm nitrocellulose membranes (GE Healthcare) by wet blotting in NuPAGE transfer buffer (Invitrogen). The membrane was blocked with intercept T20 antibody diluent (LI-COR Bioscience) for 1 h at room temperature on the shaker and incubated with mouse anti-GFP (Abcam, 1:5000), rabbit anti-TRPC6 (Merck Millipore 1:300) antibody and rabbit ß-actin (New England Biolabs GmbH, clone 13E5, 1:1000) in Intercept T20 antibody

diluent (LI-COR Biosciences) at 4 °C overnight. Membranes were washed twice with tris-buffer saline 0.1% Tween 20 (TBS-T) for 10 min and once with tris-buffer saline (TBS). The samples were incubated with IRDye 800 CW donkey anti-mouse IgG (LI-COR Biosciences, 1:10,000) and IRDye 680 RD donkey anti-rabbit IgG (LI-COR Biosciences, 1:10,000) for 1 h at room temperature under shaking. After washing twice in TBS-T for 5 min, membranes were kept in Tris-buffered saline (TBS) and visualized with the ChemiDoc MP Imaging system (BIO-RAD).

3.6.5 Transmission electron microscopy

Cultivated cells were fixed with 2.5 % glutaraldehyde (Serva) in 0.1 M sodium cacodylate buffer (Serva) for 30 min at RT and stored at 4°C. The samples were postfixed with 1 % osmium tetroxide (Electron Microscopy Sciences, Hatfield, USA) and 0.8 % potassium ferrocyanide II (Roth) in 0.1 M cacodylate buffer followed by embedding in agarose overnight. After cutting the agarose into smaller blocks, the samples were dehydrated in a graded ethanol series and transferred to Epon resin (Roth). Finally, ultrathin sections of the samples (70 nm) were stained with uranyl acetate and lead citrate. The samples were examined with a Zeiss Leo 906 electron microscope (Carl Zeiss) at 80 kV acceleration voltage equipped with a slow scan 2K CCD camera (TRS).

3.6.6 Scanning electron microscopy

Cultured cells on coverslips were fixed with 2.5% glutaraldehyde in cacodylate buffer (pH 7.3) for 30 min at RT and stored at 4°C. Postfixation was done with 2 % osmium tetroxide (electron microscopy sciences) in 0.1 M cacodylate for 1.5 h, followed by dehydration in an increasing ethanol series. Finally, the samples were critical point dried (Leica). Before analysis by scanning electron microscope (GeminiSEM 300, Carl Zeiss) the samples were subjected to gold-palladium sputtering (Balzer) and stored in a vacuum until their examination at the microscope.

3.7 Reprogramming protocol:

3.7.1 Urinary cell isolation and expansion

Urinary cells (UCs) were isolated from the urine of FSGS patients by adapting the protocol of Zhou et al.(T. Zhou et al., 2012). Briefly, UCs were thawed and cultured in proliferation medium (PM) containing a 1:1 mixture of DMEM high glucose and the REBM basal medium (Lonza), supplemented with 5% (v/v) fetal bovine serum (FBS, Biochrom),

1.25mM GlutaMax™ (Gibco), 0.5% (v/v) non-essential amino acids (NEAA, Gibco), P/S (50 U/ml, 50 µg/mL), 2.5 ng/mL basic fibroblast growth factor (bFGF), 2,5 ng/mL platelet-derived growth factor (PDGF-AB), and 2,5 ng/mL human epidermal growth factor (hEGF, all Peprotech) and the REGM singleQuote kit (Lonza), on Geltrex-coated plates. UCs ($1x10^6$) were transfected with episomal vectors (1-2µL, Epi5, Invitrogen) by using the Neon™ system (Invitrogen, settings: 1400 V, 20 ms, and 2 times). Transfected cells were transferred to a Geltrex-coated 6-well plate in PM medium and incubated for 24 h. On day 1, the medium waschangedto N2B27/basic fibroblast growth factor (bFGF) medium (DMEM/F12 w/ HEPES, containing N2 supplement (1×), B27 supplement (1×), MEM-non-essential amino acids (MEM-NEAA) (1×), GlutaMAX™-1 (100X) (1×), β-mercaptoethanol (55 µM) (all Gibco) and bFGF (Peprotech, 100 ng/ml). On day 9, the medium was changed to serum-free defined Essential 8 (E8) medium (STEMCELL Technologies). On day 25, hiPSC colonies were picked and transferred on Geltrex-coated 24 well plates (Corning) containing E8 medium supplemented with 1% P/S and 10µM Rock inhibitor Y-27632 (Wako). The hiPSC were EDTA passaged every 5-6 days in the ratio of 1:6 at 37°C and 5% CO_2. A frozen stock of other obtained clones from different iPSC lines was kept. hiPSC were tested negative for HIV 1+2, hepatitis B and C virus as well as for mycoplasma contamination using the MycoAlert™ mycoplasma detection kit.

3.7.2 Episomal vector loss

DNA was isolated from the hiPSC line using a DNeasy kit (Qiagen). PCR was performed using Q5 high fidelity 2X master mix (New England Biolabs) following a three-step thermocycling protocol: 94°C for 2 min (1x cycle), 94°C for 30 sec, 53°C for 30 sec, 72°C for 1 min (30x cycle) and 72°C for 7 min (1x cycle) using the primer sequence provided by the for OriP and EBNA1, Epi5 vectors (Invitrogen). DNA from passage 2 was used as a positive control and DNA from BCRTi005-A cells as a negative control.

3.7.3 Karyotyping and short tandem repeat (STR) analysis

For the detection of chromosomal aberrations, karyotyping was perofmred by LIFE & BRAIN Biomedical & Scientific Technology Platform (genomics@lifeandbrain.com). STR analysis was performed by external diagnostic laboratories IDEXX BioAnalytics, Kornwestheim, Germany). The genome of hiPSC and their PBMCs was analyzed for 16 different loci**.**

4 RESULTS

4.1 Conditional expression of TRPC6 to study podocyte phenotype changes

The Strategy- Various studies suggest that alterations in the TRPC6 ion channel in podocytes lead to the reorganization of the actin cytoskeleton and changes in Calcium (Ca^{2+}) regulation cause FSGS (Liu et al., 2015; Möller et al., 2007; Winn et al., 2005). To achieve cell-specific and inducible expression of TRPC6 wild-type and mutant variants in target cells and to assess Ca^{2+} regulation, the Tet-On system was used.

In the present study, two different gene delivery strategies, transgene configurations, and functional characterization of TRPC6 mutants were first evaluated in reporter cell lines (HeLA/HEK293) to optimize the gene engineering strategies and later applied to the renal lineage differentiation of hiPSCs *in vitro*.

4.1.1 Generation of transgenic HeLa and HEK293 cells with regulated expression of TRPC6 mutants

The results of this work have been published in Batool et al. (2023). To study the effect of TRPC6 mutations on intracellular Ca^{2+} levels, DNA plasmids (Tet-on all-in-one) encoding TRPC6 wild-type and known mutants (P112Q (Winn et al., 2005) and G757D (Riehle et al., 2016)) were first tested in HeLa and HEK 293 cells. In addition, the novel TRPC6 mutation Val691Lysfs* (V691Kfs*) was used, which was identified in a large kindred. This novel mutation results in a truncated TRPC6 protein lacking the C-terminal coiled-coil domain, a highly conserved region essential for the TRPC6 channel regulation. However, contrary to current theory, affected family members did not show signs of FSGS-related pathology. This chapter provides further characterization of each mutant.

4.1.2 Clinical history and pedigree analysis of a family with a novel dominant heterozygous TRPC6 mutation (V691Kfs*)

Clinical data was collected through my collaborating partner Dr. Susane Krone and Dr. Maik Gollasch at Charité Universitaetsmedizin Berlin, Germany. A 45-year-old woman was identified with a dominant heterozygous TRPC6 mutation (V691Kfs*). The index patient presented with nephrotic syndrome developed end-stage renal disease within less than 3 years. She was first presented to the nephrology clinic in 2018 with bilateral lower limb edema and an altered renal profile. Her serum creatinine was 0.9 mg/dL with low serum albumin of 20 g/L and proteinuria in the nephrotic range, with a urine protein

creatinine index (UPCI) of 34 g/g in the urine. Renal biopsy showed minimal change in glomerulopathy (MCD) with diffuse predominant mesangial immunoglobulin M (IgM) and C1q deposition. Despite treatment with prednisolone, serum creatinine and proteinuria increased to 3.3 mg/dL and 26 g/g, respectively, within 3 months. Partial remission was achieved with cyclophosphamide within 6 months (creatinine 1.3 mg/dL, proteinuria 9.6 g/g, albuminuria 8.3 g/g). The patient did not return for follow-up and sought alternative medications for her renal insufficiency. Compliance was reduced due to depressive episodes. In 2020, she presented again to the emergency department with an obvious nephrotic syndrome, severe edema, and ascites. Her serum creatinine was 5.0 g/dL (eGFR CKD-EPI <15 mL/min per 1.73m^2), serum albumin 10 g/dL, UPCI 18 g/g, urinary albumin-creatinine index 8.5 g/g. A dialysis fistula was constructed.

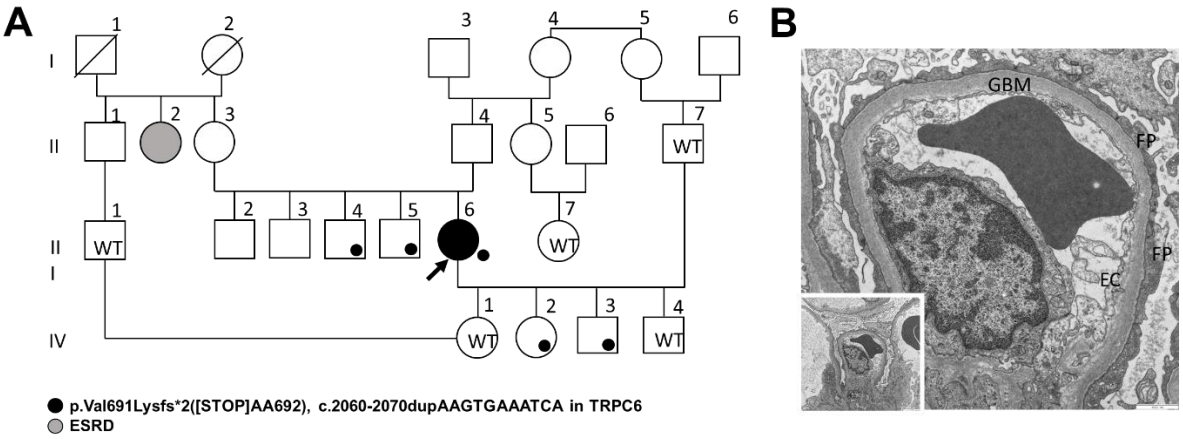

Figure 10: (A) Pedigree of Large kindred with the novel p.Val691Lysfs*2 (V691Kfs*) ([STOP]AA692) mutation. Small closed circle, V691Kfs*; WT, wild-type genotype. ESRD, end-stage renal disease. **(B)** Electron micrograph of the glomerulus of index patient III-6 showing loss of foot processes (FP) of the podocytes; glomerular basement membranes (GBM) are of regular width and without structural alterations. Endothelial cells (EC) are typical. Magnification: 1000nm. Adapted from (Batool et al., 2023)

From the pedigree analysis (Figure 10), in addition to the index patient, four other members share the same V691Kfs* mutation. Two siblings both male, aged 23 (III-c) and 39 (III-d) years, who were younger than the index patient at the time of presentation, had no renal disease and showed normal renal function. In sibling III-c, serum creatinine was 0.8mg/dl, serum albumin was 45g/L, and urinary protein creatinine index (UPCI) was 55mg/g. In sibling III-d, serum creatinine was 0.78mg/dl, serum albumin 42.3g/L, UPCI 58mg/g, and urinary albumin-creatinine index 4mg/g. All these values are within the normal range. Two other brothers refused genetic testing because they did not have renal disease (Figure 10). Similarly, two out of four children (IV-f and g) of the index patient

carried the V691Kfs* mutation, and none had renal disease (Figure 10). In child IV-f, serum creatinine was 0.7mg/dl, serum albumin 48.4g/L, UPCI 58mg/g, and urinary albumin-creatinine index 4.8mg/g. In child IV-g, serum creatinine was 0.4mg/dl, UPCI 55mg/g, and urinary albumin creatinine index 3mg/g. All these values are within the normal range. The patient's aunt was reportedly on dialysis (Figure 10); however, her underlying renal disease is unknown, and a request for genetic testing was denied. Thus, except for the index patient with histologically proven adult-onset C1q minimal change nephrotic syndrome, none of the other 22 members shown in pedigree had renal disease.

4.1.3 *In silico* modeling reveals the structural architecture of the truncated tetrameric TRPC6 mutant

The structural consequences of the new mutation were studied by a collaborator, Dr. Björn-Oliver Gohlke at Charité Universitätsmedizin Berlin, Germany, using a tri-dimensional cryo-electron microscopy (cryo-EM) model (Bai et al., 2020). This structure was solved to a resolution of 4.36Å (Bai et al., 2020). The structure (6UZ8) from the protein data bank (PDB) was used to examine and highlight the respective positions and effects of the novel truncated mutant. The tri-dimensional morphology is shown from the extracellular side (Figure 11A) and the side view with a typical bell-shaped structure (Figure 11B). The observed shapes are consistent with the bell-shaped swollen structure previously reported for other TRP cation channels (Liao et al., 2013; Maruyama et al., 2007; Tang et al., 2018). Based on the proposed structure, the two-layer architecture of the channel is packed symmetrically forming the intracellular cytoplasmic domain layer and the TM domain layer. The intracellular cytoplasmic domain is folded by both N- and C-terminal residues. The central four-fold rotation is perpendicular to both layers. The intracellular cytoplasmic domain is the bell-shaped part and is located below the ion channel pore of the TM domain. This domain harbors crucial sites that act as an element to sense the intracellular signals and communicate to the TM domain through the TRP domain that bridges the TM domain and intracellular cytoplasmic domain. The amino acids of the cytoplasmic C-terminus of TRPC6 fold into four long helices is shown in green at the top of the protein complex (Figure 11B). These helices are connected at the center of the channel to form an ion channel pore. The position of the novel FSGS-related truncating mutation was analyzed in this model.

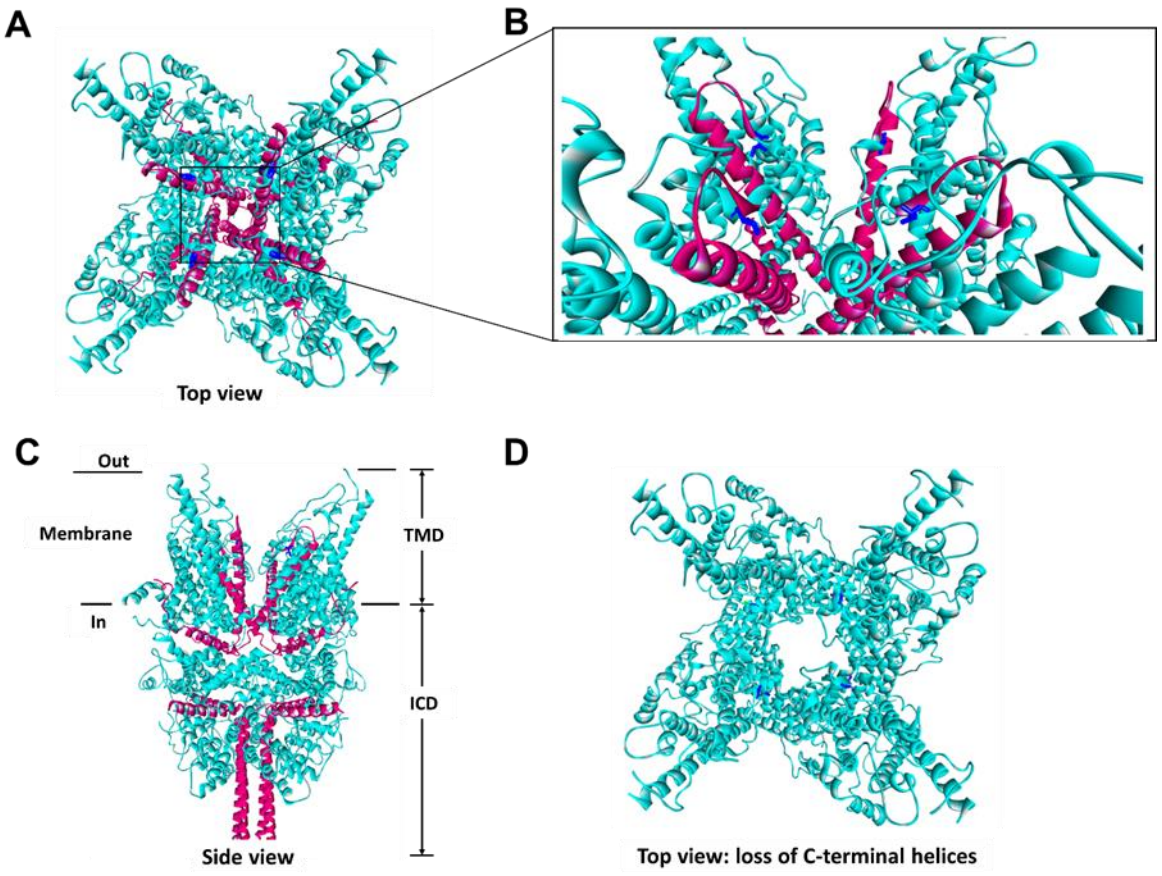

Figure 11: Tridimensional cryo-EM structure of tetrameric TRPC6 novel truncated p.Val691Lysfs*2 (V691Kfs*) ([STOP]AA692) protein. (A) View from the extracellular side, representing four monomeric TRPC6 subunits forming the ion channel complex. **(B)** Close-up view of the helices showing an exchange of valine to lysine at amino acid position p.691 and in a stop codon at p.692 resulting in a truncated protein. **(C)** Full homology side view parallel to the membrane. The position of the V691 protein is indicated in dark blue and the red color illustrates the truncated part of the closed channel. TMD transmembrane domain, ICD intracellular cytoplasmic domain. **(D)** Truncation results in complete loss of the - terminal helices. Cryo-EM modeling was performed by Dr. Björn-Oliver Gohlke at Charité – Universitätsmedizin Berlin, Germany.

4.1.4 Identification of novel truncated mutant by genetic testing

Genetic testing was performed on the index patient and six family members (IIIc and d, IVe, f, g, and h). Together with the index patient, 4 members (IIIc and d, IVf and g) were identified as heterozygous for a novel TRPC6 frameshift mutation resulting from the insertion of 11 base pair AAGTGAAATCA in exon 8 [c. 2060–2070 ins AAGTGAAATCA, Val691Lysfs*2] (Figure 12). The reported mutation is novel, as it has not been reported in any dbSNP or exome sequencing database of normal controls and rare diseases and has not been previously reported in TRPC6. The substitution of valine to lysine at amino acid position p.691 and a stop codon at p.692 resulted in a truncated protein. V691 is

located at the top of the pore, which affects the gating and ion conductance of the channel (highlighted in dark blue in the model structure, (Figure 11A, B). Truncation of the protein by the stop codon resulted in the complete loss of the C-terminal helices at the top of the complex (Figure 11D), which together with the valine-to-lysine exchange at position 691 is expected to suppress ion permeability through the TRPC6 channel pore.

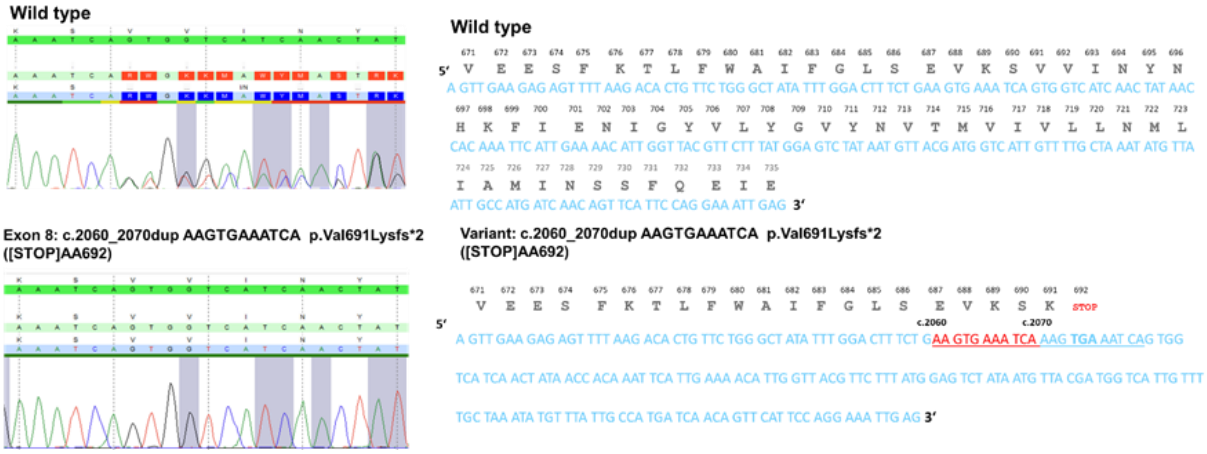

Figure 12: Verification of c.2060_2070dup AAGTGAAATCA variant compared with wild-type TRPC6 sequence. Comparison of variant sequence with nucleotide insertion and addition of stop codon at p.692, with wild-type TRPC6 sequence. Sequencing data was obtained from Dr. Maik Gollasch at Universitätsmedizin Greifswald, Greifswald.

4.1.5 Inducible overexpression of TRPC6 gene reveals mutant functionality

To achieve an inducible and tunable expression of TRPC6, a single vector construct based on the Tet-ON system, often referred to as the "Tet-ON-all-in-one" or "Tet-on 3G" system, was designed. This single vector combines all the necessary elements for conditional expression in one construct. These elements include the reverse tetracycline-controlled transactivator (rtTA) and the Tet promoter. This configuration simplifies the genetic engineering process by combining all the essential components in a single vector. It also reduces the risk of insertional mutagenesis or gene disruption that can be associated with multiple vector systems. This Tet-ON system allows for precise and overexpression of TRPC6 in response to specific inducers or conditions, making it a valuable tool for functional studies and potential therapeutic applications.

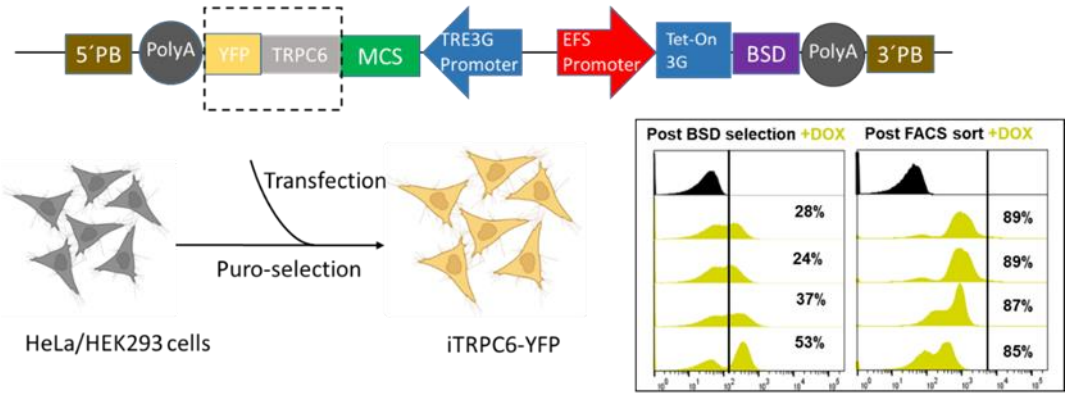

Figure 13: Design and generation of XLone transgenic HeLa cells. Schematic design shows the transposable plasmid cassette (5' PB: 5' piggybac terminal repeat; 3' PB: 3'piggybac terminal repeat; MCS: multiple cloning sites; Bsd: blasticidin resistance gene; EFS: alpha promoter; TRE3G: tetracycline responsive element 3G promoter. Flow cytometry analysis of the cells after Bsd drug selection and FACS live cell sorting of respective wild-type, P112Q, G757D, and V691Kfs*.

For an inducible and temporal control of TRPC6, an XLone plasmid containing PiggyBac transposase inverted terminal repeats, two promoters, and poly (A) sequences was used. In this plasmid, the first promoter, the TRE3G promoter, drives the expression of elements inserted into the multiple cloning sites; TRPC6 wild-type (WT), P112Q, V691Kfs*, and G757D N-terminally fused to a yellow fluorescent protein (YFP), located downstream of the promoter. The second promoter, the EF-1α promoter, controls the expression of a resistance gene for the drug blasticidin (Bsd) and the Tet-On 3G transactivator protein (Figure 13). After transfection and Bsd selection of HeLa cells, a heterogeneous population of cells was observed expressing between 28% and 53% YFP signals (Figure 13). However, FACS sorting after Dox induction alone without Bsd selection yielded more TRPC6/YFP positive cells (Figure 13, 14). Therefore, FACS live sorting was used to purify cells with Dox-inducible TRCP6/YFP expression. The expression of TRPC6 protein in HeLa cells was confirmed by western blot. The data showed the relative expression levels of wild-type and mutant V691Kfs*, which differ sufficiently in their molecular weight (Figure 15).

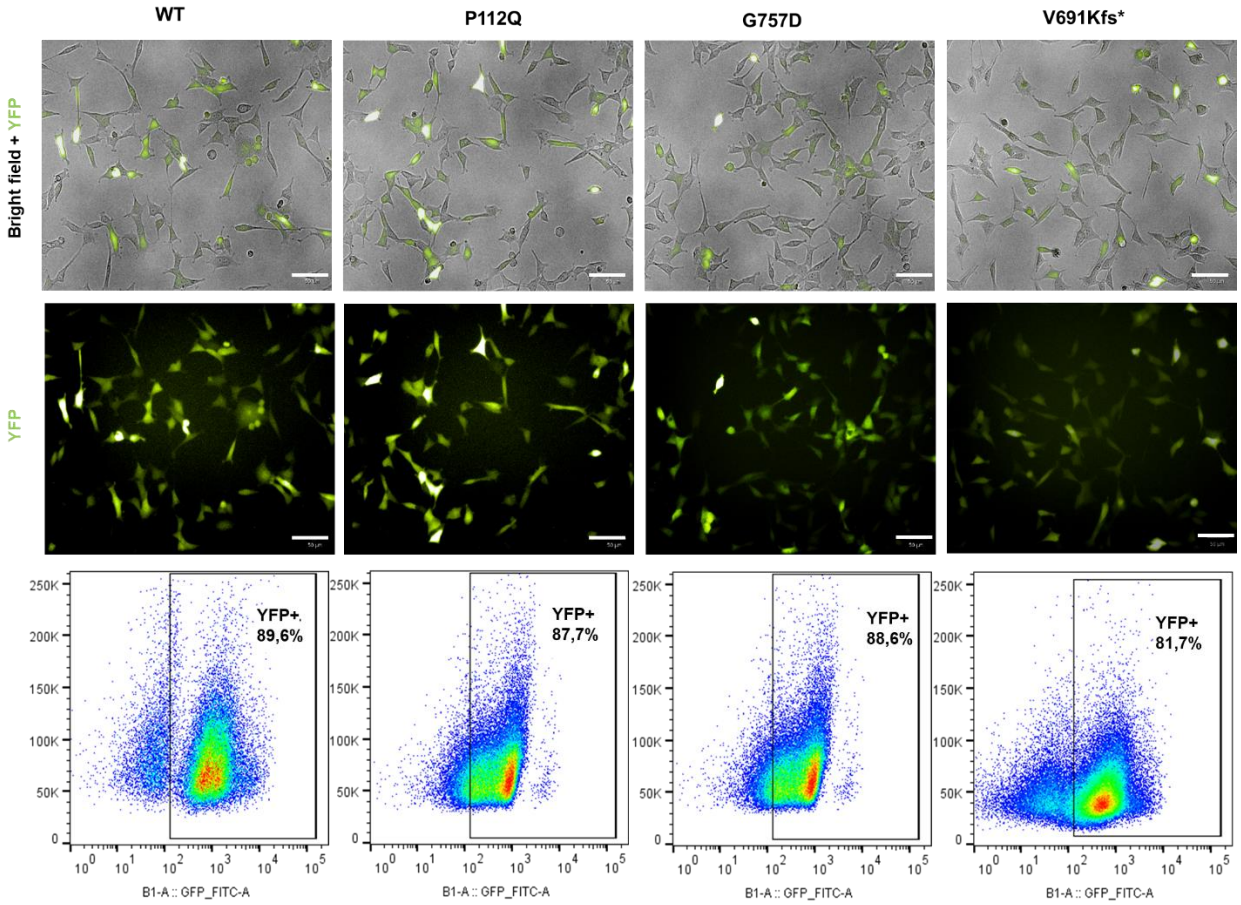

Figure 14: Expression of YFP reporter (green) in HeLa cells after transfection, Bsd selection, and FACS sorting, as shown by the merged image of the bright field and YFP signal for each of the variants studied. Scale bar 50 µm. Representative FACS plots of transgenic HeLa cells show an enriched population of up to a maximum of 89% YFP-positive cells.

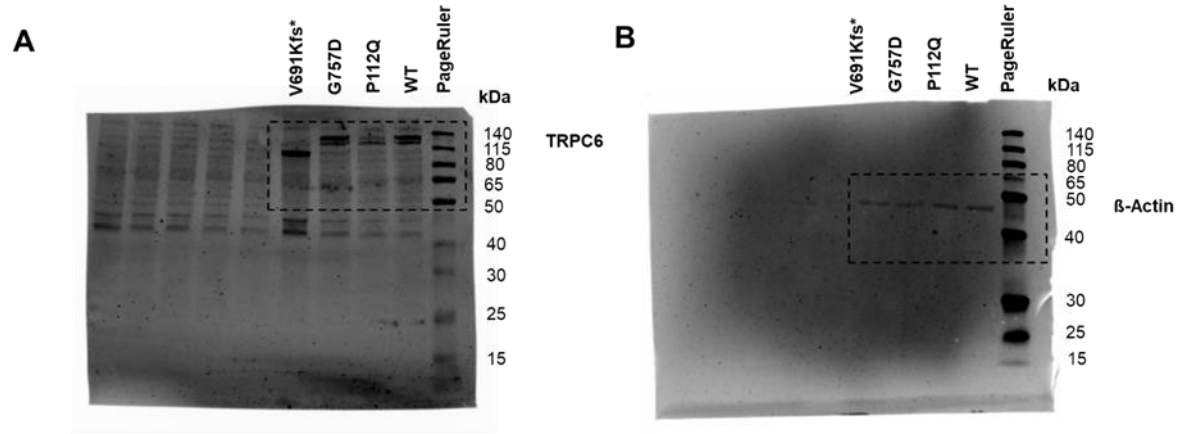

Figure 15: Western blot for TRPC6 protein in HeLa cells. **(A)** TRPC6 protein from wild-type, p112Q, G757D, and V691kfs* (~ 130 kDa) **(B)** β-actin (~45 kDa).

4.1.6 V691Kfs* is nonfunctional and inactivates TRPC6 channel as indicated by Ca^{2+} influx studies

The discovery of the new truncated mutation and the availability of known disease-ssociated TRPC6 mutations allowed us to comprehensively study their functional significance in a novel cellular system. In the first set of experiments, TRPC6 activity was measured in response to the broad channel activator Carbachol (Hofmann et al., 1999). TRPC6 P112Q showed increased Ca^{2+} influx compared to TRPC6 wild-type, whereas TRPC6 G757D showed decreased Ca^{2+} influx compared to TRPC6 wild-type and P112Q (Figure 16), which would be consistent with their respective GOF or LOF phenotypes. Interestingly, the new truncated mutant TRPC6 V691Kfs* showed a reduced Ca^{2+} influx in response to Carbachol (100 µM) compared to TRPC6 wild-type, P112Q, and G757D mutants (Figure 16A). Based on the measurements of basal Ca^{2+} concentration and Carbachol-induced amplitudes, the phenotype of the mutants appears to be heterogeneous. To investigate this further, TRPC6 activity was measured in response to a direct TRPC6 channel activator, 1, 2-dioctanoyl-sn-glycerol (DOG), to measure Ca^{2+} influx. TRPC6 P112Q showed increased Ca^{2+} signal amplitudes, consistent with the GOF phenotype (Figure 16B) and TRPC6 G757D responded to DOG with a significantly reduced signal amplitude, consistent with the LOF phenotype (Figure 16B). TRPC6 V691Kfs* showed the lowest response to DOG (Figure 16B), which can be distinguished from the wild-type, P112Q, and G757D mutants. The limited response of V691Kfs* against Carbachol and DOG supports the inactivity of the TRPC6 channel and argues for the closure of the ion transport pore. Part of the remaining Ca^{2+} influx in TRPC6 V691Kfs* expressing cells could be caused by the tetracycline-controlled gene regulatory system used for TRPC6 expression, which could have resulted from uncontrolled Tet promotor to express the transgene after Dox induction (Duran et al., 2022).

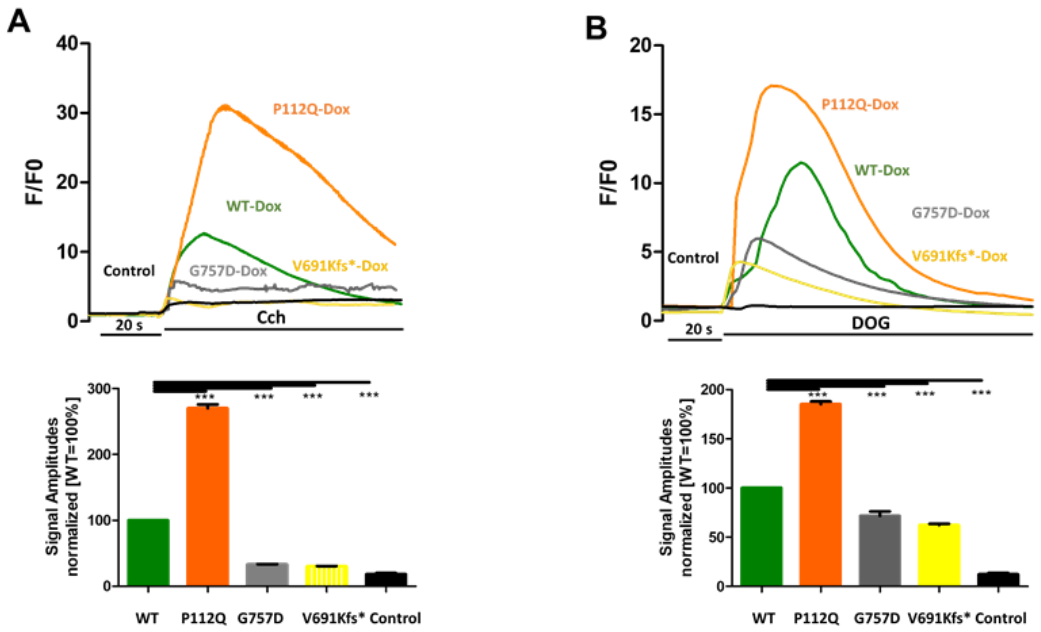

Figure 16: Functional characterization reveals GOF, LOF, and truncated phenotype in FSGS-related TRPC6 mutations. Changes in intracellular Ca^{2+} concentration (F/F0) were measured in Fluo-4 AM-loaded HeLa cells pretreated with doxycycline (Dox) (24h prior) expressing either wild-type (WT), P112Q, G757D, or V691Kfs*. Each condition was performed in 3 replicates, while non-transfected HeLa cells served as control. **(A)** Carbachol (Cch) (100 µM) was added 20 seconds after the start of the measurement. Representative measurement for all samples is shown in the upper panel, while a summary is shown as a bar graph (n = 3, mean ± SEM) in the lower panel. The graph shows the differences in the amplitudes of the responses to Cch. **(B)** DOG (100 µM) was added 20 seconds after the start of the measurement. Representative measurement for all samples is shown in the upper panel, while a summary is shown as a bar graph (n = 3, mean ± SEM) in the bottom panel. The graph shows the differences in the amplitudes of the responses to DOG. Adapted from (Batool et al., 2023)

Furthermore, the response of wild-type, P112Q, G757D, and V691Kfs* mutants against TRPC6 channel inhibitors, SAR7334 (100 nM)(Maier et al., 2015) and SH045 (100 nM) (Häfner et al., 2018) was measured, which were previously reported to show high selectivity, particularly for TRPC6, but also for TRPC3 and TRPC7. The data show that 10 min pretreatment of TRPC6 mutant-expressing cells with SAR7334 and SH045 individually inhibits TRPC6-mediated Ca^{2+} influx when stimulated with Carbachol or DOG (Figure 17, A-H), indicating that both the antagonists are specific for the TRPC6 channel.

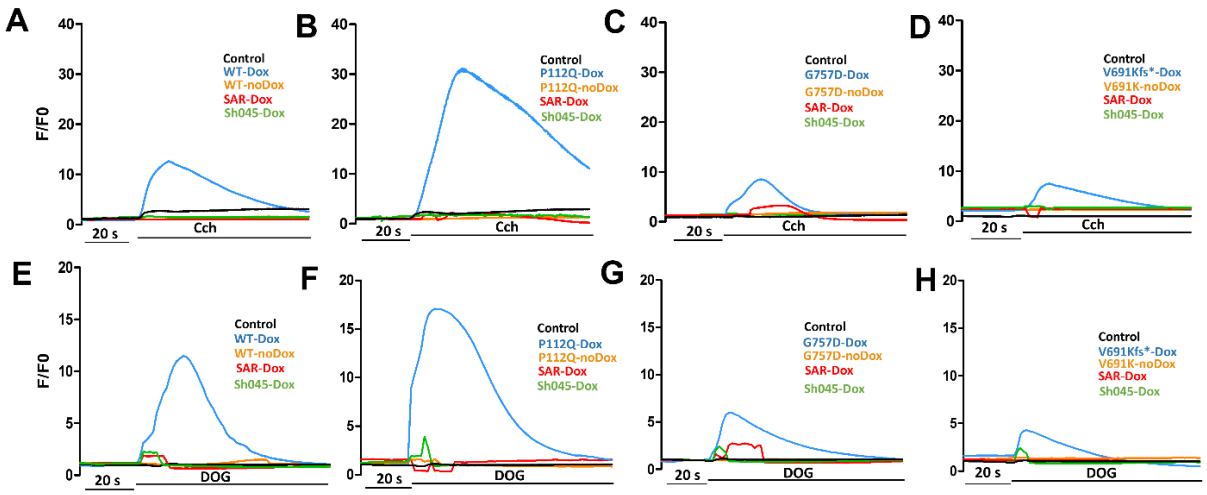

Figure 17: Functional characterization of disease related TRPC6 mutants in Ca2+ influx measurements. Changes in intracellular Ca^{2+} concentration (F/F0) were measured in Fluo-4-AM loaded HeLa cells expressing wild-type (WT), P112Q, G757D, or V691Kfs* treated with doxycycline (Dox) (0.5µg/ml) 24h before measurement and no Dox treated cells. **(A-D)** Treatment with the agonist Carbachol (Cch: 100 µM): Cch was added approximately 20 sec after the start of the measurement. Effects of TRPC6 blockers SAR7334 (SAR; 100 µM) and SH045 (100 µM) are observed in each TRPC6 mutant. **(E-H)** DOG (100 µM) was added approximately 20 sec after the start of the measurement. Effects of SAR7334 (SAR; 100 nM) and SH045 (100 nM) are observed in each TRPC6 mutant. Adapted from (Batool et al., 2023)

Whole-cell currents were measured to directly examine the difference between TRPC6 wild-type, V691Kfs*, and P112Q mutants, in transfected HEK293 cells (Riehle et al., 2016). Whole-cell membrane currents with distinctive inward and outward rectification were activated by Carbachol (100 µM) in wild-type TRPC6-expressing cells (Figure 18A, B). The Carbachol-induced current was inhibited by gadolinium chloride (Gd^{3+}, 100 µM) (Figure 18A, B). In contrast, Carbachol was unable to induce Gd^{3+}-sensitive TRPC6 currents in HEK293 cells transfected with TRPC6 V691Kfs* (Figure 18C, D). These findings were validated by recording whole-cell currents in cells transfected with P112Q, which was previously described as a GOF (Riehle et al., 2016). Consistent with the previous findings (Riehle et al., 2016), whole-cell currents in response to Carbachol were largely increased in P112Q-expressing cells (Figure 18E, F). However, almost no current amplitudes were observed in V691Kfs*-expressing cells as compared to wild-type and P112Q current amplitudes, confirming the non-functionality of the TRPC6 channel (Figure 18G). Statistical analysis showed that the differences between WT/V691Kfs* and WT/P112Q were significant. Carbachol-induced whole-cell currents obtained in co-transfected wild-type/V691Kfs*-expressing cells were negligibly small (Figure 18H, I) and could be distinguished from whole-cell currents obtained in wild-type and P112Q-

expressing cells (Figure 18B, F), indicating non-functionality of the TRPC6 channel. Statistical analysis is shown in Figure 18G.

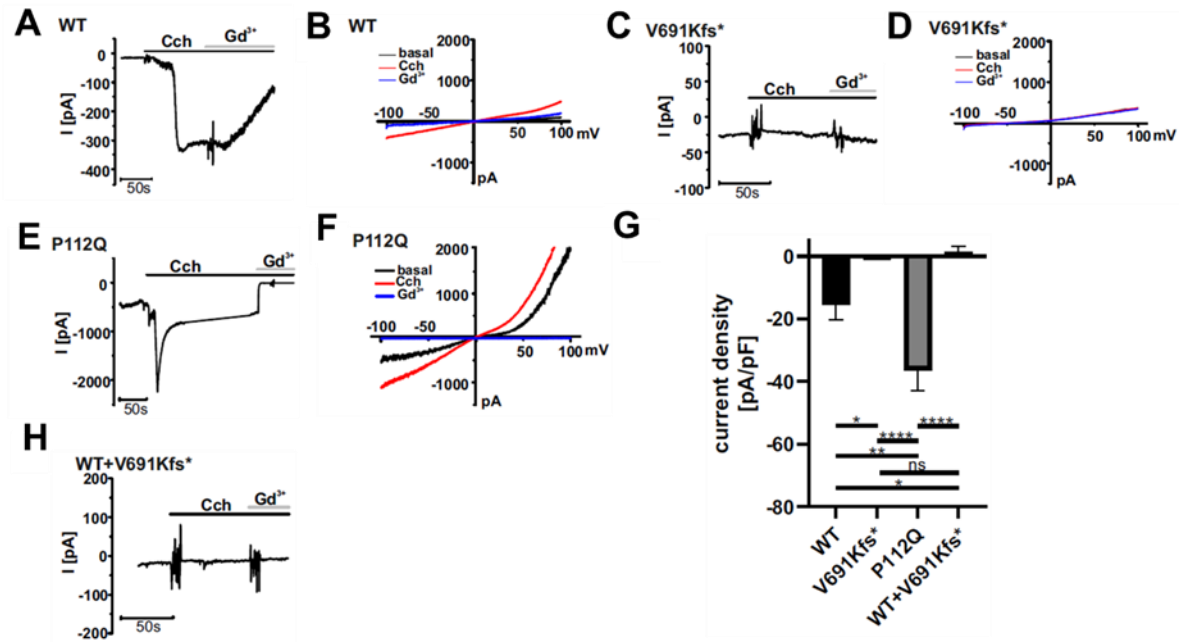

Figure 18: Electrophysiological characterization of TRPC6 WT, V691Kfs*, P112Q, and WT+V691Kfs*. Whole-cell currents were recorded in transfected HEK293 cells using the protocol described in the Methods section. After obtaining the whole-cell configuration, currents were recorded from -100 to +100 mV during voltage ramps. **(A, C, E,** and **H)** Inward currents at -60 mV were plotted against time. **(B, D, F,** and **I)** Current-voltage relationships obtained during voltage ramps from -100 to +100 mV: 1, basal currents (black); 2, 100 µM Carbachol (Cch)-induced currents (red); and 3, 100 µM Cch-induced currents in the presence of 100 µM gadolinium chloride (Gd^{3+}, blue). **(A** and **B)** Currents were measured in WT cells. **(C** and **D)** Currents were recorded in TRPC6 V691Kfs*-transfected cells. **(E** and **F)** Currents were recorded in P112Q-expressing cells. **(H)** Currents were recorded in WT+V691Kfs*–transfected cells. **(G)** Statistical analysis of the Cch-activated currents (plotted as the current density at -60 mV). Data are mean ±SEMs in each group: 6 cells (WT, black), 7 cells (truncated), 8 cells (WT+V691Kfs*), and 5 cells (P112Q, gray). *P≤0.05; **P≤0.01; ****P≤0.0001. Adapted from (Batool et al., 2023)

4.1.7 Co-expression shows a dominant-negative effect

To determine the dominant phenotypic characteristics of TRPC6 mutants that are consistent with the heterozygosity of TRPC6 *in vivo* and the tetrameric nature of the channel, *in vitro* experiments were performed to categorize the effect of P112Q and G757D individually in a channel complex composed of wild-type and TRPC6 mutants. For this purpose, Carbachol and DOG-induced Ca^{2+} responses were studied in HeLa cells expressing wild-type and TRPC6 mutants in a 1:1 ratio (Figure19). To monitor equimolar expression, mCherry, and YFP fusion reporter constructs were used (Figure

19). Cells transfected with the mixture of P112Q/WT DNA responded to Carbachol with increased channel activity (Figure 20A) after induction by Dox.

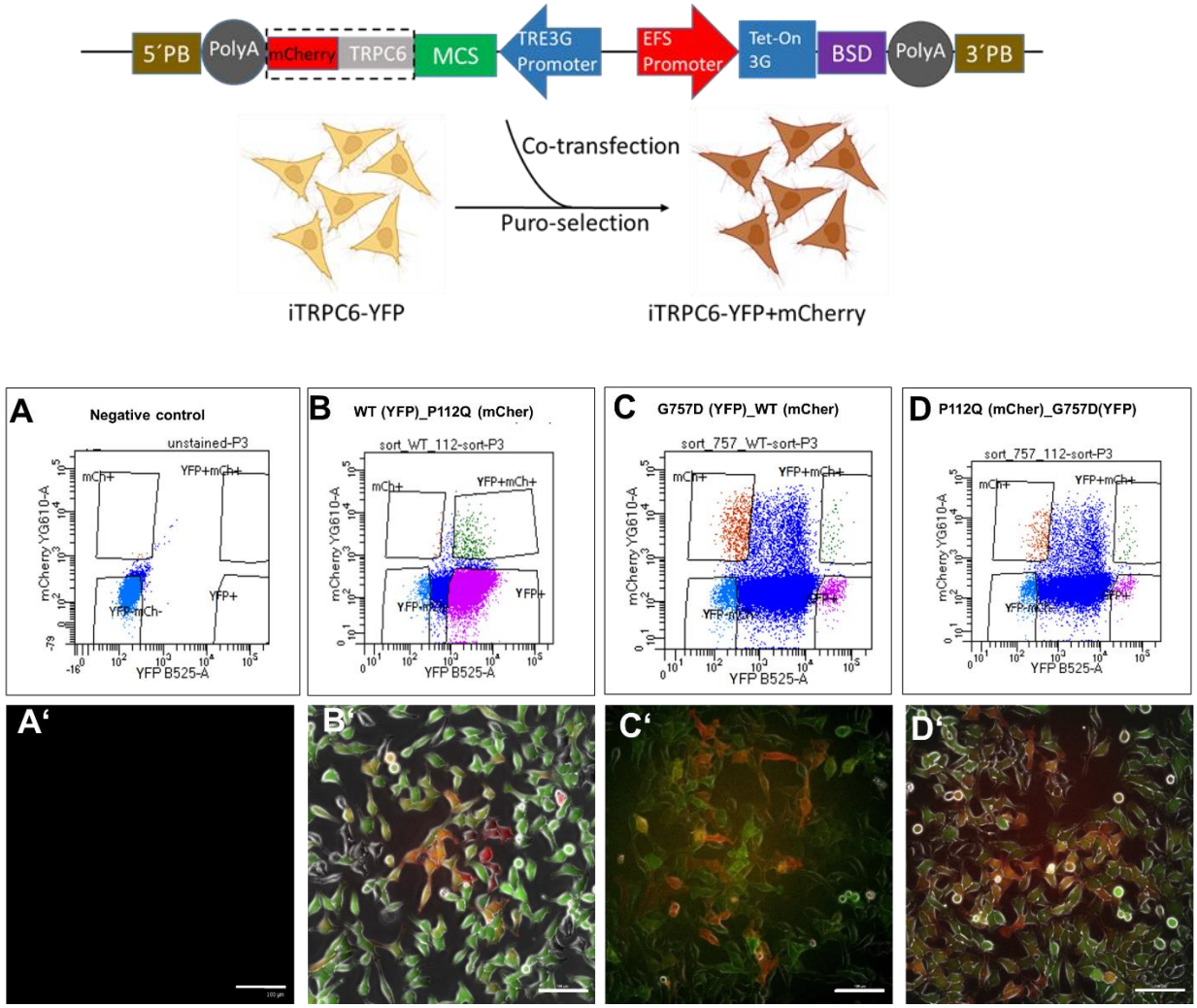

Figure 19: Co-transfection strategy to characterize the dominant phenotype of TRPC6 mutants. Upper panel: Workflow of co-transfecting TRPC6-YFP wild-type and mutant cells with TRPC6-mCherry wild-type and mutant cells. **Lower panel: (A, B, C** and **D)** Representative flow cytometry plots show the gating strategy to sort double positive cells expressing both YFP and mCherry (YFP+mCh+, top right) for each co-transfected cells and the remaining 3 gates to sort cells expressing only mChr+ (Top left), YFP (bottom right) and non-transfected cells (bottom left). Microscopic images of **(A')** negative control showing no transfection. **(B')** sorted cells expressing both WT-YFP/P112Q-mCh represented in combined image as YFP+mCh+. **(C')** sorted cells expressing both G757D-YFP/WT-mCh represented in combined image as YFP+mCh+. **(D')** sorted cells expressing both G757D-YFP/P112Q-mCh represented in combined image as YFP+mCh+. Scale bar 100 µm.

Quantitative analysis revealed that cells transfected with the P112Q/wild-type mixture responded with an approximately 2-fold increase in the response to the wild-type TRPC6, which is similar to the effect of P112Q (Figure 20G). The same mixture of cells responded to DOG with a 50% increase in the Ca^{2+} response; this is similar to the effect

of GOF alone compared to the wild-type channel (Figure 20H). The 1:1 ratio of TRPC6 wild-type and P112Q confirms that, on average, at least one P112Q protein is integrated into each tetrameric complex. Considering that the mutant affects only one channel protein within the tetrameric complex, this already results in an increased amplitude on the overall channel activity, typical for a dominant GOF effect. This suggest that the GOF-induced phenotype is the true cause of podocyte cell death in FSGS. Statistical analysis shows that DOG Ca^{2+} amplitudes are smaller than Carbachol-induced amplitudes, but the differences between wild-type and mutants are statistically significant.

Consistent with previous findings (Riehle et al., 2016), cells transfected with the TRPC6 G757D/wild-type mixture showed reduced responses to Carbachol (Figure 20B) and DOG (Figure 20E). Statistical analysis revealed that the G757D/wild-type mixture responded to DOG and Carbachol with approximately 40% of the response of the wild-type TRPC6, which is similar to G757D (Figure 20G, H), suggesting that the LOF-associated response is lower than the TRPC6 wild-type response. Similarly, cells transfected with P112Q/G757D together after Dox treatment showed a similar response as the wild-type when treated with Carbachol (Figure 20C, G) and DOG (Figure 20F, H). Thus, the mixture of both the GOF/LOF TRPC6 mutants restored the wild-type activity and the existence of a negative-dominant phenomenon with genetic variants of the TRPC6 renal channel.

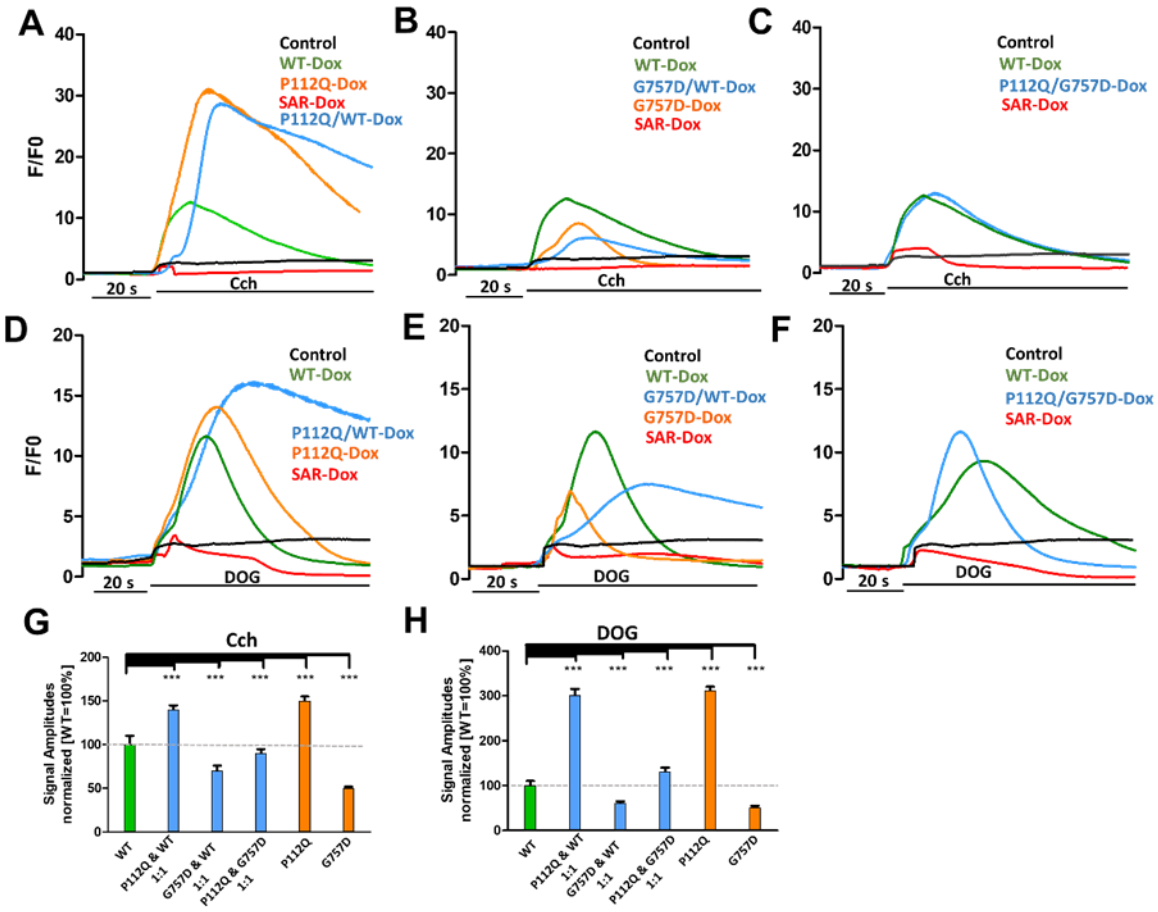

Figure 20: Co-transfection strategy to characterize the dominant phenotype of TRPC6 mutants. Changes in intracellular Ca^{2+} concentration (F/F0) were measured in Fluo-4-AM loaded HeLa cells expressing wild-type (WT), P112Q/WT, G757D/WT, or P112Q/ G757D TRPC6 C-terminally fused to YFP and mCherry treated with doxycycline (Dox) (0.5 µg/ml) 24h before measurement. **(A-C)** Carbachol (Cch: 100 µM) was added approximately 20 sec after the start of the measurement. Effects of SAR7334 (SAR; 100 µM) and SH045 (100 µM) are observed in each TRPC6 mutant. **(D-F)** DOG (100 µM) was added approximately 20 sec after the start of the measurement. Effects of SAR7334 (SAR; 100 µM) and SH045 (100 µM) are observed in each TRPC6 mutant. **(G)** Statistical analysis of data obtained from at least three independent experiments is shown as bar graphs. The graphs show the differences in the amplitudes of the responses on Cch application. **(H)** Statistical analysis of data obtained from at least three independent experiments is shown as bar graphs. The graphs show the differences in the amplitudes of the responses to the DOG application (n = 3, mean ± SEM). ***P≤0.0001. Adapted from (Batool et al., 2023)

4.2 Generation of transgenic hiPSC lines with a regulated expression of TRPC6 mutants

Stable and reproducible transgene expression has been the goal of genetic engineering from past decades, so that the transgene is expressed at constant level in each cell for an extended period of time. However, transgenes that are stably integrated into the genome often become silenced or reduced in expression over time. This can be

due to the removal of the transgene from the genome or by mechanisms related to transcription and post-translation. The thriving results of the Tet-on-all-in-one system in HeLa/HEK293 cells encouraged us to transduce the system to the hiPSC. Podocytes derived from hiPSC could be used to assess the effect of the increased/decreased Ca^{2+} levels on cell function directly in a cell type relevant for FSGS. This requires a rather homogenous expression of the transgene in the majority of the cells. Unexpectedly, the generation of mosaic expression patterns was observed in hiPSCs transduced with the Tet-on 3G system. The following section compare the use of the use of single-vector and two-vector Tet systems.

4.2.1 Single-vector Tet vs. two-vector Tet system in hiPSC

To achieve the Tet-On-all-in-one system (Randolph et al., 2017), here, I used the hiPSC - line (WISCi004-A) to integrate YFP-tagged TRPC6 wild-type and mutant genes for Tet-inducible expression. However, this system generated a mosaic transgenic cell population despite Bsd drug selection followed by fluorescence activated cell sorting (FACS) (Figure 21) and then transgene silencing after several passages.

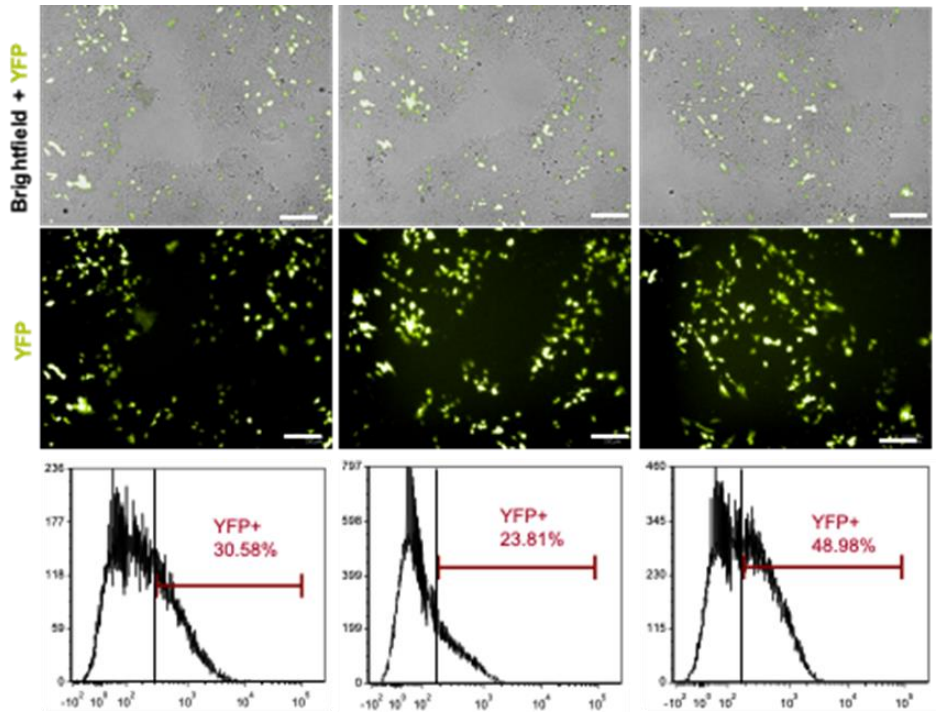

Figure 21: Generation of an inducible TRPC6 iPS-derived expression system. Representative images illustrate the development of Tet-On all-in-one vector TRPC6 hiPSCs, expressing YFP after transfection, Bsd selection, and FACs sorting, as shown by the merged images of bright field and YFP signal for each variant studied. Scale bar 100µm. The bottom panel is a representative flow cytometry analysis showing a depleted population of up to 40% YFP-positive cells.

As a result, the original system was replaced by a two-vector Tet system, and experiments were performed with hiPSCs using the OPTi-OX® cell line. This particular hiPSC line, known as CAMi014-A, is commercially available and has a built-in expression of rTA3G in the ROSA26 locus under the control of the CAG promoter. To evaluate the functionality of this cell platform, a genetic construct consisting of the Tet promoter and the TRPC6-EGFP gene was introduced into the AAVS1 safe harbor locus of the CAMi014-A cell using ZFN (Figure 22).

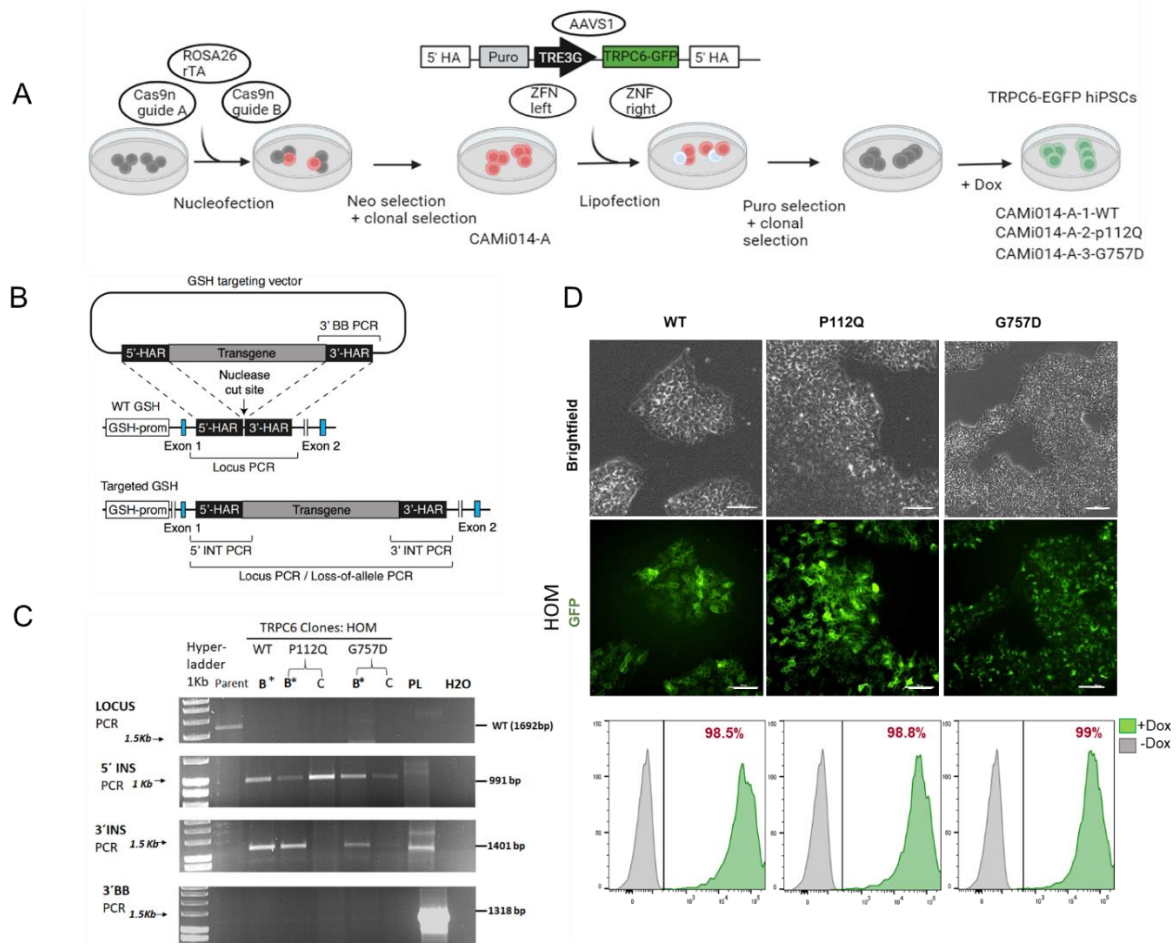

Figure 22: Genotypic and phenotypic characterization of hiPSC-TRPC6 cell lines. (A) Schematic targeting of hROSA26 and AAVS1 loci engineered with Tet ON system in hiPSC indicating the TRPC6-GFP expression. ZNF: zinc finger nucleases; rTtA: reverse tetracycline transactivator, TRE: Tet responsive element. **(B)** Genotyping strategy to identify the correct target of hROSA26 and AAVS1 in hiPSC lines. Figure adapted from Pawlowski et al. (Pawlowski et al., 2017a). For each genotyped reaction, the amplicons are indicated as locus PCR, 5'INT, 3'INT, and 3'BB. GSH-prom: genomic safe harbor ROSA26 and AAVS1 promoter. **(C)** PCR results of one clone from WT, 2 clones from P112Q, and 2 clones from G757D. Plasmid (PL) and water (H2O) are the control samples. Homozygous (HOM) lines for each allele indicate successfully targeted alleles of the AAVS1 loci. Identified HOM clones are marked with an asterisk (*) and were used for further studies. **(D)** GFP signals indicate TRPC6 expression. Scale bar 50µm. The bottom panel is a representative flow cytometry analysis of transgenic hiPSCs showing an enriched population of up to 90% GFP positive after 24hr of Dox treatment.

Following the puromycin selection process, isogenic cell lines were isolated and then expanded. These cell lines were then genotyped to confirm their genetic makeup and consistency (Figure 22C). From the genotyped clones, homozygous clones of each variant i.e. wild-type, P112Q, and G757D carrying two copies of each transgene and high transgene expression were selected for the experiments. Expression of the TRPC6 (EGFP-tagged) variants was homogenously induced by Dox, consistent across multiple clones and passages, with >90% of cells expressing TRPC6-EGFP as observed by FACS analysis (Figure 22D).

4.2.2 Transgene expression characterization in hiPSC

To determine whether the iPSC clones retained pluripotency characteristics, expression of stem cell markers and differentiation potency were analyzed in each of the established iTRPC6 cell lines (CAMi014-A-1 refers to iTRPC6-WT, CAMi014-A-2 refers to iTRPC6-P112Q, CAMi014-A-3 refers to iTRPC6-G757D). Specifically, the expression of tumor rejection antigen (Tra-1-60), stage-specific embryonic antigen 4 (SSEA4), octamer-binding transcription factor 3/4 (Oct3/4), NANOG, and sex determining region Y-box 2 (SOX2) was analyzed (Figure 23A). Induced TRPC6 (iTRPC6) gene expression was quantified and confirmed by real-time quantitative PCR (qPCR) in the presence and/or absence of Dox (Figure 23B). The differentiation potential into three germ layers was assessed *in vitro* by embryoid body formation (Figure 23C). Markers of ectoderm (NESTIN and NEUROD1), mesoderm (brachyury and MIXL1), and endoderm (gooscoid and SOX17) were successfully detected by reverse transcriptase polymerase chain reaction (RT-PCR) (Figure 23C).

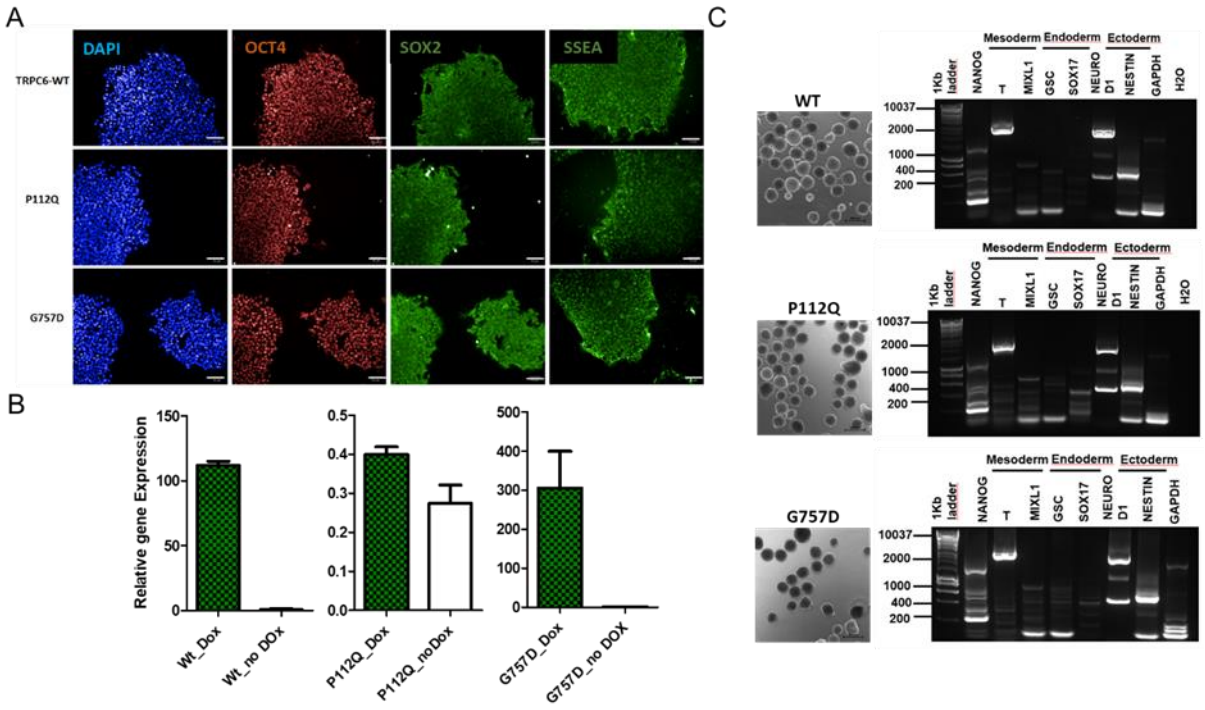

Figure 23: Characterization of CAMi014-A-1, CAMi014-A-2, CAMi014-A-3. (**A**) Cells expressing the pluripotency markers Oct4, Sox2, and SSEEA. (**B**) Relative TRPC6 expression after Dox treatment and untreated treated cells. (**C**) PCR for three germ layer markers.

4.2.3 Kidney differentiation: Inducing mesoderm, intermediate mesoderm, and renal vesicle formation

The inducible TRPC6 wild-type and mutant (iTRPC6-WT, iTRPC6-P112Q, and iTRPC6-G757D) hiPSC lines were then successfully differentiated into the mesoderm, renal progenitor cells, and podocytes. Additional screening for transcription factors crucial to the developmental cascade was performed by high-content screening using immunofluorescence. The first time point chosen was day 4 to assess the onset of mesoderm induction and specification into intermediate mesoderm. Subsequently, day 8 served as a second time point to evaluate the induction of renal vesicle formation.

To obtain intermediate mesoderm cells, I initiated the formation of mesodermal cells by exposing the cells to a medium containing activin A, BMP4, and RA. This resulted in an increase in the expression of specific markers such as SIX2, PAX2, and WT1 (Figure 24). The initiation of nephrogenesis with the intermediate mesoderm specification was further promoted by the addition of GDNF, which has been shown to enhance the differentiation of ureteric bud cells and stimulate branching. This addition of GDNF created a positive feedback loop for metanephric mesenchyme cells (Majumdar et al.,

2003; Sainio et al., 1997). At the end of the 8-day treatment, the cells showed increased expression of markers such as WT1, HOXB7, and JAG1 (as shown in Figure 24). This indicates the progression of the hiPSC lines toward renal vesicle cells. In addition, the complete loss of OCT4 confirmed the loss of pluripotency and the successful differentiation of all pluripotent stem cells. The presence of LHX1 in the majority of the cells at this stage, together with PAX2, corresponds to the development of the nephric duct and renal vesicle cells.

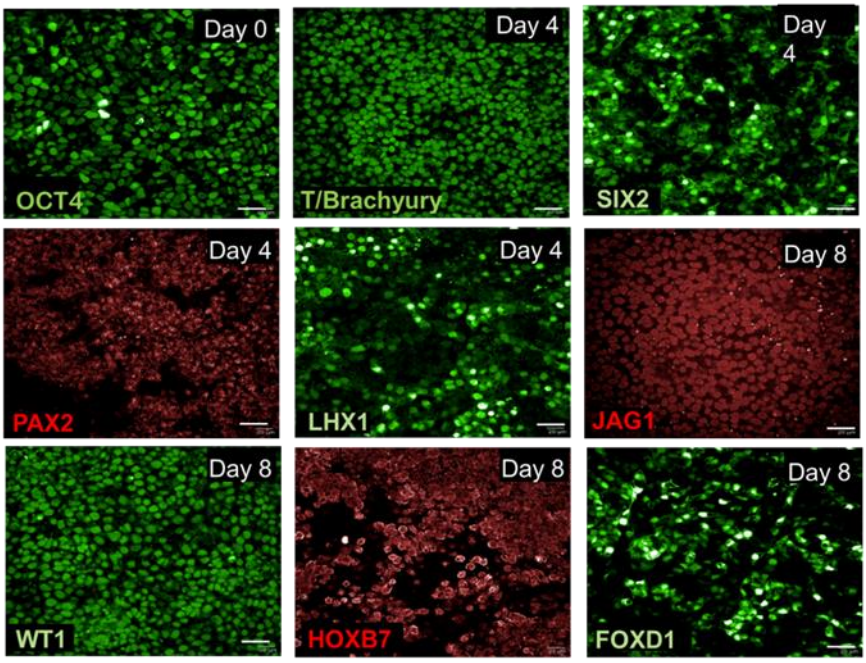

Figure 24: Expression patterns of intermediate mesoderm, metanephric mesenchyme, and ureteric bud-related transcription factors in hiPSC–derived cells. On day 4**,** Intermediate mesoderm and metanephric mesenchyme markers SIX2, PAX2, and LHX1 were observed. On day 8, the expression of the uretic progenitor markers HOXB7, JAG1, WT1, and FOXD1 can be seen. Scale bar=20µm.

4.2.4 Morphological characterization

During the differentiation process, significant morphological changes were observed in all three TRPC6 clonal lines. Within the first 2 days, hiPSCs began to lose their compact structure and spread over the culture surface. This was accompanied by cell proliferation as well as a significant amount of cell death during the treatment with activin A, BMP4, and RA. Over the next 2 days, the differentiating cells began to form dome-like structures within the culture, as shown in Figure 25. The addition of GDNF for the next 4 days resulted in the loss of these dome-like structures and a significant decrease in cell death. By the day 8 of differentiation, a heterogeneous cell mass was

observed, characterized by the presence of epithelial islands surrounded by mesenchymal cells (Figure 25). Starting from an initial hiPSCs culture of approximately 800,000 cells, the differentiation process yielded approximately 3.5 million cells, representing a substantial increase in cell number of up to five-fold. By day 14 cells showed arborized structures indicating podocyte formation (Figure 25).

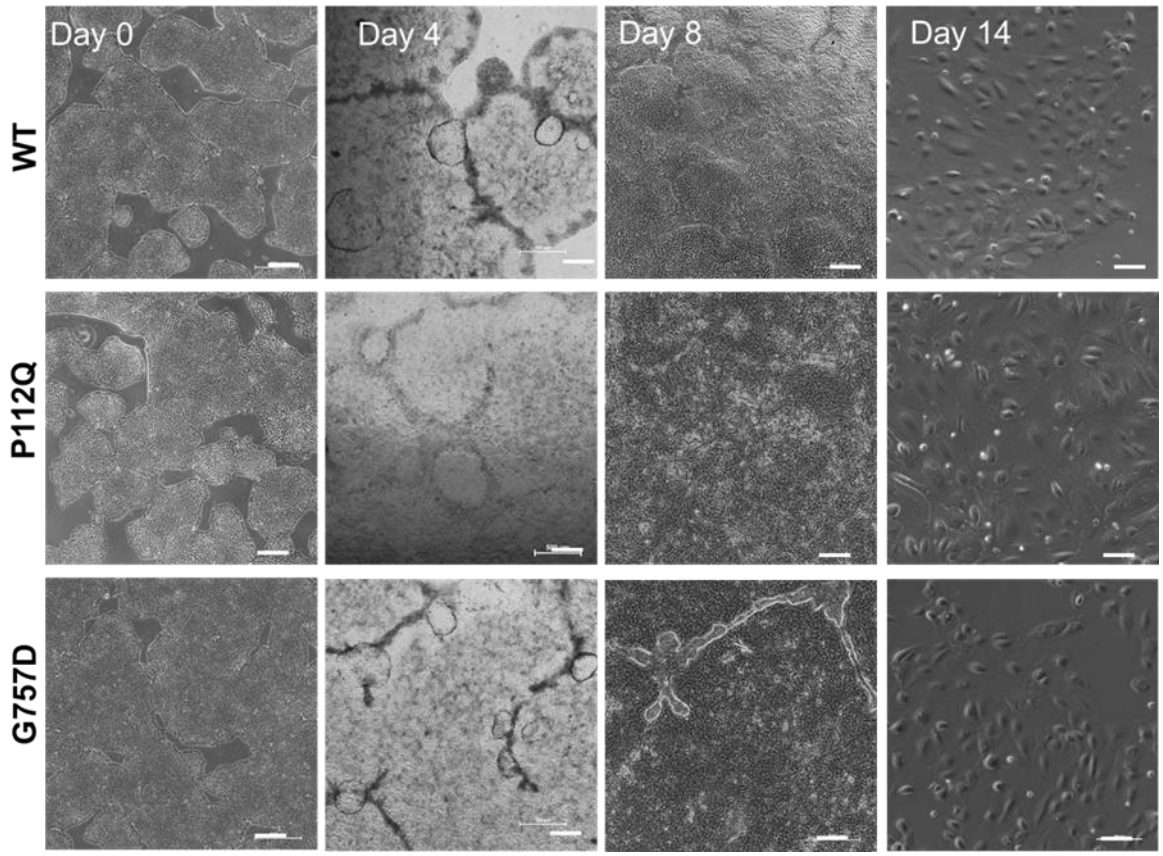

Figure 25: Morphological characterization of hiPSC- CAMi014-A-1-WT, CAMi014-A-2-P112Q, CAMi014-A-3-G757D. Podocyte differentiation patterns were similar in all three TRPC6 clonal lines. Starting day 0 treatment with activin A, BMP4, and RA results in cell proliferation. On day 4 cells appear to show dome-like structures on treatment with GDNF in culture. On day 8, mesenchymal cells were replated which led to the formation of podocytes until day 14.

4.3 Derivation of the glomerular compartment cells of the nephron from renal vesicle -like day 8 transgenic cells

4.3.1 Podocyte precursor cells

To promote podocyte differentiation, day 8 renal precursor cells were seeded at low density on laminin521-coated plates in the presence of hepatocyte growth factor (HGF). Every renal precursor cell generated from an iTRPC6 mutation exhibited a podocyte-like phenotype by day 14 and had an arborized cell body with multiple undivided nuclei (Figure 26B). Approximately 71% of the cells were podocalyxin (PODXL1) positive

and expressed synaptopodin (SYNPO) and podocin (NPHS2, Figure 27). The expression of podocyte developmental transcription factors at day 14 was analyzed at the RNA level as shown in Figure 28, confirming the specificity of the cells for the podocyte cell lineage.

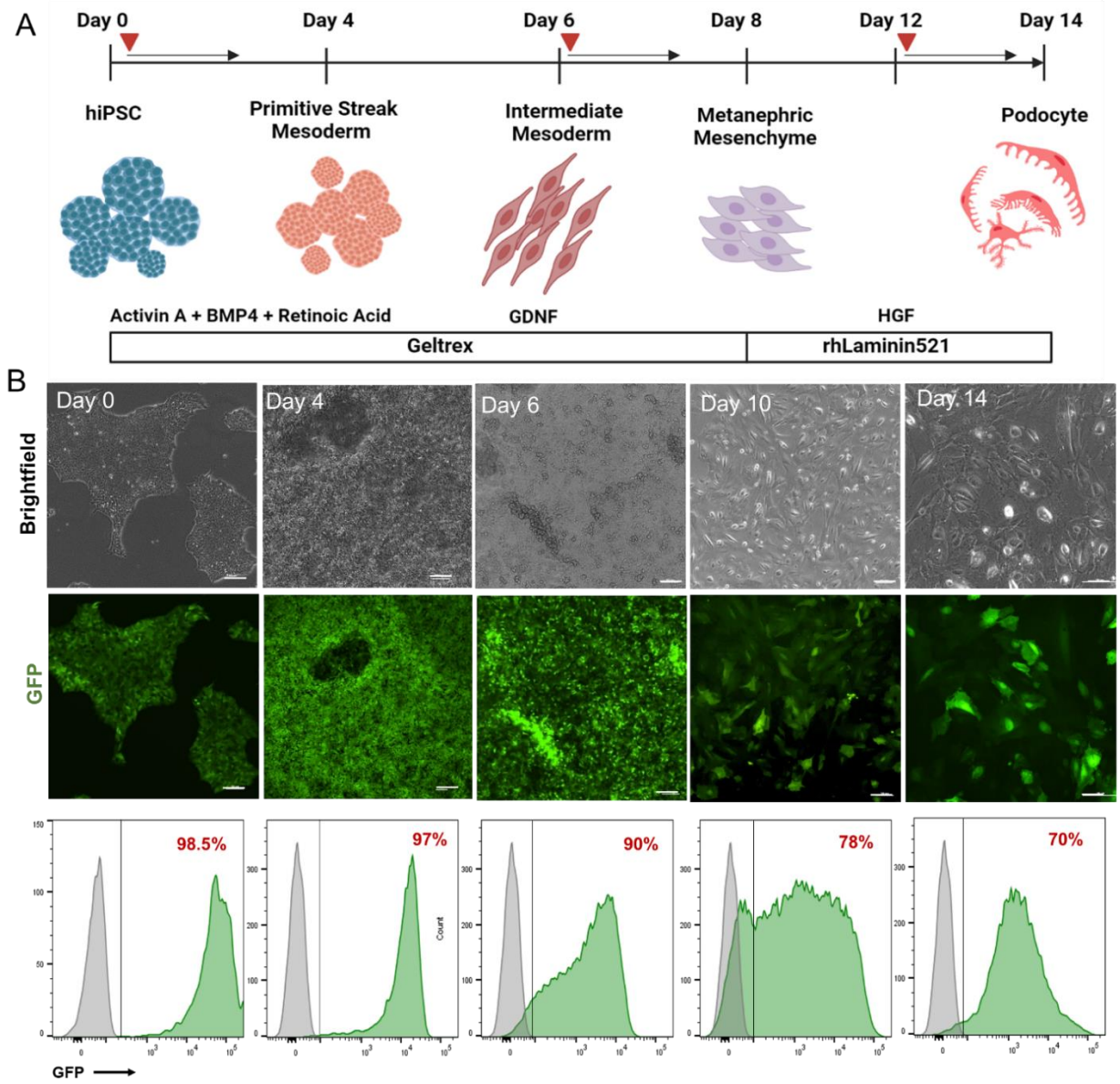

Figure 26: Directed differentiation of hiPSCs iTRPC6-WT into podocytes. (A) Workflow for the generation of mature glomerular podocytes. **(B)** Morphological changes of hiPSCs at each stage of differentiation. Panel below is a representative flow cytometry analysis of transgenic hiPSCs demonstrating iTRPC6-WT expression on day 0, day 4, day 6, day 8, and day 14.

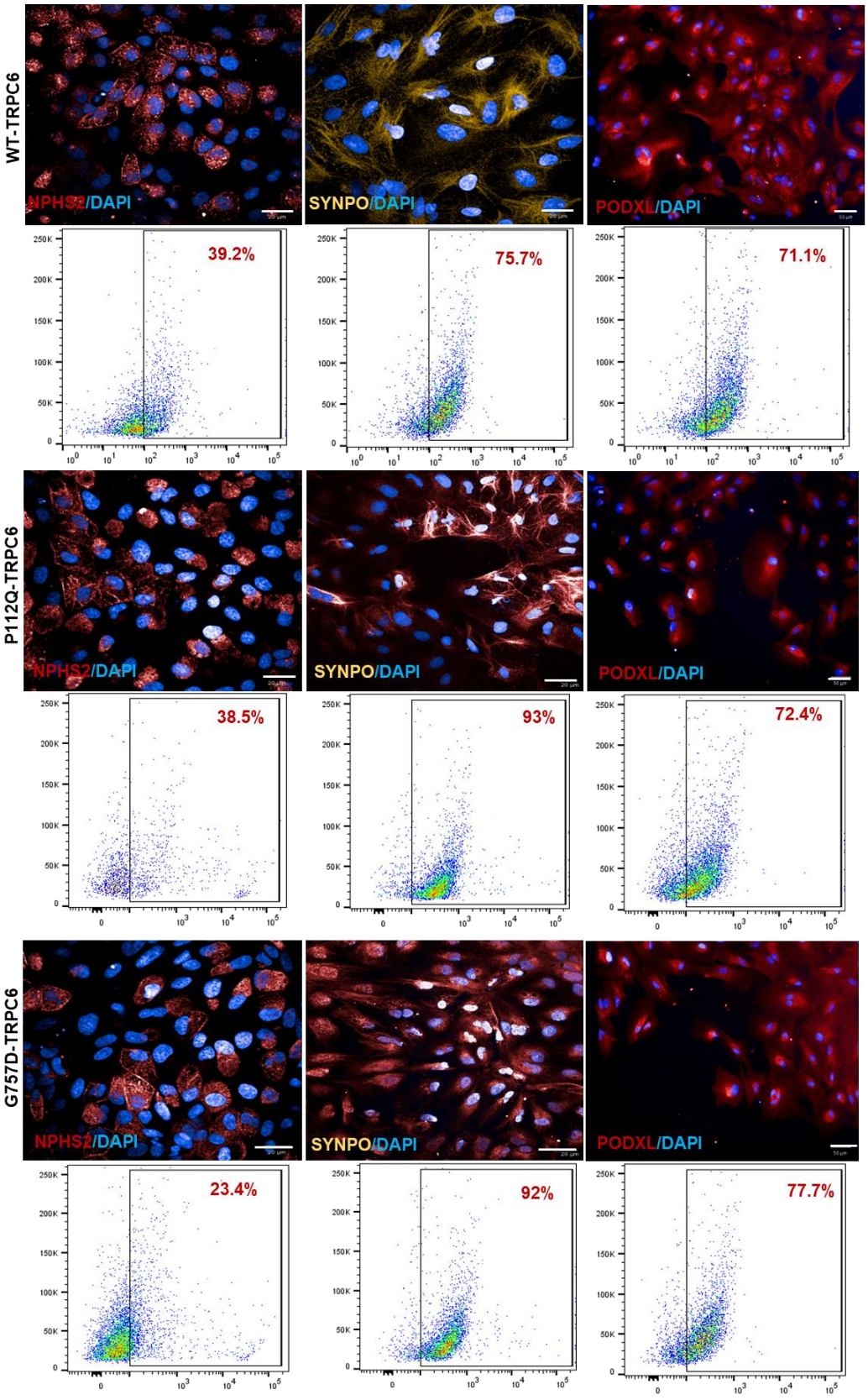

Figure 27: Immunofluorescence staining of podocyte markers in WT-TRPC6, P112Q-TRPC6, G757D-TRPC6: NPHS2, SYNPO, and PODXL. Scale bar=20µm. Alongside each panel is a representative flow cytometry analysis of podocyte markers — NPHS2, SYNPO, and PODXL.

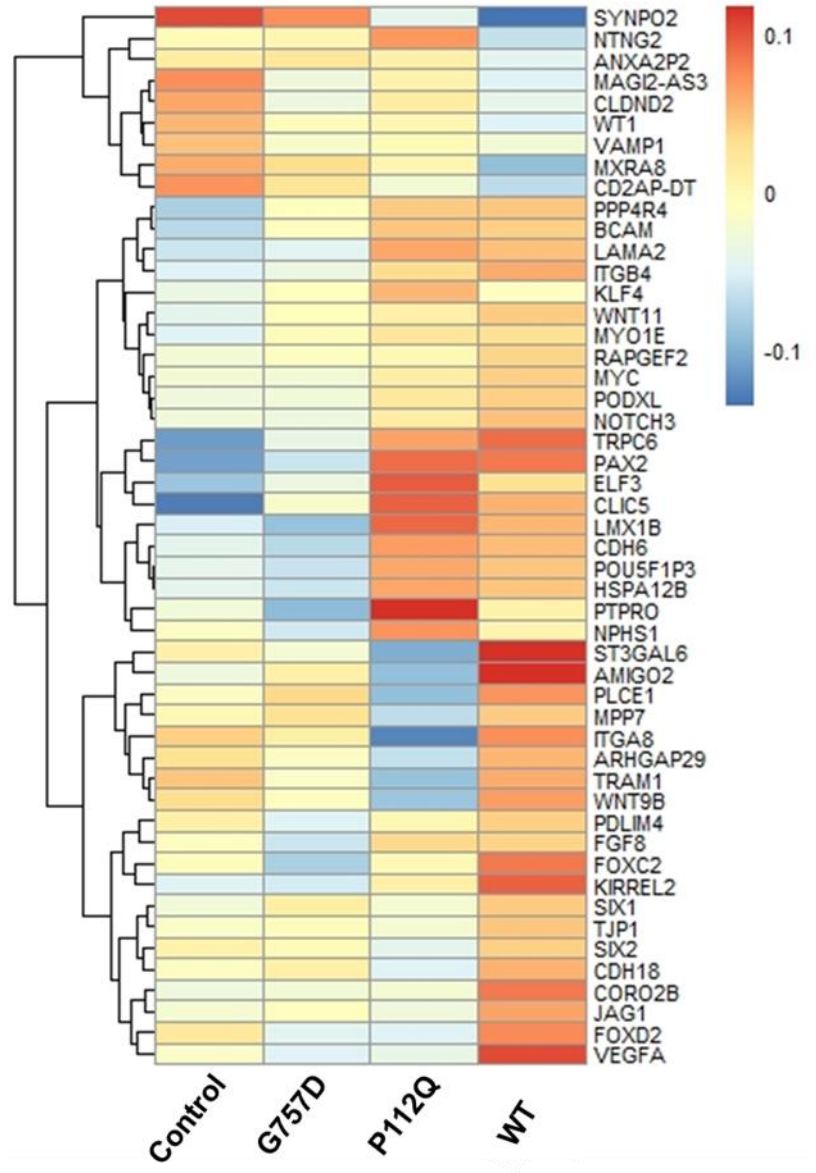

Figure 28: Heat map showing the onset of podocyte developmental genes on day 14. Analysis of podocyte developmental transcription factors on day 14 at RNA level

Furthermore, the ultrastructure of the podocytes on day 14 was visualized by scanning electron microscopy (SEM) and transmission electron microscopy (TEM). SEM revealed the development of primary and secondary foot processes while the adjacent interdigital processes are connected by molecular complexes known as slit diaphragms (Figure 29A) (Andersen et al., 1987). TEM images of the podocyte revealed a well-developed golgi apparatus, several endoplasmic reticulum structures, and mitochondria dispersed throughout the cell. Podocytes were equipped with numerous large lysosomes

at various stages of development (Figure 29B). In addition, the functionality of podocytes is demonstrated by endocytosis of albumin-FITC on day 14 (Figure 29C).

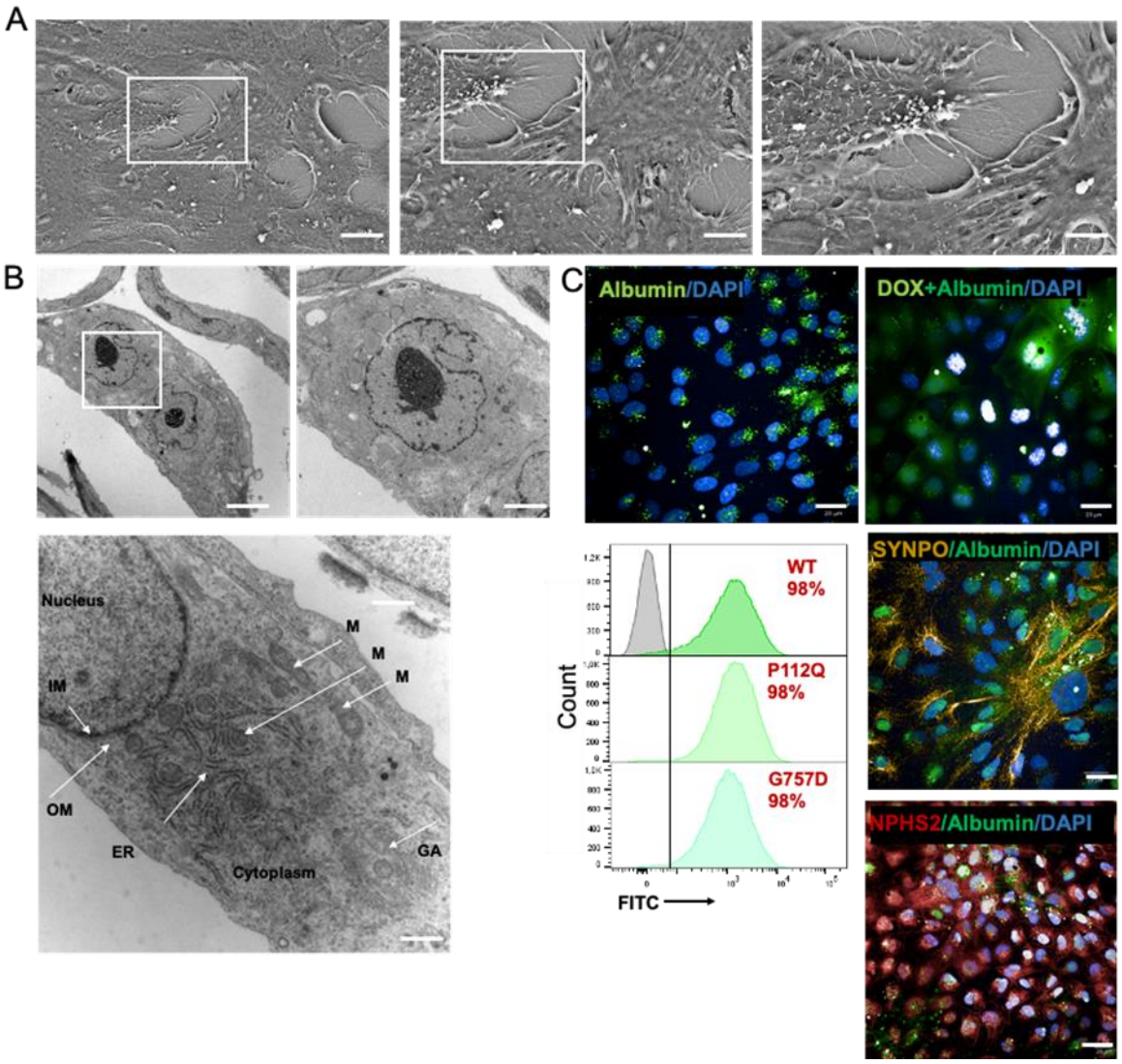

Figure 29: Human TRPC6 iPS-derived podocytes exhibit primary and secondary cell processes and albumin endocytosis. (A) Scanning electron microscopy (SEM) images of podocytes at day 14. Scale bar= 2µm**. (B)** Transmission electron microscopy (TEM) images of podocytes of day 14. (IM) Inner membrane, (OM) outer membrane, (ER) endoplasmic reticulum, (M) mitochondria, and (GA) golgi apparatus. Scale bar 1000nm. **(C)** The functionality of podocytes, top panel, marked by no Dox and Dox-induced endocytosing albumin-FITC, Bottom panel, marked by NPHS2 (red), SYNPO (yellow) endocytosing albumin-FITC. Flow cytometry analysis of albumin-positive TRPC6 mutant podocytes. Scale bar 20µm.

4.3.1.1 Reduced expression of TRPC6 after overexpressing rtTA in a GSH locus

To test the applicability of the applied GSH platform for the induction of TRPC6 transgenes, cells were treated with Dox in a chemically defined medium on alternate days according to the differentiation protocol. GFP indicating TRPC6 expression decreased

from 99% of the cells on day 0 (undifferentiated hiPSC) to 70% of cells on day 14 (differentiated podocytes) (Figure 30). To exclude a negative feedback effect due to continuous expression during the differentiation process, transgene induction was limited to the last differentiation phase. However, the same phenomena were observed when iTRPC6 expression was induced by Dox only on day 12 to visualize the TRPC6 expression on day 14. Accordingly, TRPC6-GFP protein expression in the induced state (+ Dox) was confirmed by immunoblotting (Figure 31). However, the TRPC6-GFP protein expression also decreased on day 14 compared to day 0.

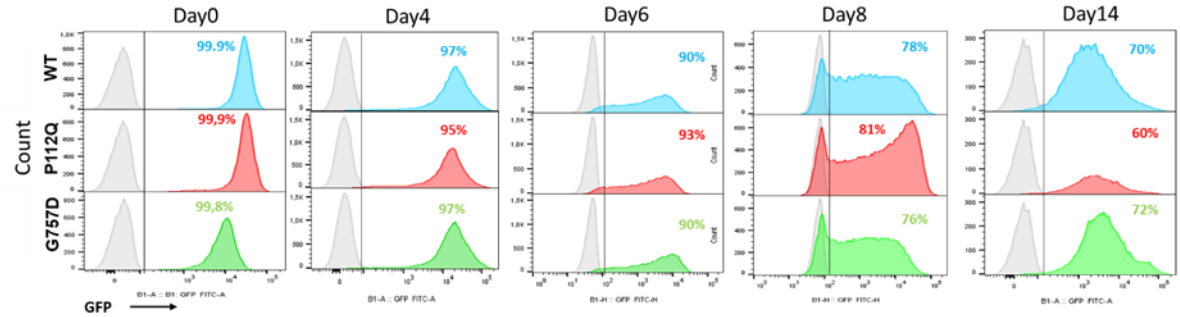

Figure 30: Flow cytometry analysis of hiPSCs-iTRPC6 EGFP for the expression of GFP signals on the alternative days of podocyte differentiation. WT: wild-type, P112Q (gain of function), and G757 (loss of function) TRPC6 mutants show a decrease in TRPC6-GFP expression on day 14 compared to day 0, day 4, day 6 and day 8.

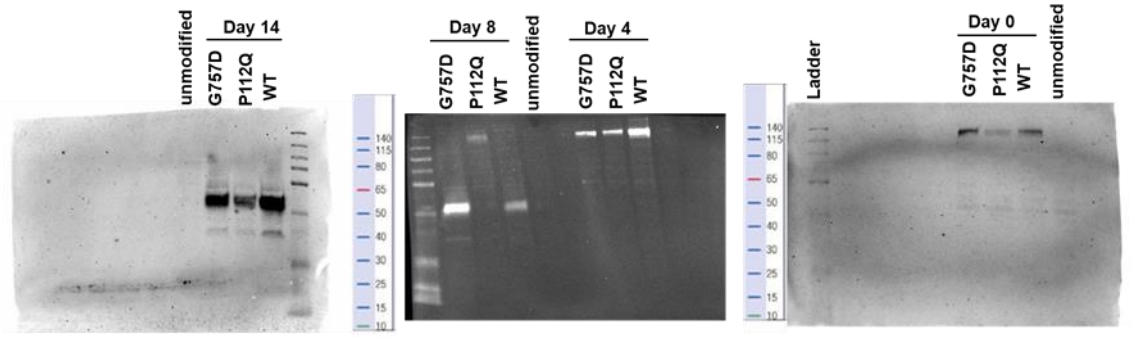

Figure 31: Western blot performed on day 0, day 4, day 8, and day 14. WT: wild-type, P112Q (gain of function), and G757 (loss of function) TRPC6 mutants show a normal protein expression on day and day 4 of the podocyte differentiation while TRPC6 protein expression was degraded on day 8 and day 14. Unmodified: un-transfected cells.

4.3.2 Ca^{2+} influx measurements on iPodocytes

The generated iPodocyte model was used to measure TRPC6 activity in response to Carbachol, an activator of the TRP channel. iTRPC6 P112Q (GOF) showed increased Ca^{2+} influx compared to the iTRPC6 wild-type podocytes whereas G757D (LOF) expressing cells showed decreased Ca^{2+} influx compared to wild-type and P112Q (Figure 32 A). Furthermore, Ca^{2+} influx was measured in response to 1, 2-dioctanoyl-sn-glycerol (DOG), a direct activator of TRPC6 channel. iTRPC6 wild-type and P112Q showed a small and insignificant signal amplitude, indicating that DOG was unable to stimulate the TRPC6 activity. This may be due to gene silencing during the differentiation protocol in the majority of the hiPSC-derived podocytes (Figure 32C). No channel activity was detected in the G757D (LOF) expressing cells. In addition, Ca^{2+}-influx was measured in TRPC6 wild-type, P112Q, and G757D mutants upon the addition of the TRPC6 channel inhibitor SAR7334 (Maier et al., 2015). Pretreatment of TRPC6-expressing cells with SAR7334 for 10 min showed a significant response to Carbachol-induced Ca^{2+} influx and no signal amplitude to DOG-induced Ca^{2+} influx in fura-2-loaded cells (Figure 32B, D), indicating that the antagonist did not block the TRPC6 channel activity in the iPodocytes.

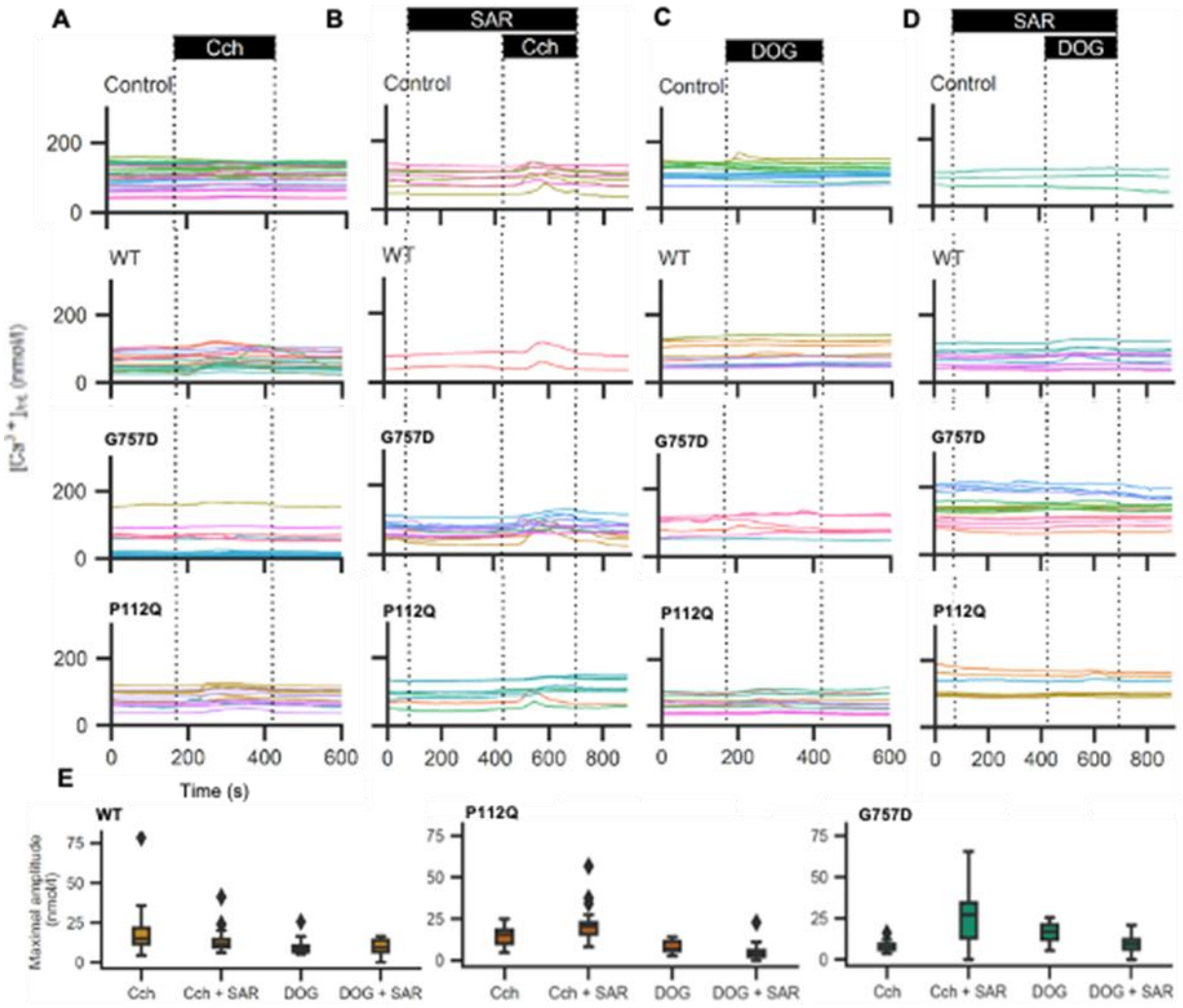

Figure 32: Functional characterization of disease-related TRPC6 mutations in Ca2+ influx measurement. Changes in intracellular Ca^{2+} concentration were measured in Fura-2 AM loaded ipodocytes expressing wild-type (WT), P112Q, and G757D treated with Dox (0.5µg/ml) 24h before measurement and control cells without genetic modification. **(A)** Carbachol (Cch: 100 µM): Cch was added about 3 min after the start of the measurement for approximately 5 min. **(B)** Effects of TRPC6 blocker SAR7334 (SAR; 100 µM) are observed in each TRPC6 mutant. **(C)** DOG (100 µM) was added about 3 min after the start of the measurement for approximately 5 min. **(D)** Effects of SAR7334 (SAR; 100 nM) were observed in each TRPC6 mutant. **(E)** Box plots show differences in the amplitude of the responses of TRPC6 wild-type, P112Q, and G757D-expressing podocytes.

4.3.3 Proximal tubular epithelial cells (PTEC)

To further explore the renal-specific differential potential of the generated iTRPC6 lines for the forward programming of hiPSCs, I focused on generating PTEC (Hariharan et al., 2019; Ngo et al., 2022). To obtain this particular cell type, the renal vesicle-like cells obtained on day 8 were collected and seeded at a cell density of 10,000 cells/cm^2 on a well in the presence of renal epithelial growth medium (REGM). After 6 days of continuous culture in REGM, the cells showed a heterogeneous appearance, with the presence of

several tubular epithelial cells (as shown in Figure 33). In particular, the expression of proximal tubular markers such as Na+/K+-ATPase, AQP1, and SGLT2 became evident by day 14. The presence of these markers, Na+/K+-ATPase, AQP1, and SGLT2, confirmed that these cells had adopted a phenotype similar to PTECs (Figure 33).

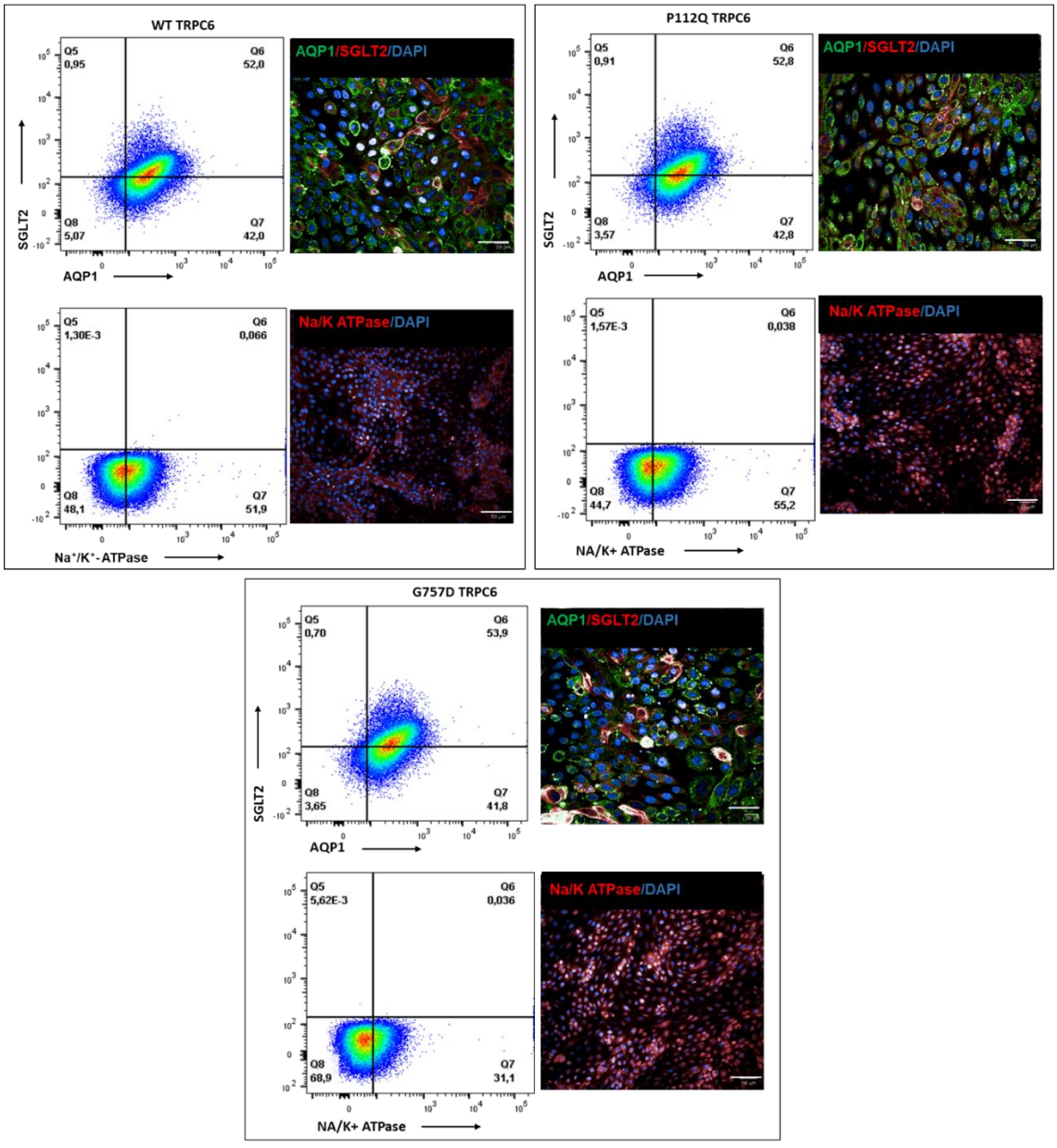

Figure 33: Efficiency of hiPSC-derived PTEC. Flow cytometry analysis and fluorescence microscopy of PTEC on day 16 expressing AQP1, SGLT2, and Na^+/K^+- ATPase markers.

4.3.4 Differentiation of transgenic TRPC6 cells to cardiomyocytes (CM)

During podocyte differentiation, transgene silencing hindered the TRPC6 expression, so I wanted to generate CM to assess whether TRPC6 transgene silencing is podocyte-specific or a general differentiation phenomenon. TRP channels are

ubiquitously expressed in various cell types of the cardiovascular system. TRPC6 has been detected in the sinoartrial nodal cells and cardiomyocytes (Kuwahara et al., 2006; Yue et al., 2015). The generated iTRPC6-EGFP cell lines were differentiated into cardiomyocytes by adapting the protocol from the Conklin Laboratory (Allen Institute for Cell Science, 2018). Briefly, iTRPC6-EGFP cell lines were subjected to WNT activation (by addition of CHIR99021) for 48h, followed by a WNT off-phase influenced by the addition of a WNT inhibitor (IWR-2) for 48h, which is crucial for cardiac specification of hiPSC. The cells began to contract (beat) on day 6. These cardiomyocytes were assessed by flow cytometry on day day8 and showed approximately 95% cardiac troponin (cTNT) marker of cardiomyocytes (Figure 34). Titration of cell seeding density and CHIR99021 concentration was necessary for the proliferation of this cell line. A reduced GFP expression was analyzed on day 8 compared to day 0 of the differentiation procedure (Figure 34C). Similarly, TRPC6 GFP protein expression in the induced state (+ Dox) was confirmed by immunoblotting on day 8 (Figure 34D). The blot analysis showed a decreased protein expression compared to day 0.

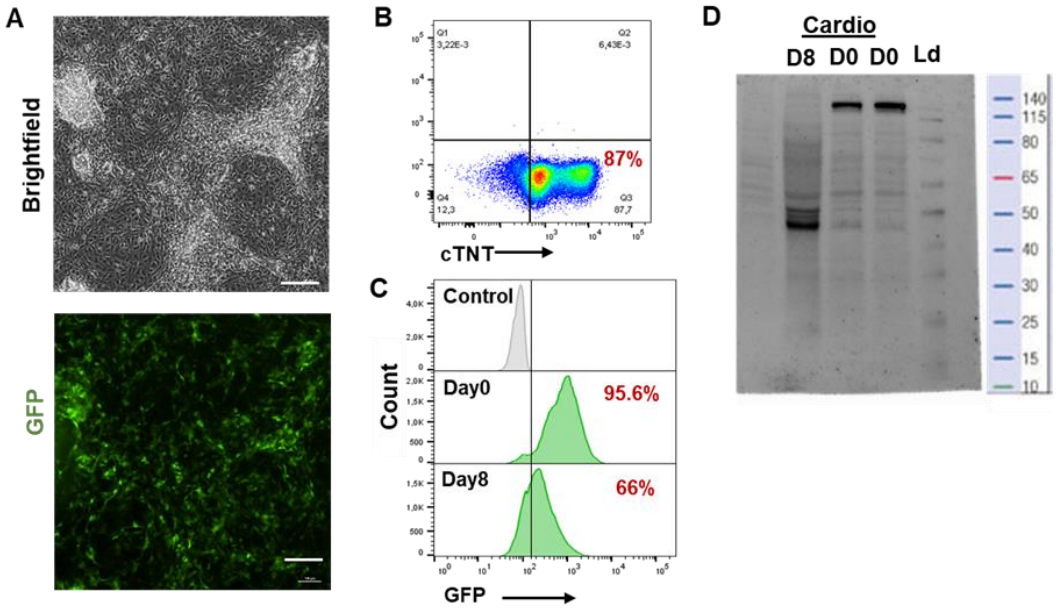

Figure 34: Efficiency of hiPSC-derived cardiomyocytes. **(A)** Day 8 cardiomyocytes shown in bright field, and Dox-induced GFP expression. **(B)** Flow cytometric analysis of day 8 cells for cTNT cardiomyocyte marker**. (C)** Flow cytometry analysis of hiPSCs-iTRPC6 wild-type cells for the o GFP signal expression at day 0 and day 8 of cardiac differentiation. **(D)** Western blot analysis of hiPSCs-iTRPC6 wild-type cells for the TRPC6 protein expression at day 0 and day 8 of cardiac differentiation.

4.4 Development of a personalized glomerulus model

The use of iPSC-derived cells provides the opportunity to personalize cell-based models. To study the role of podocytes in glomerular diseases such as FSGS, I developed a personalized glomerulus model, that recapitulates the human kidney glomerular capillary wall. hiPSC-derived podocytes were co-cultured with a layer of human primary endothelial cells to form a functional endothelium-podocyte interface useful to study glomerular filtration function and podocyte damage. Here, I used a multi-organ tissue flow (MOTiF) microfluidic chip to culture podocytes and endothelial cells recapitulating the capillary wall (Figure 35D).

To form the epithelial podocyte layer, iTRPC6 lines were differentiated on culture plates until day 8. The cells were then harvested and reseeded into the lower chamber of the biochip, followed by further differentiation into podocytes. HUVECs were seeded in the upper chamber to mimic the endothelial circuit of the glomerular wall of the kidney. Brightfield microscopy of the upper and lower chambers of the chip showed a uniform monolayer of iTRPC6-derived podocytes and endothelial cells in their respective channels (Figure 35C). To determine the maturation state of the podocytes, the lower chamber was immunostained with podocyte-specific markers; NPHS2, SYNPO, and PODXL. The arborized network of podocytes on the biochip closely resembled the structure of the glomerular filtration barrier (Figure 35C).

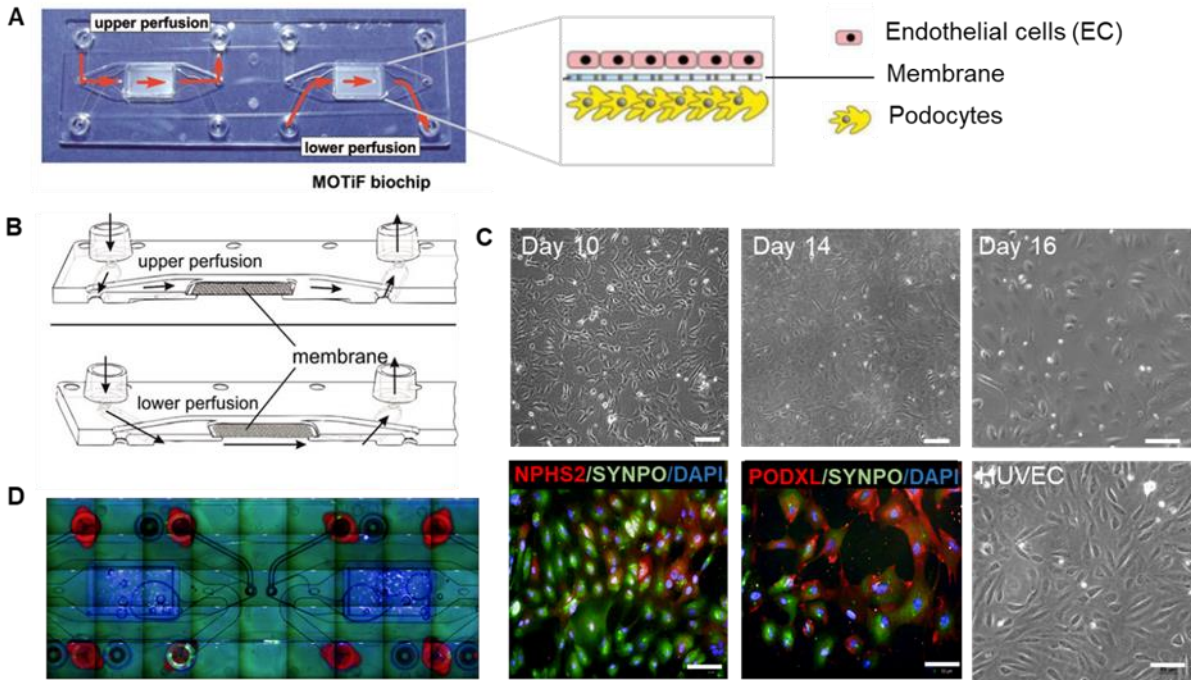

Figure 35: MOTiF biochip design and chamber flow. **(A,** and **B)** Design of two-dimensional perfused flow chambers, with two channels, each containing a porous membrane serving as a cell culture area. Cultured cells on the membrane can be perfused independently from both the apical and basal sides through upward-directed (Upper perfusion) and downward-directed (lower perfusion) chambers. Adapted from Raasch et al. 2015. **(C)** Differentiated iTRPC6 podocytes cultured on the lower compartment and endothelial cells (iEC) cultured on the upper compartment of the MOTiF biochip until day 16. The lower panel shows immunofluorescence staining of podocyte markers expressing: NPHS2, SYNPO, and PODXL. **(D)** MOTiF biochip showing cultured podocytes stained with DAPI.

4.5 Toolbox for patient-derived iPSC reprogramming and differentiation

In this thesis, I have reprogrammed four hiPSC lines, including a healthy donor and three different patients with genetic predisposition that includes FSGS (Batool et al., 2023), polycystic kidney disease (PKD) (Batool et al., 2023), and neurofibromatosis type 1 (NF1) (Batool et al., 2023). These lines are available and registered in the human pluripotent stem cell registry (hPSCreg) and are available through the European bank for induced pluripotent stem cells (EBiSCs) (Table 9). The hiPSC-derived FSGS cell line (BCRTi006-A) was further differentiated into podocytes to verify that they were phenotypically comparable to podocytes derived from healthy donor iPSC lines.

4.5.1 Generation of hiPSC lines from a patient carrying FSGS disease (BCRTi006-A) and a patient with ADPKD (BCRTi007-A)

The results of the presented work have been published by Batool et al. (2023). Urinary cells from an FSGS patient carrying a mutant variant of TRPC6 (V691Kfs*) and

an ADPKD patient were isolated, expanded (T. Zhou et al., 2012) and reprogrammed into hiPSC under feeder-free conditions using episomal vectors (OCT3/4, SOX2, LIN28, L-MYC, and KLF4). Cells were maintained under culture conditions as shown in Figure 36A. Multiple colonies appeared on day 19 and were individually picked and sub-cultured on day 25 of reprogramming. The derived hiPSC line was named as BCRTi006-A and BCRTi007-A and was subsequently characterized. When maintained in Essential E8 medium, the cells exhibited a typical morphology of undifferentiated hiPSC (Figure 36B and 37A). The cell line no longer exhibited episomal vectors at passage 6 of BCRTi006-A and passage 9 of BCRTi007-A (Figure 36E and 37B) and were subsequently expanded into a master cell bank. After vector loss, immunofluorescence staining was performed, which revealed the expression of stem cell markers, namely, octamer-binding transcription factor 3/4 (Oct3/4), tumor rejection antigen (Tra-1–60), stage-specific embryonic antigen 4 (SSEA4), sex-determining region Y-box 2 (SOX2), and NANOG confirming the pluripotency of the derived hiPSC lines (Figure 36C and 37C). A high number of pluripotency markers were detected within the hiPSC lines by flow cytometry analysis (Figure 36D and 37D). The differentiation potential of these cell lines into three germ layers was assessed *in vitro* by embryoid body formation (Figure 36F and 37E). RT-PCR was performed to detect the markers of ectoderm (NESTIN and NEUROD1), mesoderm (brachyury and MIXL1), and endoderm (gooscoid and SOX17). Furthermore, a normal karyotype was conducted for each cell line using SNP analysis. Short tandem repeat (STR) analysis confirmed the authenticity of each cell line using 16 genomic loci including AMEL, CSF1PO, TPOX, D16S539, D18S51, D3S1358, D5S818, D7S820, D13S317, D8S1179, D21S11, FGA, Penta_E, TH01, Penta_D, vWA. Identical DNA profiles were observed between the patient's urinary cell and the generated hiPSC line (Tables 15 and 16). Both hiPSC lines were negative for mycoplasma contamination and human immunodeficiency virus 1 and 2 (HIV 1 + 2), hepatitis B, and hepatitis C.

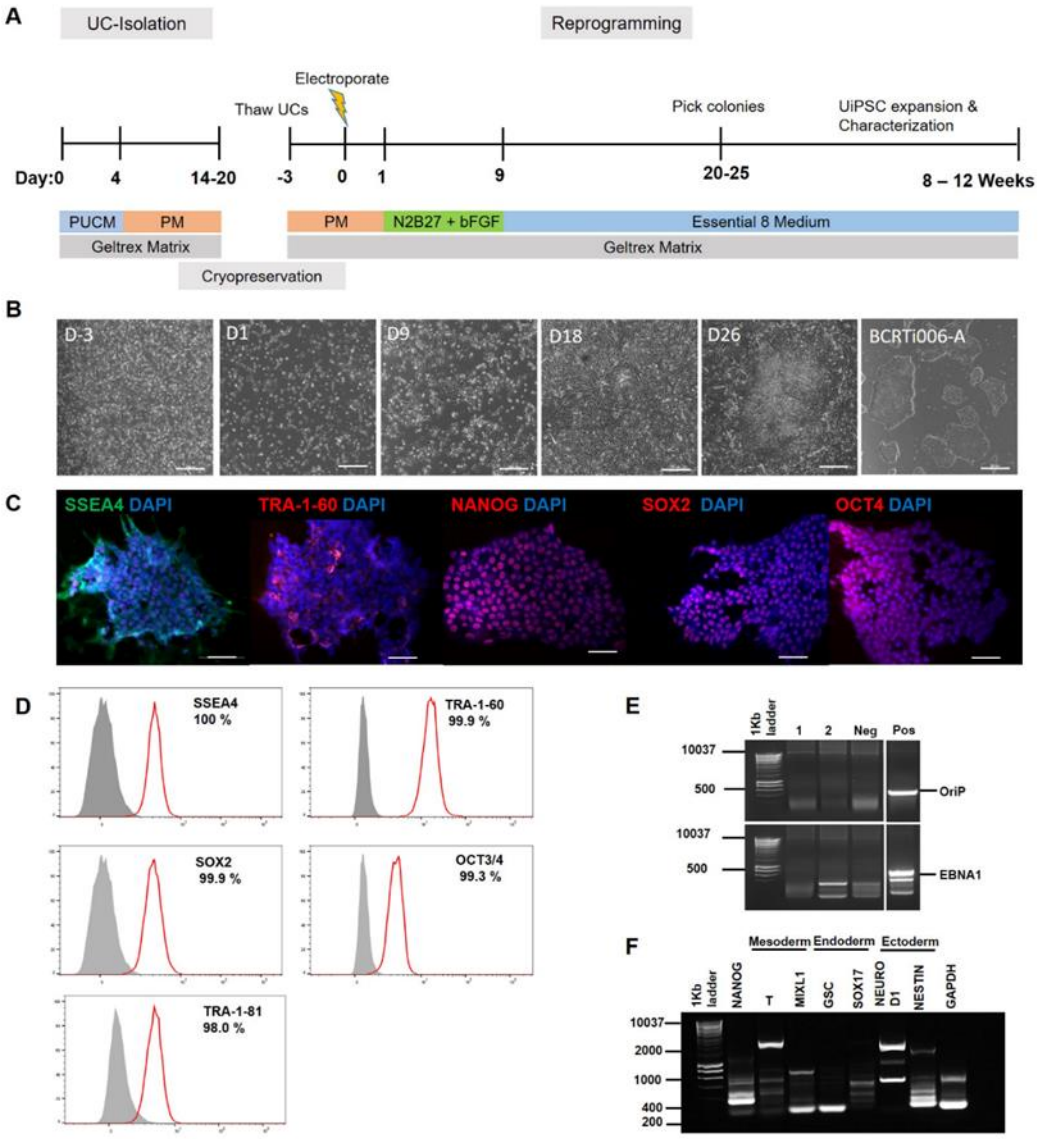

Figure 36: Generation and characterization BCRTi006-A. **(A)** Scheme of urinary cell (UC) isolation and hiPSC generation protocol: PUCM, primary UC medium, PM, proliferation medium. **(B)** Proliferation of cells before and after electroporation at different day points until hiPSC colony emerged (scale bar 100µm). **(C)** Immunostaining for stem cell markers (scale bar 100µm). **(D)** Flow cytometry analysis showing stem cell expressing cells **(E)** PCR check for episomal reprogramming vector loss: clone 1 and 2, Neg: negative control (DNA form BCRTi005-A cells), Pos: positive control (DNA from early passage 2 of BCRTi006-A). **(F)** RT-PCR to verify the expression of ectoderm (NESTIN and NEUROD), mesoderm (brachyury and MIXL1), and endoderm (goosecoid and SOX17) markers. Adapted from (Batool et al. 2023)

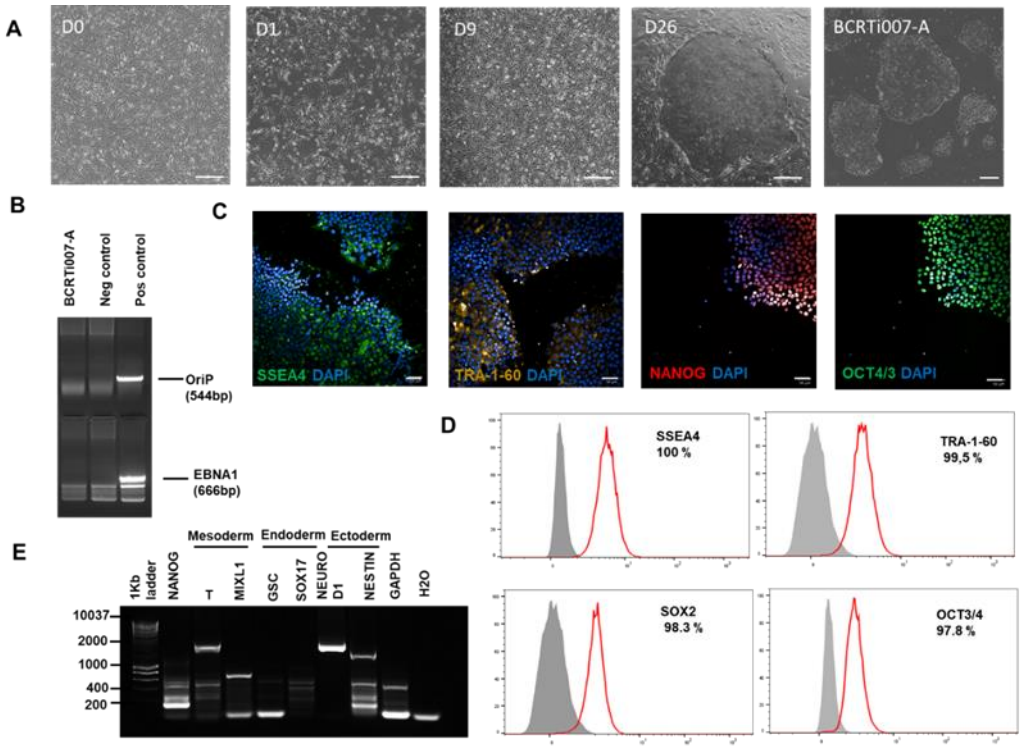

Figure 37: Generation and characterization BCRTi007-A. **(A)** Proliferation of cells before and after electroporation at different day points until hiPSC colony emerged (scale bar 100µm). **(B)** PCR check for episomal reprogramming vector loss: clones 1 and 2, Neg: negative control (DNA form BCRTi005-A cells), Pos: positive control (DNA from early passage 2 of BCRTi006-A). **(C)** Immunostaining for stem cell markers (Scale bar 100µm). **(D)** Flow cytometry analysis showing stem cell expressing cells. **(E)** RT-PCR to check marker expression in three germ layers. Adapted from (Batool et al., 2023)

Table 15: Result of STR analysis BCRTi006-A

Marker Name	Donor Primary cells	BCRTi006-A
AMEL	X	X
CSF1PO	11, 12	11, 12
D13S317	8, 12	8, 12
D16S539	11, 12	11, 12
D18S51	14	14
D21S11	28, 32.2	28, 32.2
D3S1358	16, 18	16, 18
D5S818	9	9
D7S820	12	12
D8S1179	12	12

Marker Name	Donor Primary cells	BCRTi006-A
FGA	22, 24	22, 24
Penta_D	9, 13	9, 13
Penta_E	5, 20	5, 20
TH01	6, 9.3	6, 9.3
TPOX	8, 11	8, 11
vWA	17, 18	17, 18

Table 16: Result of STR analysis BCRTi007-A

Marker Name	Donor Primary cells	BCRTi007
AMEL	X	X
CSF1PO	11	11
D13S317	10,14	10,14
D16S539	11	11
D18S51	13, 15	13, 15
D21S11	28, 31	28, 31
D3S1358	16, 18	16, 18
D5S818	9, 11	9, 11
D7S820	10, 11	10, 11
D8S1179	10, 13	10, 13
Penta_D	12, 13	12, 13
Penta_E	12,15	12, 15
TH01	9, 9.3	9, 9.3
TPOX	10, 12	10, 12
vWA	15, 18	15, 18
FGA	21, 22	21, 22

4.5.1.1 Podocyte differentiation of BCRTi006-A

One of the main goals of my research was to compare podocyte function in the presence of TRPC6 mutants. This require developmental homology between hiPSC lines carrying the mutated genes and normal hiPSC lines. Therefore, I differentiated patient-

derived FSGS hiPSCs, the synthetic hiPSC lines carrying TRPC6 GOF and LOF genes, and healthy control hiPSCs into podocytes. Podocytes derived from BCRTi006-A expressed podocyte markers (PODXL, SYNPO, and podocin) on day 14 (Figure 38). However, the endocytosis of albumin-FITC in these cells showed a lower uptake of albumin as compared to a healthy (BCRTi005-A) cell line (Figure 38). The data show that BCRTi006-A cells can produce podocytes similar in morphology to those from healthy cells, but that the disease genotype selectively impairs aspects of podocyte functionality. In particular, the hiPSC line carries a truncated TRPC6 mutation (V691Kfs*), which may be a reason for the improper endocytosis process. Further studies are needed to characterize the functional properties of BCRTi006-A.

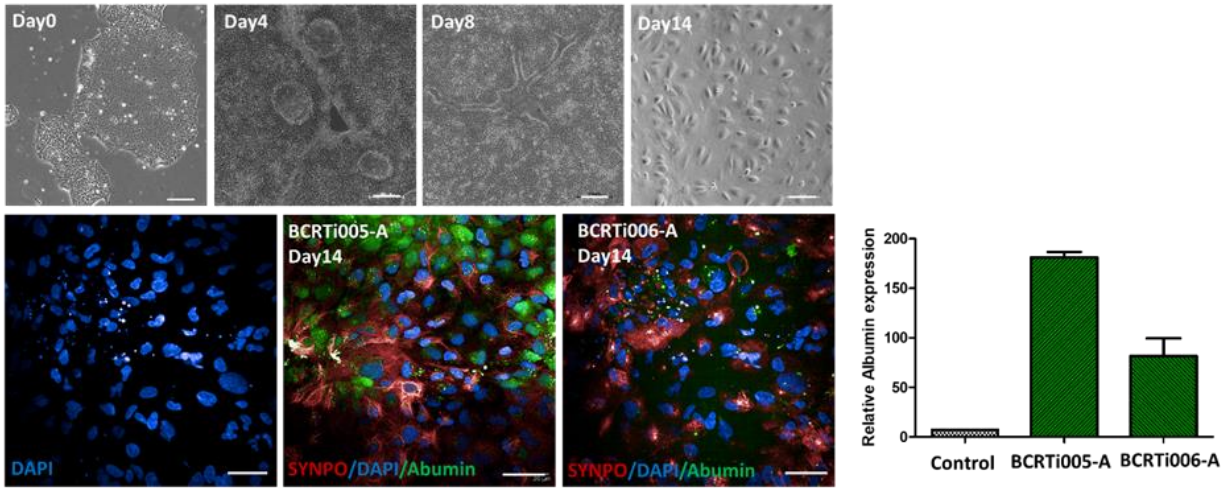

Figure 38: Podocyte differentiation of BCRTi006-A. Endocytosis of Albumin-FITC in BCRTi006-A-derived podocytes. Sclae bar: 500µm, 20µM

4.5.2 Generation of two hiPSC lines from a patient with neurofibromatosis type 1 (NF1) with the pathogenic variant p.Y489C (c.1466 A>G) in the *NF1* gene (BCRTi011-A) and a first degree healthy relative (BCRT010-A)

Like FSGS and ADPKD, neurofibromatosis type 1 (NF1) is a rare disease. NF1 is characterized by an inherited tumor predisposition that develops in the brain and spinal cord with multiple neoplastic abnormalities in neural crest derived tissues. It has an incidence of 1/2000 to 1/5000 in most population-based studies. NF1 is inherited as an autosomal dominant trait, with approximately 50% of affected individuals carrying pathogenic germline variants in the *NF1* gene at 17q11.2. Skeletal malformations, cognitive deficits, brain tumors, malignant peripheral nerve sheath tumors (MPNST), and

other malignancies have been significantly associated with NF1 patients (Uusitalo et al., 2016). No curative therapy has yet been developed for patients with this genetic disorder.

The results of the presented work were published in Batool et al. (2023). Reprogramming of peripheral blood mononuclear cells (PBMCs) from an NF1 patient and a healthy relative was performed using episomal vectors. The generated hiPSC lines (BCRTi010-A and BCRTi011-A) showed the typical morphology of undifferentiated hiPSC maintained in E8 medium (Figure 39A). The absence of episomal vectors was confirmed by RT-PCR in BCRTi010-A at passage 10 and in BCRTi011-A at passage 12 (Figure 39E). The pluripotency of the derived hiPSC lines was confirmed by the detection of OCT3/4, NANOG and SOX2, TRA-1-60, and SSEA4 by fluorescence microscopy (Figure 39B). Flow cytometric analysis revealed the expression of pluripotency markers (Figure 39C, D). Embryoid bodies were generated to demonstrate the potential pluripotency differentiation of both lines by differentiating into endodermal (goosecoid, Sox17), mesodermal (brachyury and MIXL1), and ectodermal cells (NESTIN and NEUROD) as confirmed by RT-PCR (Figure 39F). Normal karyotypes were observed when tested by SNP analysis. The authenticity of both hiPSC lines was confirmed by short tandem repeat (STR) analysis of 16 genomic loci including, AMEL, D13S317, D16S539, CSF1PO, D18S51, D3S1358, D5S818, D21S11, D7S820, vWA, D8S1179, FGA, Penta_E, TH01, Penta_D, TPOX. The patient's PBMCs and the generated hiPSC line showed identical DNA profiles (Tables 17 and 18). Moreover, mycoplasma contamination and HIV 1 + 2, hepatitis B, and hepatitis C tests were negative for both the iPSC lines. After characterization, cells were expanded and cryopreserved in a master cell bank.

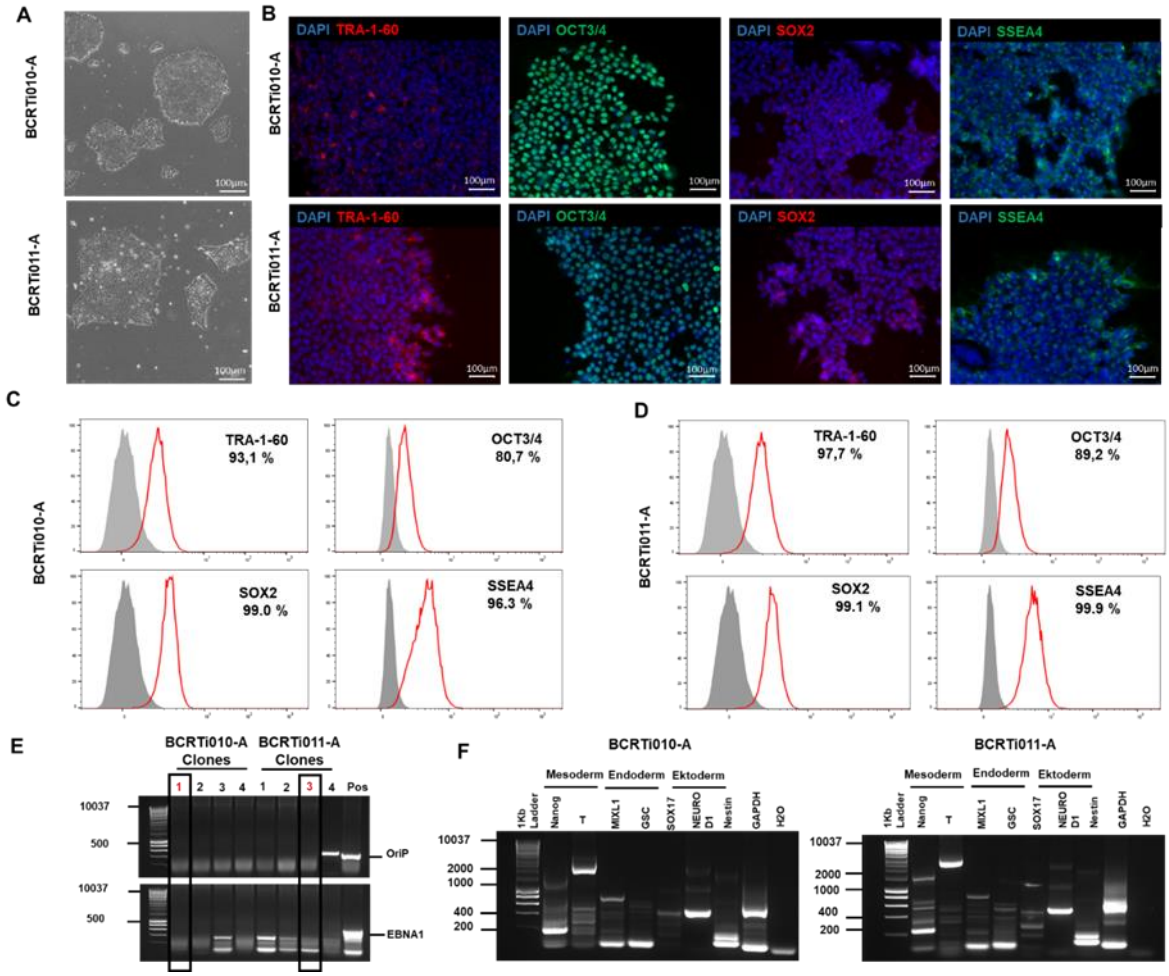

Figure 39. Characterization of BCRTi010-A and BCRTi011-A. (A) hiPSC colonies (scale bar 100µm). **(B)** Immunostaining for stem cell markers (scale bar 100µm). (**C** and **D)** Flow cytometry analysis showing stem cell expressing cells. **(E)** PCR check for episomal reprogramming vector loss: clone 1 of BCRTi010-A and clone 3 of BCRTi011-A were selected for further characterization; negative control (DNA form BCRTi005-A cells), Pos positive control (DNA from early passage 2 of BCRTi010-A). **(F)** RT-PCR to verify the marker expression of three germ layers. Adapted from (Batool et al. 2023)

Table 17: Result of STR Analysis of BCRTi010-A

Marker Name	Donor Primary cells	BCRTi010-A
AMEL	X	X
CSF1PO	11, 12	11, 12
D13S317	11, 12	11, 12
D16S539	12	12
D18S51	15	15
D21S11	28, 29	28, 29
D3S1358	17	17

Marker Name	Donor Primary cells	BCRTi010-A
D5S818	12	12
D7S820	9, 10	9, 10
D8S1179	10, 13	10, 13
FGA	19, 24	19, 24
Penta_D	11, 12	11, 12
Penta_E	7	7
TH01	6, 7	6, 7
TPOX	8, 10	8, 10
vWA	17, 19	17, 19

Table 18: Result of STR Analysis of BCRTi011-A

Marker Name	Donor Primary cells	BCRTi011-A
AMEL	X, Y	X, Y
CSF1PO	12	12
D13S317	8, 11	8, 11
D16S539	11, 12	11, 12
D18S51	15	15
D21S11	29	29
D3S1358	14, 17	14, 17
D5S818	12	12
D7S820	9	9
D8S1179	13	13
FGA	21, 24	21, 24
Penta_D	11	11
Penta_E	7, 12	7, 12
TH01	7, 9.3	7, 9.3
TPOX	8, 10	8, 10
vWA	17	17

5 DISCUSSION

5.1 A hitherto narrative of FSGS

Proteinuria is a hallmark of FSGS and it occurs due to the disruption of the glomerular filtration barrier. This barrier controls the selective permeability of substances through close interactions between fenestrated endothelial cells, glomerular basement membrane, and podocytes (D'Agati, 2008). Approximately 10% to 40% of FSGS cases are genetic, resulting in podocyte damage leading to the effacement of podocyte foot processes (Miao et al., 2021). This effacement is a major structural change associated with nephrotic proteinuria (D'Agati, 2008).

Since the identification of nephrin as the major component of the slit diaphragm in 1998 (Kestilä et al., 1998; Ruotsalainen et al., 1999), the number of identified proteins involved in familial and sporadic FSGS has increased. Mutations in genes encoding for various podocyte-specific proteins affect the actin cytoskeleton, slit diaphragm, cytosol, plasma membrane, nucleus, mitochondria, and lysosomes (Bierzynska et al., 2014). However, one of the most recent advances in familial FSGS has been the discovery of a mutant variant of TRPC6 in a large New Zealand kindred by Winn et al. (2005). This mutation follows an autosomal dominant inheritance pattern and is associated with an exceptionally aggressive form of the disease. It is characterized by high-grade proteinuria, ultimately leading to end-stage renal disease in 60% of affected individuals. Further studies using Calcium measurements showed that this mutation leads to a GOF effect, resulting in increased Calcium transients and the mislocalization of the ion channel on the podocyte cell membrane (Winn et al., 2005). Notably, this was the first time that an ion channel mutation was linked to the development of FSGS. In addition, research from other scientific groups has contributed to the expanding spectrum of diseases associated with abnormal Calcium homeostasis, particularly due to mutations in the TRPC6 channel.

In the present study, a new TRPC6 mutation V691Kfs* was reported, which leads to the production of a largely truncated TRPC6 protein. Furthermore, I developed cell models to assess the effect of GOF and LOF mutations in TRPC6 on Calcium transients. These models were designed to directly analyze whether TRPC6 mediated Calcium transients lead to podocyte damage. Furthermore, the correlation of the data obtained

from these cell models was used to exclude loss of Calcium channel function as a cause for the development FSGS.

5.2 Proof of concept: TRPC6-related FSGS mutant analysis

I have described and characterized a novel TRPC6 variant V691Kfs* in a large kindred with no signs of FSGS-related pathology. The characterization was performed along with two other TRPC6 variants P112Q (GOF) and G757D (LOF). The novel heterozygous TRPC6 frameshift mutation encodes a truncated TRPC6 protein lacking the intracellular cytosolic C-terminal tail, a highly conserved domain that plays a significant role in the TRPC6 channel activity, and results in an exchange of valine-to-lysine at amino acid position p.691. The cryo-EM structure of TRPC6 protein resolved at 4.36Å, which provides information on ion channel structures, shows that V691Kfs* is located in the pore-opening region of the tetrameric channel complex. The truncation introduced by V691Kfs* is predicted to cause a complete closure of the ion-conducting pore, resulting in a dominant downstream loss of Calcium ions, consistent with a LOF channel phenotype. To substantiate this hypothesis, my study showed that this mutant manifests channel activity below the activation level of wild-type TRPC6, P112Q (GOF), and even lower than the previously described G757D (Riehle et al., 2016) (LOF) mutation, confirming an inactive TRPC6 channel. Pedigree analysis of kidney disease in the index family showed that despite the presence of the truncated FSGS mutant across generations, kidney function is normal. This finding together with my *in vitro* cell data therefore argue against the loss of TRPC6 function as a generalized concept of hereditary FSGS in humans (Batool et al., 2023).

TRPC6 gene is mainly expressed in the podocytes of the glomeruli. The membrane topology and structural domain of TRPC6 shows a cytosolic N-terminus consisting of 4 ankyrin repeats (AR), a C-terminus, and 6 TM domains with an ion channel pore opening at TM 5 and 6 for ion transport. Multiple sequence alignment studies revealed that all the identified TRPC6-related mutations are located in these highly conserved regions. In addition, *in-silico* analysis revealed that these mutations have damaging effects that adversely affect protein function (Guo et al., 2022; Guo & Chen, 2019; Jardin et al., 2020; Tang et al., 2018). A structural study of the TRPC6 channel by Tang et al. (2018) showed that the truncation of N-terminal amino acids 1-71 did not affect the tetramer assembly. This suggests that the flexible N-terminal 71 residues are not necessary for TRPC6 gating

and assembly. On the other hand, 4 ankyrin repeats (residues: 96-243) and subsequent linker helices (residues: 256-393) form a major structural component of the intracellular cytoplasmic domain as shown in Figure 40. At the cytoplasmic C-terminus of TRPC6, the amino acids folds into two long helices, C-terminal helix 1 (CH1) and C-terminal helix 2 (CH2). These sites are the binding sites for inositol hexaphosphate (IP6, 842-868), calmodulin and IP3 receptor binding regions (838-872). Calmodulin and IP3 receptors are the crucial binding sites for modulating TRPC6 channel activity (Tang et al., 2018). Deletion of the entire CH2 helix (901-931) do not disrupt the TRPC6 assembly and gating (Tang et al., 2018), however, when the entire CH2 was deleted alongside CH1-CH2 linker (878-931), it was observed that the entire assembly of the tetrameric TRPC6 channel was largely disrupted (Boulay, 2002; Kwon et al., 2007).

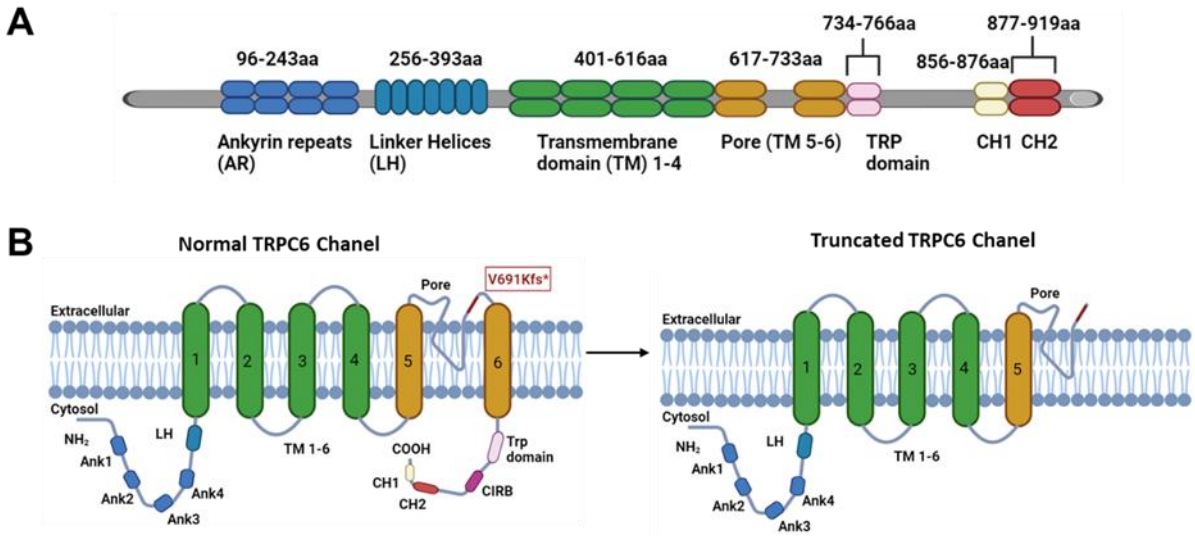

Figure 40: Membrane topology and domain structure of the TRPC6 subunit. **(A)** Linearized organization of TRPC6. **(B)** Proposed tetrameric structure of normal TRPC6 channel vs truncated TRPC6 channel in the plasma membrane. The subunit contains 6 transmembrane domains (TM) with an ion channel pore between TM 5 and 6. Structural domains for channel assembly and protein interaction sites are present at the NH_2 and COOH termini: ankyrin repeats (Ank1-4), linker helices (LH), calmodulin-IP_3R binding site (CIRB), TRPC binding site (TRP).

In my study, P112Q (GOF) is located in the N-terminal and one mutation G757D (LOF) is located in the C-terminus. So far, 10 different mutations (Hofstra et al., 2013; Mottl et al., 2013; Santín et al., 2009; Winn et al., 2005) affecting the same domains have been reported, highlighting the essential role of these domains for protein function. The novel p.V691Kfs* TRPC6 mutation identified in this study is the first mutation located in the extracellular or pore-forming TM segment 6 region of the channel. Although the majority of the mutations in the N/C terminal tails are more susceptible to acquiring the

disease phenotype, the depicted mutation in the TM-6 does not lead to any clinical (renal) phenotype. I thus conclude that the LOF TRPC6 character is not a direct cause of FSGS in humans (Batool et al., 2023).

The co-expression experiments showed that different disease-causing mutations have a negative-dominant effect on the renal channel TRPC6. This phenomenon is known for many genetic variants of different multimeric cardiac K^+, Ca^{2+}, Cl^-, and Na^+ channels, and in particular Brugada syndrome variants of $Na_v1.5$ (Sottas & Abriel, 2016). For example, epidemiological studies have shown that patients carrying KCNQ1 missense mutations with a dominant negative effect have a worse outcome than individuals with nonsense mutations leading to haploinsufficiency (Moss et al., 2007). Furthermore, if such distinct heterogeneous ion channel complexes exist in renal TRPC channels, it would be interesting to determine whether a dominant negative mutant of one type of channel affects the activity of another type of channel that affects the renal outcome. In this regard, my data support the novel concept that inhibition of TRPC6 channels, possibly in cross-talk with TRPC3 (Saliba et al., 2015), represents a promising new therapeutic approach to ameliorate renal stress-induced disease with fibrosis (E. Y. Kim et al., 2018; E. Y. Kim & Dryer, 2021; W. Kong et al., 2019; Lin et al., 2019; Wu et al., 2017; Zheng et al., 2022)

To date, two C-terminal truncated TRPC6 mutations (K874X and D873fsX878) have been identified that exhibit an autosomal dominant GOF effect (Farmer et al., 2019; Hindi & Reiser, 2011; Mottl et al., 2013; Reiser et al., 2005). However, the functional characterization of these mutants remains unclear. A family with frameshift TRPC6 mutation (D873fsX878) at the C-terminus was identified by Mottle et al. 2013, in a 34-year-old pregnant woman with minimal change disease, recalling it as an early clinical stage of FSGS with dominant GOF effect (Mottl et al., 2013). However, their argument was not supported by further *in vitro* experiments. In addition, Reiser et al. 2005 reported a TRPC6 truncated mutation (K874X) with an earlier stop codon near to the C-terminus. This mutation showed a pattern of co-segregation in disease inheritance, although with less than complete penetrance (Reiser et al., 2005). However, the identified mutation showed no changes in the current amplitude compared to the wild-type TRPC6 channels. Other reports show a delay in Calcium channel inactivation, resulting in increased channel opening associated with this mutation. (Heeringa, Ller, et al., 2009; Schlöndorff et al.,

2009). In my study, the V691Kfs* mutant showed a LOF phenotype. The Calcium imaging experiments and whole-cell electrophysiological recordings in the V691Kfs* mutant revealed a non-functional, fully inactivated TRCP6 channel, which is consistent with a complete LOF phenotype. In contrast, the functional characterization of the GOF (P112Q) variant in recombinant expression systems showed that replacement of these amino acids results in increased TRPC6 activity in this expression system by increasing Calcium influx 2-fold compared to other TRPC6 variants, linking GOF mutations to the cause of FSGS (Reiser et al., 2005; Winn et al., 2005). Nevertheless, I believe that the family pedigree featuring the V691Kfs* mutation illustrates the substantial variability in clinical presentation that can result from a single genetic mutation. The progression of kidney disease in the index patient is not consistent with the typical renal pathology associated with TRPC6-FSGS. Moreover, the histological results of the renal biopsy were not consistent with what is commonly observed in TRPC6-associated FSGS cases. In addition, although the pedigree is relatively large, only two family members, one of whom had an unknown genotype, had renal disease. This is unusual for a disease with autosomal dominant inheritance, where one would typically expect more affected individuals within the family. Finally, the pattern of the TRPC6 variant and its inheritance do not follow a pattern of co-segregation, even when taking into account the age differences among mutation carriers.

To date, the reported GOF mutations in TRPC6 channels have resulted in severe familial nephrotic syndrome with an autosomal dominant mode of inheritance. However, there have been animal studies that have shown that TRPC6 knockouts are protective in some, but not all, models of acquired forms of chronic kidney disease in animals, the most robust of which is in chronic adaptive forms of FSGS, such as that induced in rats by puromycin aminonucleoside (E. Y. Kim et al., 2018). The TRPC6 inactivation was found to have a significant protective effect on the severity of glomerular damage, particularly glomerulosclerosis. This protective effect was confirmed by semi-quantitative analysis of light microscopy (E. Y. Kim et al., 2019). In mouse models where tubulointerstitial disease developed after an initial insult due to unilateral ureteral obstruction (UUO), TRPC6 knockout showed protective effects. Specifically, it helped to mitigate the damage caused to the tubules in this context (Wu et al., 2017). Furthermore, a study conducted by Kim and Dryer showed that the LOF TRPC6 channels in rats neither improved nor worsened the overall renal function typically associated with aging. These animals also show no

reduction in inflammation or tubulointerstitial fibrosis (E. Y. Kim & Dryer, 2021). The degree of the protection is highly species and model dependent. However, the data collectively suggest that the development of TRPC6 inhibitors as therapeutic agents for nephrotic syndromes, renal fibrosis, and possibly other diseases has merits. Nevertheless, a publication appeared in 2015 showing that some of the TRPC6 mutations associated with particularly early-onset FSGS are not GOF at all (Riehle et al., 2016). In fact, at least one of them has a dominant negative effect on TRPC6 function. None of these were pore mutations, all were in parts of TRPC6 that allow it to form large complexes with other slit diaphragm proteins such as nephrin, podocin, other channels, etc. These observations had a major impact on the scientific community on drug discovery because they suggested that inhibition of TRPC6 could be pathogenic. This is why the discovery of this new mutation, V691Kfs*, is so important, as it affects the pore domain (the first to occur naturally in humans) and has a LOF, and indeed dominant-negative effects when co-expressed with wild-type TRPC6. This variant has been found in a large kindred in which there are no signs of FSGS except in the initial index patient. In other words, there may be expression of a dominant-negative form of TRPC6 without any signs of nephrosis.

Therefore, it is clear from the present study and the large amount of animal data that a loss of function TRPC6 does not inevitably lead to kidney disease. Perhaps the mutations observed by Riehle et al. (2015) cause toxicity in podocytes through some effect unrelated to its role as a channel. Perhaps its interactions with other proteins are dysregulated, thereby affecting the function or trafficking of other proteins. Farmer et al. (2019) provided clear evidence that the degradation of focal adhesion proteins, involving enzymes called calpains plays a crucial role in the development of FSGS. In this context, calpain activity was significantly reduced in TRPC6 knockout podocytes, similar to what was observed in podocytes treated with the calpain inhibitor calpeptin and in TRPC6 wild-type cells. Importantly, TRPC6 regulation of calpain activity was found to be independent of any changes in its calcium conductance (Farmer et al., 2019). Furthermore, recent reports suggest that TRPC6 activity is associated with increased activity of calpain 1 and calcineurin, both of which contribute to podocyte injury induced by puromycin aminonucleoside (Ding et al., 2016) and promote the pathogenesis of nephrotic syndrome (X. Tian et al., 2014; Verheijden et al., 2018). Other TRPC channels, such as TRPC3 and TRPC5, contribute to calcium entry in podocytes as shown by electrophysiological

studies, and are expressed in glomerular podocytes in addition to TRPC6. Greka and coworkers (Schaldecker et al., 2013) investigated the pathogenic role of TRPC5 in animal models with proteinuric kidney disease. They found that whole body knockout of TRPC5 effectively inhibited albuminuria and foot process effacement in the lipopolysaccharide-induced proteinuria model. Furthermore, their group identified a specific TRPC5 inhibitor (AC1903) that was tested in a proteinuria model induced by transgenic (TG) overexpression of the human type 1 angiotensin II receptor (AT1R) specifically in podocytes in rats (AT1R TG rats) and Dahl salt-sensitive rats. These animals are models of hypertension-induced glomerulosclerosis (Y. Zhou et al., 2017) in which AC1903 not only suppresses proteinuria but also reduces podocyte loss and improves glomerular histology. While TRPC5 and TRPC6 have been the primary focus, there is a growing evidence to suggest that TRPC3 is also an important contributor to kidney diseases (Hall et al., 2019). Like TRPC6, TRPC3 upregulation is mediated by calcineurin-dependent mechanisms in pathological processes. Notably, an increase in TRPC3 expression was observed in the renal cortex of TRPC6 knockout rats under basal conditions. Consequently, selective blockade of TRPC6 may lead to compensatory upregulation of other TRPC family members and may not be sufficient to inhibit calcium influx induced by TRPC activation in pathological conditions (E. Y. Kim et al., 2018, 2019).

The results of my experiments with HeLa cells suggest that the loss of TRPC6 channel function alone is unlikely to be the sole cause of early- or late-onset FSGS. These findings highlight the importance of conducting further research to explore the mechanisms of TRPC6 channels and their interactions with other podocyte proteins in the development of human FSGS.

5.3 Establishment of a novel FSGS podocyte model using transgenic hiPSC

5.3.1 All in one Tet-on 3G: an obstacle to homogenous expression

I used the lentiviral Tet-On all-in-one vector to induce TRPC6 expression in hiPSCs. This single vector Tet system is appealing for therapeutic application because it streamlines genetic engineering. The functionality of this system was previously reported in HeLa cells (Duran et al., 2022). However, in the case of hiPSCs, achieving homogeneous expression across large populations proved to be challenging. Within days of expanding genetically identical cells, continuous selective pressure and clonal expansion efforts resulted in mosaic transgene expression. Monitoring transactivation

through the expression of a reporter protein revealed that a higher percentage of transduced cells, particularly those that were antibiotic resistant, lost inducibility after the initial antibiotic selection cycle (Duran et al., 2022). Thus, clonal cells exhibit high variability in transgene expression despite the selective pressure. A common strategy to avoid transgene expression loss by continuous gene expression activation (Oyer et al., 2009) failed to eliminate mosaicism in clonally expanded cells cultured with doxycycline (Dox) since transfection. It is possible that cells that do not express the reporter still carry at least one copy of the antibiotic resistance gene, given that the mosaic hiPSCs are all antibiotic resistant. Similarly, other gene regulatory mechanisms may also be responsible for the lack of reporter expression. This hypothesis would need to be supported by genome sequencing or PCR to validate the presence of the transgene in the non-expressing cells.

FACS-based sorting of YFP-expressing cells to achieve a stable population of transgene expressing cells is another strategy that was previously performed on HeLa cells in this study. It can be argued that this procedure is more efficient than drug selection, but it failed when applied to hiPSCs, as mosaicism was observed again after 2-3 passages.

Gene silencing, transgene loss, and post-translational regulatory processes are all possible causes of reduced transgene expression (Pankiewicz et al., 2005). Among the factors contributing to this phenomenon are (i) high copy number of the transgene (Q. Kong et al., 2009); (ii) promoter selection and methylation in this region (Q. Kong et al., 2009); (iii) deacetylation of histones (Gödecke et al., 2017); (iv) repeated sequences within transgene cassettes, as in the Tet promoter (Oyer et al., 2009); (v) nature of integration sites (Garrick et al., 1998); and (vi) incorporation near transcriptional enhancers or silencers (Singer et al., 2012). All of these factors highlight the need to tailor the gene delivery approach to each application.

To fully understand the mechanisms behind reduced gene expression in Tet-ON all-in-one vectors, it is crucial to examine the methylation status of the Tet promoter in iPSCs that do not express the gene.

5.3.2 Two-vector Tet system: OPTi-OX system to generate induced podocytes (iPodocytes)

In particular, the use of a two-vector Tet system in a hiPSC line with a single copy of the transgene in the AAVS1 locus showed homogenous GFP transgene expression even after multiple passages without inducing selection criteria on the cells.

Once stable TRPC6 transgene-expressing hiPSC lines were generated, it was possible to generate terminal kidney cell types, in particular podocytes. For this, I adapted the protocol of Hariharan et al. (2019). Podocyte precursors were generated within 14 days. The expression pattern of the Dox-induced TRPC6 transgene was high during the initial phase of differentiation, however, the percentage of transgene-expressing cells decreased at the end of differentiation protocol. The same phenomena were observed at the protein level, where the TRPC6 expression pattern was obscured as seen by the reduced protein size. Here, I speculated that the heterogeneity or mosaicism of the transgene expression in the iPodocytes may be caused by differentiation-associated epigenetic silencing or differences in Tet promoter activation kinetics (Rand et al., 2015). Still, this phenomenon requires further investigation.

I used the mosaic-induced podocytes (iPodocytes) to reciprocate the Ca^{2+} measurement performed in HeLa cells to functionally characterize the TRPC6 wild-type and variants. The Ca^{2+} imaging experiments on iPodocytes with P112Q and G757D mutants in this expression system showed increased and decreased calcium activity in response to carbachol, consistent with a complete GOF and LOF phenotype, respectively. However, when treated with DOG, the proposed expression was not observed.

There is an urgent need for effective tools to address genetic interference issues in transgenic cells. This problem is exacerbated by improper enhancer-promoter interactions, integration site-dependent chromatin positions, and epigenetic modifications leading to transgene misexpression. One potential solution is the incorporation of insulators into the transgenic constructs, which are placed between the transcriptional units. This strategy aims to minimize the impact of DNA methylation on the stability of the transgene expression, prevent inappropriate interactions, reduce interference from nearby endogenous enhancers, and mitigate chromatin-mediated silencing.

Podocyte differentiation protocols have several applications, including simulating the development and function of the kidney glomerulus, understanding the factors that contribute to podocyte injury in glomerulopathies, and creating *in vitro* models for assessing nephrotoxicity and drug discovery. (Hendry et al., 2013; Lam et al., 2014; Morizane & Bonventre, 2017; Takasato et al., 2014). While recent advances in stem cell differentiation have contributed to our understanding of nephron progenitor development, my approach to investigate the factors that influence the function of fully differentiated kidney glomerulus cells provides opportunities to study a wide range of kidney diseases, including early- and late-onset FSGS, SRNS, and congenital nephrotic syndrome (Büscher & Weber, 2012; Reiser & Sever, 2013). To date, I have generated isogenic iPSC - lines that differ only by specific mutations and then differentiated them into kidney podocytes (Hariharan et al., 2019) to study disease phenotype and facilitate therapeutic discovery. The microfluidic human kidney glomerulus chip represents a significant advancement in tissue culture methods. It provides a unique platform that allows the simultaneous study of the effects of multiple factors on the performance of the glomerular capillary wall. These include factors such as cell-cell interactions, fluid shear stress, and mechanical or cellular deformation forces. This innovative technology has the potential to improve our understanding of kidney development and pathophysiology. Therefore, I have established a model system using the isogenic hiPSC-TRPC6 cell lines to mimic FSGS on-chip and recapitulate human glomerular function in the disease state. Although I do not claim to have reconstructed a complete human glomerulus in this study; however, I have reconstituted the human glomerular capillary wall with TRPC6 wild-type and TRPC6 mutants which has never been modeled *in vitro* and that may greatly benefit research and drug development in this field. The functionality of the established FSGS model on the biochip was not further tested (including with iPSC-derived endothelial cells) due to the observed transgene silencing effect. In a broader context, this approach opens up possibilities for the construction of *in vitro* kidney models. The glomerulus chip can be fluidically connected to other units of the human kidney, such as the proximal tubules, to study glomerular reabsorption and filtration. In addition, the glomerulus capillary chip can be connected to other organ chips that replicate vascularized organs, such as liver, lung, intestine, and bone marrow (Benam et al., 2016; Chang et al., 2016; Maschmeyer et al., 2015; Materne et al., 2015; Torisawa et al., 2014). This interconnected system could be used to simulate a "kidney-on-a-chip" or "body-on-a-chip", allowing functional studies of

pharmacokinetic and pharmacodynamic parameters *in vitro* (Bhatia & Ingber, 2014; Ingber, 2016; Picollet-D'hahan et al., 2021) (Figure 41).

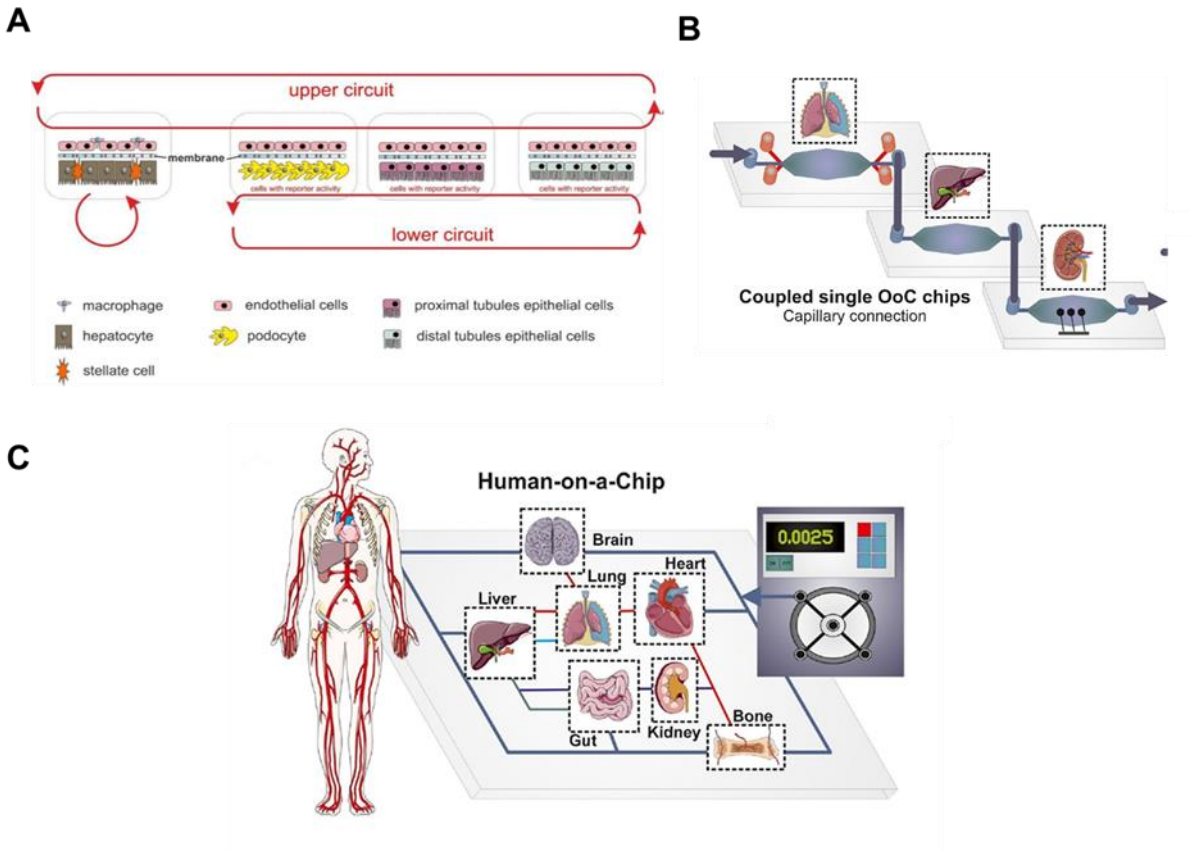

Figure 41: Schematic representation of approaches to model multi-organ on chip (OoC). (A) Human kidney subunits, each modeling a different kidney compartment on a chip. **(B** and **C)** Integration of different organ models in a single plate, representing a body-on-a-chip model. Adapted from (Picollet-D'ahan et al. 2020)

The fact that many human diseases cannot be accurately modeled in animals, coupled with the need to study disease under controlled conditions, has given rise to a new field at the intersection of pathology and tissue engineering. This field is dedicated to the development of *in vitro* disease models. Indeed, reprogramming technology has proved to be a highly valuable tool for developing *in vitro* disease models, particularly for the study of diseases with a significant genetic component. For example, neurons derived from pluripotent stem cells carrying mutations in the alpha-synuclein or LRRK2 genes exhibited pathological features associated with synucleinopathies (Linta et al., 2012). Another study by Ebert et al. (2009) generated iPSC-derived motor neurons from a patient with a genetic form of spinal muscular atrophy, a neurodegenerative disease that results in the loss of lower motor neurons. Initially, these motor neurons were similar in

morphology and number to those derived from wild-type iPSCs. However, after eight weeks in culture, there was a selective decline in their number and size. In addition, these cells exhibited a lack of survival of motor neuron protein aggregates, a characteristic phenotype of spinal muscular atrophy. Notably, drug treatment can reverse the deficiency in motor neuron protein levels (Ebert et al., 2009). Furthermore, iPSCs have also been generated from patients with inherited liver diseases resulting from loss-of-function mutations, providing a promising avenue for studying liver diseases (Ghodsizadeh et al., 2010; Rashid et al., 2010). Similarly, researchers have recently generated *in vitro* models of human congenital long QT (LQT) syndrome, a disorder of myocardial repolarization defined by a prolonged QT interval, delayed repolarization, and potentially fetal polymorphic ventricular tachycardia (Itzhaki et al., 2011). To model this syndrome, hiPSCs were generated from dermal fibroblasts derived from patients diagnosed with familial type 2 LQT syndrome, caused by a missense mutation in the *KCNH2* gene. These hiPSCs were then differentiated into cardiomyocytes. Electrophysiological recordings showed that cardiomyocytes derived from LQT iPSCs exhibited significantly prolonged action potential duration compared to cardiomyocytes derived from control iPSCs, both during paced and spontaneous beating. This *in vitro* model of LQT syndrome model has also been used to evaluate the effects of drugs on the disease phenotype, potentially identifying compounds that exacerbate or alleviate the condition (Itzhaki et al., 2011). In summary, cell types derived from hiPSCs are well suited for the development of personalized drug treatments due to their inherent patient-specific nature. By combining multi-lineage modeling approaches *in vitro*, *in vivo*, and even *in silico*, researchers can expect to obtain the most accurate, reproducible, and translatable results in the quest for effective personalized medicine. This potency is reflected in the recent guidelines from the U.S. Food and Drug Administration that call for the preferred use of *in vitro* cell models for preclinical drug proof-of-concept, efficacy, and toxicity testing. This shift from animal models also reflects the improved translatability when using human models (Wadman, M. (2023). FDA no longer needs to require animal tests before human drug trails. Science. Available from: https://www.science.org/content/article/fda-no-longer-needs-require-animal-tests-human-drug-trials [Accessed 24 August 2023]).

The first application of iPSC-based modeling of kidney disease was in the context of autosomal dominant polycystic kidney disease (ADPKD), the most common monogenic kidney disease characterized by progressive renal cyst formation and gradual

loss of renal function. Freedman et al. (2013) pioneered the modeling of PKD using iPSCs derived from ADPKD patients. They demonstrated that these hiPSC-derived kidney cells could self-organize into kidney organoids when treated with a GSK3-beta inhibitor during the epiblast stage of development. These organoids exhibited morphological and functional features similar to nephrons, including proximal tubules, podocytes, and endothelium. Furthermore, the knockout of PKD1 or PKD2, the causative genes for ADPKD, resulted in cyst formation in the renal tubules (Freedman et al., 2015). Morizane et al. (2015) investigated the critical role of BMP4 levels in the differentiation of hiPSCs into mesoderm and subsequently into renal vesicles and nephrons. The generated nephron organoids exhibited cell-type-specific responses to nephrotoxic agents, highlighting their potential for drug testing (Morizane et al., 2015). Little et al. (2015) supported the application of hiPSCs in modeling nephrogenesis and identifying dysfunctional cellular pathways beyond the ciliopathic renal phenotype. In 2021, Facioli and colleagues used iPSCs reprogrammed from ADPKD patients to generate organoids that closely resembled the architectural features of kidney progenitors. These organoids were able to form cysts when stimulated with forskolin, providing valuable insight into the pathogenesis of ADPKD and a potential therapeutic target (Facioli et al., 2021).

Taken together, the data of this study highlight the potential of the hiPSC-derived FSGS model as a valuable tool for studying various forms of human kidney disease, including hereditary and chronic conditions. This model system holds great promise for advancing our understanding of the precise mechanisms underlying renal glomerulosclerosis, renal cyst formation, and nephropathy. Despite the progress made, several key questions in the field of nephrology remain unanswered. However, the use of *in vitro* models, such as hiPSC-derived kidney cells, has the potential to provide critical insights into these unresolved issues and may even stimulate further research in the field of kidney regenerative medicine.

REFERENCES

Akilesh, S., Suleiman, H., Yu, H., Stander, M. C., Lavin, P., Gbadegesin, R., Antignac, C., Pollak, M., Kopp, J. B., Winn, M. P., & Shaw, A. S. (2011). Arhgap24 inactivates Rac1 in mouse podocytes, and a mutant form is associated with familial focal segmental glomerulosclerosis. *Journal of Clinical Investigation*, *121*(10), 4127–4137. https://doi.org/10.1172/JCI46458

Al-Awqati, Q., & Oliver, J. A. (2002). Stem cells in the kidney. *Kidney International*, *61*(2), 387–395. https://doi.org/10.1046/j.1523-1755.2002.00164.x

Allen Institute for Cell Science. (2018). *Cardiomyocyte Differentiation Methods v1.0*. 3–8. https://www.allencell.org/methods-for-cells-in-the-lab.html

Amaya, E., Stein, P. A., Musci, T. J., & Kirschner, M. W. (1993). *Amaya 1993 - XFD*. *487*, 477–487.

Andersen, K. J., Haga, H. J., & Dobrota, M. (1987). Lysosomes of the renal cortex: Heterogeneity and role in protein handling. *Kidney International*, *31*(4), 886–897. https://doi.org/10.1038/ki.1987.82

Anderson, M., Kim, E. Y., Hagmann, H., Benzing, T., & Dryer, S. E. (2013). Opposing effects of podocin on the gating of podocyte TRPC6 channels evoked by membrane stretch or diacylglycerol. *American Journal of Physiology - Cell Physiology*, *305*(3). https://doi.org/10.1152/ajpcell.00095.2013

Angelotti, M. L., Ronconi, E., Ballerini, L., Peired, A., Mazzinghi, B., Sagrinati, C., Parente, E., Gacci, M., Carini, M., Rotondi, M., Fogo, A. B., Lazzeri, E., Lasagni, L., & Romagnani, P. (2012). Characterization of renal progenitors committed toward tubular lineage and their regenerative potential in renal tubular injury. *Stem Cells*, *30*(8), 1714–1725. https://doi.org/10.1002/stem.1130

Asanuma, K., & Mundel, P. (2003a). The role of podocytes in glomerular pathobiology. *Clinical and Experimental Nephrology*, *7*(4), 255–259. https://doi.org/10.1007/s10157-003-0259-6

Asanuma, K., & Mundel, P. (2003b). The role of podocytes in glomerular pathobiology. *Clinical and Experimental Nephrology*, *7*(4), 255–259. https://doi.org/10.1007/s10157-003-0259-6

Attia, L., Schneider, J., Yelin, R., & Schultheiss, T. M. (2015). Collective cell migration of the nephric duct requires FGF signaling. *Developmental Dynamics*, *244*(2), 157–167. https://doi.org/10.1002/dvdy.24241

Bai, Y., Yu, X., Chen, H., Horne, D., White, R., Wu, X., Lee, P., Gu, Y., Ghimire-Rijal, S., Lin, D. C. H., & Huang, X. (2020). Structural basis for pharmacological modulation of the TRPC6 channel. *ELife*, *9*, 1–18. https://doi.org/10.7554/eLife.53311

Ballermann, B. J., & Obeidat, M. (2014). Tipping the balance from angiogenesis to fibrosis in CKD. *Kidney International Supplements*, *4*(1), 45–52. https://doi.org/10.1038/kisup.2014.9

Barker, N., Rookmaaker, M. B., Kujala, P., Ng, A., Leushacke, M., Snippert, H., van de Wetering, M., Tan, S., Van Es, J. H., Huch, M., Poulsom, R., Verhaar, M. C., Peters, P. J., & Clevers, H. (2012). Lgr5+ve Stem/Progenitor Cells Contribute to Nephron Formation during Kidney Development. *Cell Reports*, *2*(3), 540–552. https://doi.org/10.1016/j.celrep.2012.08.018

Batool, L., Hariharan, K., Xu, Y., Kaßmann, M., Tsvetkov, D., & Oliver, B. (2023). An inactivating human TRPC6 channel mutation without focal segmental glomerulosclerosis. *Cellular and Molecular Life Sciences*, 1–16. https://doi.org/10.1007/s00018-023-04901-w

Batool, L., Raab, C., Beez, C. M., Hariharan, K., Kurtz, A., Gollasch, M., & Rossbach, B. (2023). Generation of human induced pluripotent stem cell line (BCRTi006-A) from a patient with focal segmental glomerulosclerosis disease. *Stem Cell Research*, *69*(March), 103070. https://doi.org/10.1016/j.scr.2023.103070

Batool, L., Raab, C., Beez, C. M., Kurtz, A., Gollasch, M., & Rossbach, B. (2023). Generation of human induced pluripotent stem cell line (BCRTi007-A) from urinary cells of a patient with autosomal dominant polycystic kidney disease. *Stem Cell Research*, *69*(March), 103071. https://doi.org/10.1016/j.scr.2023.103071

Batool, L., Storozhuk, O., Raab, C., Madlen, C., Selig, M., Harder, A., & Kurtz, A. (2023). Generation of two human induced pluripotent stem cell lines from a patient with Neurofibromatosis type 1 (NF1) and pathogenic NF1 gene variant c . 1466 A > G BCRTi011-A as well as a first-degree healthy relative. *Stem Cell Research*,

71(August), 103184. https://doi.org/10.1016/j.scr.2023.103184

Bekker, I. (2021). Chapter 28. *Polybius Tomus 2*, *5*, 1150–1158. https://doi.org/10.1515/9783112389423-028

Benam, K. H., Villenave, R., Lucchesi, C., Varone, A., Hubeau, C., Lee, H. H., Alves, S. E., Salmon, M., Ferrante, T. C., Weaver, J. C., Bahinski, A., Hamilton, G. A., & Ingber, D. E. (2016). Small airway-on-a-chip enables analysis of human lung inflammation and drug responses in vitro. *Nature Methods*, *13*(2), 151–157. https://doi.org/10.1038/nmeth.3697

Bertero, A., Pawlowski, M., Ortmann, D., Snijders, K., Yiangou, L., De Brito, M. C., Brown, S., Bernard, W. G., Cooper, J. D., Giacomelli, E., Gambardella, L., Hannan, N. R. F., Iyer, D., Sampaziotis, F., Serrano, F., Zonneveld, M. C. F., Sinha, S., Kotter, M., & Vallier, L. (2016). Optimized inducible shRNA and CRISPR/Cas9 platforms for in vitro studies of human development using hPSCs. *Development (Cambridge)*, *143*(23), 4405–4418. https://doi.org/10.1242/dev.138081

Bhatia, S. N., & Ingber, D. E. (2014). Microfluidic organs-on-chips. *Nature Biotechnology*, *32*(8), 760–772. https://doi.org/10.1038/nbt.2989

Bierzynska, A., Soderquest, K., & Koziell, A. (2014). Genes and podocytes - new insights into mechanisms of podocytopathy. *Frontiers in Endocrinology*, *5*(DEC), 1–7. https://doi.org/10.3389/fendo.2014.00226

Bouchard, M., Souabni, A., Mandler, M., Neubüser, A., & Busslinger, M. (2002). Nephric lineage specification by Pax2 and Pax8. *Genes and Development*, *16*(22), 2958–2970. https://doi.org/10.1101/gad.240102

Boulay, G. (2002). Ca2+-calmodulin regulates receptor-operated Ca2+ entry activity of TRPC6 in HEK-293 cells. *Cell Calcium*, *32*(4), 201–207. https://doi.org/10.1016/S0143416002001550

Boulay, G., Zhu, X., Peyton, M., Jiang, M., Hurst, R., Stefani, E., & Birnbaumer, L. (1997). Cloning and expression of a novel mammalian homolog of Drosophila Transient receptor potential (Trp) involved in calcium entry secondary to activation of receptors coupled by the G(q) class of g protein. *Journal of Biological Chemistry*, *272*(47), 29672–29680. https://doi.org/10.1074/jbc.272.47.29672

Boute, N. (2000). Erratum: NPHS2, encoding the glomerular protein podocin, is mutated in autosomal recessive steroid-resistant nephrotic syndrome (Nature Genetics (2000) 24 (349-354)). *Nature Genetics*, *25*(1), 125. https://doi.org/10.1038/75532

Bréchard, S., Melchior, C., Plançon, S., Schenten, V., & Tschirhart, E. J. (2008). Store-operated Ca2+ channels formed by TRPC1, TRPC6 and Orai1 and non-store-operated channels formed by TRPC3 are involved in the regulation of NADPH oxidase in HL-60 granulocytes. *Cell Calcium*, *44*(5), 492–506. https://doi.org/10.1016/j.ceca.2008.03.002

Brown, B. J., Boekell, K. L., Stotter, B. R., Talbot, B. E., Schlondorff, J. S., Israel, B., Medical, D., & Medical, H. (2022). *Gain-of-function, focal segmental glomerulosclerosis*.

Brown, E. J., Schlöndorff, J. S., Becker, D. J., Tsukaguchi, H., Uscinski, A. L., Higgs, H. N., Henderson, J. M., & Pollak, M. R. (2010). Mutations in the formin gene INF2 cause focal segmental glomerulosclerosis. *Nature Genetics*, *42*(1), 72–76. https://doi.org/10.1038/ng.505

Bruce, S. J., Rea, R. W., Steptoe, A. L., Busslinger, M., Bertram, J. F., & Perkins, A. C. (2007). In vitro differentiation of murine embryonic stem cells toward a renal lineage. *Differentiation*, *75*(5), 337–349. https://doi.org/10.1111/j.1432-0436.2006.00149.x

Brunskill, E. W., Aronow, B. J., Georgas, K., Rumballe, B., Valerius, M. T., Aronow, J., Kaimal, V., Jegga, A. G., Grimmond, S., McMahon, A. P., Patterson, L. T., Little, M. H., & Potter, S. S. (2008). Atlas of Gene Expression in the Developing Kidney at Microanatomic Resolution. *Developmental Cell*, *15*(5), 781–791. https://doi.org/10.1016/j.devcel.2008.09.007

Büscher, A. K., Konrad, M., Nagel, M., Witzke, O., Kribben, A., Hoyer, P. F., & Weber, S. (2012). Mutations in podocyte genes are a rare cause of primary FSGS associated with ESRD in adult patients. *Clinical Nephrology*, *78*(1), 47–53. https://doi.org/10.5414/CN107320

Büscher, A. K., & Weber, S. (2012). Educational paper: The podocytopathies. *European Journal of Pediatrics*, *171*(8), 1151–1160. https://doi.org/10.1007/s00431-011-1668-2

Bussolati, B., Bruno, S., Grange, C., Buttiglieri, S., Deregibus, M. C., Cantino, D., & Camussi, G. (2005). Isolation of renal progenitor cells from adult human kidney. *American Journal of Pathology*, *166*(2), 545–555. https://doi.org/10.1016/S0002-9440(10)62276-6

Cameron, J. S. (2003a). Focal segmental glomerulosclerosis in adults. *Nephrology Dialysis Transplantation*, *18*(SUPPL. 6). https://doi.org/10.1093/ndt/gfg1058

Cameron, J. S. (2003b). Focal segmental glomerulosclerosis in adults. *Nephrology Dialysis Transplantation*, *18*(suppl_6), vi45–vi51. https://doi.org/10.1093/ndt/gfg1058

Carroll, T. J., & Vize, P. D. (1999). Synergism between Pax-8 and lim-1 in embryonic kidney development. *Developmental Biology*, *214*(1), 46–59. https://doi.org/10.1006/dbio.1999.9414

Chang, S. Y., Weber, E. J., Van Ness, K. P., Eaton, D. L., & Kelly, E. J. (2016). Liver and Kidney on Chips: Microphysiological Models to Understand Transporter Function. *Clinical Pharmacology and Therapeutics*, *100*(5), 464–478. https://doi.org/10.1002/cpt.436

Chen, H., Lun, Y., Ovchinnikov, D., Kokubo, H., Oberg, K. C., Pepicelli, C. V, Gan, L., Lee, B., & Johnson, R. L. (1998). *Limb and kidney defects in*. *19*(may), 51–55.

Chen, L., & Al-Awqati, Q. (2005). Segmental expression of Notch and Hairy genes in nephrogenesis. *American Journal of Physiology - Renal Physiology*, *288*(5 57-5), 939–952. https://doi.org/10.1152/ajprenal.00369.2004

Churg, J., Habib, R., & White, R. R. (1970). Pathology of the Nephrotic Syndrome in Children. *The Lancet*, *295*(7660), 1299–1302. https://doi.org/10.1016/s0140-6736(70)91905-7

Clapham, D. E. (2003). TRP channels as cellular sensors. *Nature*, *426*(6966), 517–524. https://doi.org/10.1038/nature02196

Costantini, F., & Kopan, R. (2010). Patterning a complex organ: Branching morphogenesis and nephron segmentation in kidney development. *Developmental Cell*, *18*(5), 698–712. https://doi.org/10.1016/j.devcel.2010.04.008

Cullen-McEwen, L., Sutherland, M. R., & Black, M. J. (2015). The Human Kidney:

Parallels in Structure, Spatial Development, and Timing of Nephrogenesis. In *Kidney Development, Disease, Repair and Regeneration* (Vol. 1). Elsevier Inc. https://doi.org/10.1016/B978-0-12-800102-8.00003-5

D'Agati, V. D. (2008). The spectrum of focal segmental glomerulosclerosis: New insights. *Current Opinion in Nephrology and Hypertension*, *17*(3), 271–281. https://doi.org/10.1097/MNH.0b013e3282f94a96

De Vriese, A. S., Sethi, S., Nath, K. A., Glassock, R. J., & Fervenza, F. C. (2018). Differentiating primary, genetic, and secondary FSGS in adults: A clinicopathologic approach. *Journal of the American Society of Nephrology*, *29*(3), 759–774. https://doi.org/10.1681/ASN.2017090958

Desgrange, A., & Cereghini, S. (2015). Nephron patterning: Lessons from xenopus, zebrafish, and mouse studies. *Cells*, *4*(3), 483–499. https://doi.org/10.3390/cells4030483

Dietrich, A., Chubanov, V., & Gudermann, T. (2010). Renal TRPathies. *Journal of the American Society of Nephrology*, *21*(5), 736–744. https://doi.org/10.1681/ASN.2009090948

Dietrich, A., & Gudermann, T. (2014). TRPC6: Physiological function and pathophysiological relevance. In *Handbook of Experimental Pharmacology* (Vol. 222). https://doi.org/10.1007/978-3-642-54215-2_7

Ding, F., Li, X., Li, B., Guo, J., Zhang, Y., & Ding, J. (2016). Calpain-mediated cleavage of calcineurin in puromycin aminonucleoside-induced podocyte injury. *PLoS ONE*, *11*(5), 1–12. https://doi.org/10.1371/journal.pone.0155504

Dressler, G. R. (2006). The cellular basis of kidney development. *Annual Review of Cell and Developmental Biology*, *22*, 509–529. https://doi.org/10.1146/annurev.cellbio.22.010305.104340

Duester, G. (2008). Retinoic Acid Synthesis and Signaling during Early Organogenesis. *Cell*, *134*(6), 921–931. https://doi.org/10.1016/j.cell.2008.09.002

Dulak, J., Szade, K., Szade, A., Nowak, W., & Józkowicz, A. (2015). Adult stem cells: Hopes and hypes of regenerative medicine. *Acta Biochimica Polonica*, *62*(3), 329–337. https://doi.org/10.18388/abp.2015_1023

Duran, A. G., Schwestka, M., Nazari-Shafti, T. Z., Neuber, S., Stamm, C., & Gossen, M. (2022). Limiting Transactivator Amounts Contribute to Transgene Mosaicism in Tet-On All-in-One Systems. *ACS Synthetic Biology*, *11*(8), 2623–2635. https://doi.org/10.1021/acssynbio.2c00036

Ebert, A. D., Yu, J., Rose, F. F., Mattis, V. B., Lorson, C. L., Thomson, J. A., & Svendsen, C. N. (2009). Induced pluripotent stem cells from a spinal muscular atrophy patient. *Nature*, *457*(7227), 277–280. https://doi.org/10.1038/nature07677

Englisch, C. N., Röhricht, D., Walz, M., Junker, K., Beckmann, A., Meier, C., Paulsen, F., Jung, M., & Tschernig, T. (2022). *TRPC6 Is Found in Distinct Compartments of the Human Kidney*. 156–163.

Eun, Y. K., Alvarez-Baron, C. P., & Dryer, S. E. (2009). Canonical transient receptor potential channel (TRPC) 3 and TRPC6 associate with large-conductance Ca 2+-activated K + (BK ca) channels: Role in BK ca trafficking to the surface of cultured podocytes. *Molecular Pharmacology*, *75*(3), 466–477. https://doi.org/10.1124/mol.108.051912

Facioli, R., Lojudice, F. H., Anauate, A. C., Maquigussa1, E., Nishiura, J. L., Heilberg, I. P., Sogayar, M. C., & Boim, M. A. (2021). Kidney organoids generated from erythroid progenitors cells of patients with autosomal dominant polycystic kidney disease. *PLoS ONE*, *16*(8 August), 1–16. https://doi.org/10.1371/journal.pone.0252156

Farmer, L. K., Rollason, R., Whitcomb, D. J., Ni, L., Goodliff, A., Lay, A. C., Birnbaumer, L., Heesom, K. J., Xu, S. Z., Saleem, M. A., & Welsh, G. I. (2019). TRPC6 Binds to and activates calpain, independent of its channel activity, and regulates podocyte cytoskeleton, cell adhesion, and motility. *Journal of the American Society of Nephrology*, *30*(10), 1910–1924. https://doi.org/10.1681/ASN.2018070729

Fleming, B. M., Yelin, R., James, R. G., & Schultheiss, T. M. (2013). A role for Vg1/nodal signaling in specification of the intermediate mesoderm. *Development (Cambridge)*, *140*(8), 1819–1829. https://doi.org/10.1242/dev.093740

Fogo, A. B. (2003). Animal models of FSGS: Lessons for pathogenesis and treatment. *Seminars in Nephrology*, *23*(2), 161–171. https://doi.org/10.1053/snep.2003.50015

Foreman, K. J., Marquez, N., Dolgert, A., Fukutaki, K., Fullman, N., McGaughey, M.,

Pletcher, M. A., Smith, A. E., Tang, K., Yuan, C. W., Brown, J. C., Friedman, J., He, J., Heuton, K. R., Holmberg, M., Patel, D. J., Reidy, P., Carter, A., Cercy, K., … Murray, C. J. L. (2018). Forecasting life expectancy, years of life lost, and all-cause and cause-specific mortality for 250 causes of death: reference and alternative scenarios for 2016–40 for 195 countries and territories. *The Lancet*, *392*(10159), 2052–2090. https://doi.org/10.1016/S0140-6736(18)31694-5

Franke, I., Aydin, M., Llamas Lopez, C. E., Kurylowicz, L., Ganschow, R., Lentze, M., & Born, M. (2018). The incidence of the nephrotic syndrome in childhood in Germany. *Clinical and Experimental Nephrology*, *22*(1), 126–132. https://doi.org/10.1007/s10157-017-1433-6

Freedman, B. S., Brooks, C. R., Lam, A. Q., Fu, H., Morizane, R., Agrawal, V., Saad, A. F., Li, M. K., Hughes, M. R., Werff, R. Vander, Peters, D. T., Lu, J., Baccei, A., Siedlecki, A. M., Valerius, M. T., Musunuru, K., McNagny, K. M., Steinman, T. I., Zhou, J., … Bonventre, J. V. (2015). Modelling kidney disease with CRISPR-mutant kidney organoids derived from human pluripotent epiblast spheroids. *Nature Communications*, *6*(May). https://doi.org/10.1038/ncomms9715

Gansevoort, R. T., Correa-Rotter, R., Hemmelgarn, B. R., Jafar, T. H., Heerspink, H. J. L., Mann, J. F., Matsushita, K., & Wen, C. P. (2013). Chronic kidney disease and cardiovascular risk: Epidemiology, mechanisms, and prevention. *The Lancet*, *382*(9889), 339–352. https://doi.org/10.1016/S0140-6736(13)60595-4

Garrick, D., Fiering, S., Martin, D. I. K., & Whitelaw, E. (1998). Repeat-induced gene silencing in mammals. *Nature Genetics*, *18*(1), 56–59. https://doi.org/10.1038/ng0198-56

Gasiunas, G., Barrangou, R., Horvath, P., & Siksnys, V. (2012). Cas9-crRNA ribonucleoprotein complex mediates specific DNA cleavage for adaptive immunity in bacteria. *Proceedings of the National Academy of Sciences of the United States of America*, *109*(39), 2579–2586. https://doi.org/10.1073/pnas.1208507109

Gbadegesin, R. A., Hall, G., Adeyemo, A., Hanke, N., Tossidou, I., Burchette, J., Wu, G., Homstad, A., Sparks, M. A., Gomez, J., Jiang, R., Alonso, A., Lavin, P., Conlon, P., Korstanje, R., Christine Stander, M., Shamsan, G., Barua, M., Spurney, R., … Winn, M. P. (2014). Mutations in the gene that encodes the F-Actin binding protein

anillin cause FSGS. *Journal of the American Society of Nephrology*, *25*(9), 1991–2002. https://doi.org/10.1681/ASN.2013090976

Gee, H. Y., Saisawat, P., Ashraf, S., Hurd, T. W., Vega-Warner, V., Fang, H., Beck, B. B., Gribouval, O., Zhou, W., Diaz, K. A., Natarajan, S., Wiggins, R. C., Lovric, S., Chernin, G., Schoeb, D. S., Ovunc, B., Frishberg, Y., Soliman, N. A., Fathy, H. M., … Hildebrandt, F. (2013). ARHGDIA mutations cause nephrotic syndrome via defective RHO GTPase signaling. *Journal of Clinical Investigation*, *123*(8), 3243–3253. https://doi.org/10.1172/JCI69134

Geurts, A. M., Cost, G. J., Freyvert, Y., Zeitler, B., Miller, J. C., Choi, V. M., Jenkins, S. S., Wood, A., Cui, X., Meng, X., Vincent, A., Lam, S., Michalkiewicz, M., Schilling, R., Foeckler, J., Kalloway, S., Weiler, H., Ménoret, S., Anegon, I., … Buelow, R. (2009). Knockout rats via embryo microinjection of zinc-finger nucleases. *Science*, *325*(5939), 433. https://doi.org/10.1126/science.1172447

Gheissari, A., Meamar, R., Kheirollahi, M., Rouigari, M., Dehbashi, M., Dehghani, L., & Abedini, A. (2018). TRPC6 mutational analysis in iranian children with focal segmental glomerulosclerosis. *Iranian Journal of Kidney Diseases*, *12*(6), 341–349.

Ghodsizadeh, A., Taei, A., Totonchi, M., Seifinejad, A., Gourabi, H., Pournasr, B., Aghdami, N., Malekzadeh, R., Almadani, N., Salekdeh, G. H., & Baharvand, H. (2010). Generation of Liver Disease-Specific Induced Pluripotent Stem Cells Along with Efficient Differentiation to Functional Hepatocyte-Like Cells. *Stem Cell Reviews and Reports*, *6*(4), 622–632. https://doi.org/10.1007/s12015-010-9189-3

Gigante, M., Caridi, G., Montemurno, E., Soccio, M., D'Apolito, M., Cerullo, G., Aucella, F., Schirinzi, A., Emma, F., Massella, L., Messina, G., de Palo, T., Ranieri, E., Ghiggeri, G. M., & Gesualdo, L. (2011). TRPC6 Mutations in children with steroid-resistant nephrotic syndrome and atypical phenotype. *Clinical Journal of the American Society of Nephrology*, *6*(7), 1626–1634. https://doi.org/10.2215/CJN.07830910

Gipson, P. E., & Gipson, D. S. (2019). Focal segmental glomerulosclerosis. *Nephrology Secrets: Fourth Edition*, 186–191. https://doi.org/10.1016/B978-0-323-47871-7.00036-8

Glassock, R. J., Fervenza, F. C., Hebert, L., & Cameron, J. S. (2015). Nephrotic

syndrome redux. *Nephrology Dialysis Transplantation*, *30*(1), 12–17. https://doi.org/10.1093/ndt/gfu077

Gödecke, N., Zha, L., Spencer, S., Behme, S., Riemer, P., Rehli, M., Hauser, H., & Wirth, D. (2017). Controlled re-activation of epigenetically silenced Tet promoter-driven transgene expression by targeted demethylation. *Nucleic Acids Research*, *45*(16). https://doi.org/10.1093/nar/gkx601

Goel, M., Sinkins, W. G., Zuo, C. Di, Estacion, M., & Schilling, W. P. (2006). Identification and localization of TRPC channels in the rat kidney. *American Journal of Physiology - Renal Physiology*, *290*(5), 1241–1252. https://doi.org/10.1152/ajprenal.00376.2005

Gough, F. (2011). Human embryonic stem cell research in Ireland: Ethical and legal issues. *Medical Law International*, *11*(4), 262–283. https://doi.org/10.1177/0968533211419124

Greka, A., & Mundel, P. (2011). Balancing calcium signals through TRPC5 and TRPC6 in podocytes. *Journal of the American Society of Nephrology*, *22*(11), 1969–1980. https://doi.org/10.1681/ASN.2011040370

Guo, W., & Chen, L. (2019). Recent progress in structural studies on canonical TRP ion channels. *Cell Calcium*, *83*, 102075. https://doi.org/10.1016/j.ceca.2019.102075

Guo, W., Tang, Q., Wei, M., Kang, Y., Wu, J. X., & Chen, L. (2022). Structural mechanism of human TRPC3 and TRPC6 channel regulation by their intracellular calcium-binding sites. *Neuron*, *110*(6), 1023-1035.e5. https://doi.org/10.1016/j.neuron.2021.12.023

Haas, M., Spargo, B. H., & Coventry, S. (1995). Increasing incidence of focal-segmental glomerulosclerosis among adult nephropathies: A 20-year renal biopsy study. *American Journal of Kidney Diseases*, *26*(5), 740–750. https://doi.org/10.1016/0272-6386(95)90437-9

Habib, R. (1973). Focal glomerular sclerosis. *Kidney International*, *4*(6), 355–361. https://doi.org/10.1038/ki.1973.131

Häfner, S., Burg, F., Kannler, M., Urban, N., Mayer, P., Dietrich, A., Trauner, D., Broichhagen, J., & Schaefer, M. (2018). A (+)-Larixol Congener with High Affinity

and Subtype Selectivity toward TRPC6. *ChemMedChem*, *13*(10), 1028–1035. https://doi.org/10.1002/cmdc.201800021

Hall, G., Gbadegesin, R. A., Lavin, P., Wu, G., Liu, Y., Oh, E. C., Wang, L., Spurney, R. F., Eckel, J., Lindsey, T., Homstad, A., Malone, A. F., Phelan, P. J., Shaw, A., Howell, D. N., Conlon, P. J., Katsanis, N., & Winn, M. P. (2015). A novel missense mutation of Wilms' Tumor 1 causes autosomal dominant FSGS. *Journal of the American Society of Nephrology*, *26*(4), 831–843. https://doi.org/10.1681/ASN.2013101053

Hall, G., Wang, L., & Spurney, R. F. (2019). TRPC Channels in Proteinuric Kidney Diseases. *Cells*, *9*(1), 1–24. https://doi.org/10.3390/cells9010044

Hariharan, K., Stachelscheid, H., Rossbach, B., Oh, S. J., Mah, N., Schmidt-Ott, K., Kurtz, A., & Reinke, P. (2019). Parallel generation of easily selectable multiple nephronal cell types from human pluripotent stem cells. *Cellular and Molecular Life Sciences*, *76*(1), 179–192. https://doi.org/10.1007/s00018-018-2929-2

Heeringa, S. F., Ller, C. C. M., Du, J., Yue, L., Hinkes, B., Chernin, G., Vlangos, C. N., Hoyer, P. F., Reiser, J., & Friedhelm Hildebrandt1. (2009). A Novel TRPC6 Mutation That Cause Childhood FSGS. *PloS One*, *4*(11), e7771. https://doi.org/10.1371/Citation

Heeringa, S. F., Möller, C. C., Du, J., Yue, L., Hinkes, B., Chernin, G., Vlangos, C. N., Hoyer, P. F., Reiser, J., & Hildebrandt, F. (2009). A Novel TRPC6 Mutation That Causes Childhood FSGS. *PLoS ONE*, *4*(11), e7771. https://doi.org/10.1371/journal.pone.0007771

Hendry, C. E., Vanslambrouck, J. M., Ineson, J., Suhaimi, N., Takasato, M., Rae, F., & Little, M. H. (2013). Direct transcriptional reprogramming of adult cells to embryonic nephron progenitors. *Journal of the American Society of Nephrology*, *24*(9), 1424–1434. https://doi.org/10.1681/ASN.2012121143

Hickson, L. J., Gera, M., Amer, H., Iqbal, C. W., Moore, T. B., Milliner, D. S., Cosio, F. G., Larson, T. S., Stegall, M. D., Ishitani, M. B., Gloor, J. M., & Griffin, M. D. (2009). Kidney transplantation for primary focal segmental glomerulosclerosis: Outcomes and response to therapy for recurrence. *Transplantation*, *87*(8), 1232–1239. https://doi.org/10.1097/TP.0b013e31819f12be

Hindi, S. El, & Reiser, J. (2011). TRPC channel modulation in podocytes-inching toward novel treatments for glomerular disease. *Pediatric Nephrology*, *26*(7), 1057–1064. https://doi.org/10.1007/s00467-010-1718-4

Hofmann, T., Obukhov, A. G., Schaefer, M., Harteneck, C., Gudermann, T., & Schultz, G. (1999). Direct activation of human TRPC6 and TRPC3 channels by diacylglycerol. *Nature*, *397*(6716), 259–263. https://doi.org/10.1038/16711

Hofstra, J. M., Coenen, M. J. H., Schijvenaars, M. M. V. A. P., Berden, J. H. M., Van Der Vlag, J., Hoefsloot, L. H., Knoers, N. V. A. M., Wetzels, J. F. M., & Nijenhuis, T. (2014). TRPC6 single nucleotide polymorphisms and progression of idiopathic membranous nephropathy. *PLoS ONE*, *9*(7). https://doi.org/10.1371/journal.pone.0102065

Hofstra, J. M., Lainez, S., Van Kuijk, W. H. M., Schoots, J., Baltissen, M. P. A., Hoefsloot, L. H., Knoers, N. V. A. M., Berden, J. H. M., Bindels, R. J. M., Van Der Vlag, J., Hoenderop, J. G. J., Wetzels, J. F. M., & Nijenhuis, T. (2013). New TRPC6 gain-of-function mutation in a non-consanguineous Dutch family with late-onset focal segmental glomerulosclerosis. *Nephrology Dialysis Transplantation*, *28*(7), 1830–1838. https://doi.org/10.1093/ndt/gfs572

Huber, T. B., Schermer, B., Müller, R. U., Höhne, M., Bartram, M., Calixto, A., Hagmann, H., Reinhardt, C., Koos, F., Kunzelmann, K., Shirokova, E., Krautwurst, D., Harteneck, C., Simons, M., Pavenstädt, H., Kerjaschki, D., Thiele, C., Walz, G., Chalfie, M., & Benzing, T. (2006). Podocin and MEC-2 bind cholesterol to regulate the activity of associated ion channels. *Proceedings of the National Academy of Sciences of the United States of America*, *103*(46), 17079–17086. https://doi.org/10.1073/pnas.0607465103

Ilatovskaya, D. V., & Staruschenko, A. (2015). TRPC6 channel as an emerging determinant of the podocyte injury susceptibility in kidney diseases. *American Journal of Physiology - Renal Physiology*, *309*(5), F393–F397. https://doi.org/10.1152/ajprenal.00186.2015

Ingber, D. E. (2016). Reverse Engineering Human Pathophysiology with Organs-on-Chips. *Cell*, *164*(6), 1105–1109. https://doi.org/10.1016/j.cell.2016.02.049

Itzhaki, I., Maizels, L., Huber, I., Zwi-Dantsis, L., Caspi, O., Winterstern, A., Feldman,

O., Gepstein, A., Arbel, G., Hammerman, H., Boulos, M., & Gepstein, L. (2011). Modelling the long QT syndrome with induced pluripotent stem cells. *Nature*, *471*(7337), 225–230. https://doi.org/10.1038/nature09747

James, R. G., & Schultheiss, T. M. (2005). Bmp signaling promotes intermediate mesoderm gene expression in a dose-dependent, cell-autonomous and translation-dependent manner. *Developmental Biology*, *288*(1), 113–125. https://doi.org/10.1016/j.ydbio.2005.09.025

Jardin, I., Nieto, J., Salido, G. M., & Rosado, J. A. (2020). TRPC6 channel and its implications in breast cancer: an overview. *Biochimica et Biophysica Acta - Molecular Cell Research*, *1867*(12), 118828. https://doi.org/10.1016/j.bbamcr.2020.118828

Joshi, B. B., Koringa, P. G., Mistry, K. N., Patel, A. K., Gang, S., & Joshi, C. G. (2015). In silico analysis of functional nsSNPs in human TRPC6 gene associated with steroid resistant nephrotic syndrome. *Gene*, *572*(1), 8–16. https://doi.org/10.1016/j.gene.2015.06.069

Kandasamy, K., Chuah, J. K. C., Su, R., Huang, P., Eng, K. G., Xiong, S., Li, Y., Chia, C. S., Loo, L. H., & Zink, D. (2015). Prediction of drug-induced nephrotoxicity and injury mechanisms with human induced pluripotent stem cell-derived cells and machine learning methods. *Scientific Reports*, *5*(July), 1–15. https://doi.org/10.1038/srep12337

Kaplan, J. M., Kim, S. H., North, K. N., Rennke, H., Correia, L. A., Tong, H. Q., Mathis, B. J., Rodríguez-Pérez, J. C., Allen, P. G., Beggs, A. H., & Pollak, M. R. (2000). Mutations in ACTN4, encoding α-actinin-4, cause familial focal segmental glomerulosclerosis. *Nature Genetics*, *24*(3), 251–256. https://doi.org/10.1038/73456

Kestilä, M., Lenkkeri, U., Männikkö, M., Lamerdin, J., McCready, P., Putaala, H., Ruotsalainen, V., Morita, T., Nissinen, M., Herva, R., Kashtan, C. E., Peltonen, L., Holmberg, C., Olsen, A., & Tryggvason, K. (1998). Positionally cloned gene for a novel glomerular protein - Nephrin - Is mutated in congenital nephrotic syndrome. *Molecular Cell*, *1*(4), 575–582. https://doi.org/10.1016/S1097-2765(00)80057-X

Khayyat, N. H., Tomilin, V. N., Zaika, O., & Pochynyuk, O. (2020). Polymodal roles of TRPC3 channel in the kidney. *Channels*, *14*(1), 257–267.

https://doi.org/10.1080/19336950.2020.1804153

Kim, E. Y., & Dryer, S. E. (2021). Effects of trpc6 inactivation on glomerulosclerosis and renal fibrosis in aging rats. *Cells*, *10*(4), 1–12. https://doi.org/10.3390/cells10040856

Kim, E. Y., Shotorbani, P. Y., & Dryer, S. E. (2019). TRPC6 inactivation does not affect loss of renal function in nephrotoxic serum glomerulonephritis in rats, but reduces severity of glomerular lesions. *Biochemistry and Biophysics Reports*, *17*(January), 139–150. https://doi.org/10.1016/j.bbrep.2018.12.006

Kim, E. Y., Yazdizadeh Shotorbani, P., & Dryer, S. E. (2018). Trpc6 inactivation confers protection in a model of severe nephrosis in rats. *Journal of Molecular Medicine*, *96*(7), 631–644. https://doi.org/10.1007/s00109-018-1648-3

Kim, J. H., Wu, H., Green, G., Winkler, C. A., Kopp, J. B., Miner, J. H., Unanue, E. R., & Shawl, A. S. (2003). CD2-associated protein haploinsufficiency is linked to glomerular disease susceptibility. *Science*, *300*(5623), 1298–1300. https://doi.org/10.1126/science.1081068

Kinder, S. J., Tsang, T. E., Quinlan, G. A., Hadjantonakis, A., Nagy, A., & Tam, P. P. L. (2017). *The orderly allocation of mesodermal cells to the extraembryonic structures and the anteroposterior axis during gastrulation of the mouse embryo*. *114*(10), 2705–2710.

Kiselyov, K., Mignery, G. A., Zhu, M. X., & Muallem, S. (1999). The N-terminal domain of the IP3 receptor gates store-operated hTrp3 channels. *Molecular Cell*, *4*(3), 423–429. https://doi.org/10.1016/S1097-2765(00)80344-5

Kitiyakara, C., Eggers, P., & Kopp, J. B. (2004). Twenty-one-year trend in ESRD due to focal segmental glomerulosclerosis in the United States. *American Journal of Kidney Diseases*, *44*(5), 815–825. https://doi.org/10.1053/j.ajkd.2004.07.008

Knoll, G. (2008). Trends in kidney transplantation over the past decade. *Drugs*, *68*(SUPPL. 1), 3–10. https://doi.org/10.2165/00003495-200868001-00002

Kobayashi, A., Kwan, K. M., Carroll, T. J., McMahon, A. P., Mendelsohn, C. L., & Behringer, R. R. (2005). Distinct and sequential tissue-specific activitites of the LIM-class homeobox gene Lim1 for tubular morphogenesis during kidney development.

Development, *132*(12), 2809–2823. https://doi.org/10.1242/dev.01858

Kobayashi, A., Valerius, M. T., Mugford, J. W., Carroll, T. J., Self, M., Oliver, G., & McMahon, A. P. (2008). Six2 Defines and Regulates a Multipotent Self-Renewing Nephron Progenitor Population throughout Mammalian Kidney Development. *Cell Stem Cell*, *3*(2), 169–181. https://doi.org/10.1016/j.stem.2008.05.020

Kong, Q., Wu, M., Huan, Y., Zhang, L., Liu, H., Bou, G., Luo, Y., Mu, Y., & Liu, Z. (2009). Transgene expression is associated with copy number and cytomegalovirus promoter methylation in transgenic pigs. *PLoS ONE*, *4*(8). https://doi.org/10.1371/journal.pone.0006679

Kong, W., Haschler, T. N., Nürnberg, B., Krämer, S., Gollasch, M., & Markó, L. (2019). Renal fibrosis, immune cell infiltration and changes of TRPC channel expression after unilateral ureteral obstruction in TRPC6-/-mice. *Cellular Physiology and Biochemistry*, *52*(6), 1484–1502. https://doi.org/10.33594/000000103

Kopan, R., Cheng, H. T., & Surendran, K. (2007). Molecular insights into segmentation along the proximal-distal axis of the nephron. *Journal of the American Society of Nephrology*, *18*(7), 2014–2020. https://doi.org/10.1681/ASN.2007040453

Krall, P., Canales, C. P., Kairath, P., Carmona-Mora, P., Molina, J., Carpio, J. D., Ruiz, P., Mezzano, S. A., Li, J., Wei, C., Reiser, J., Young, J. I., & Walz, K. (2010). Podocyte-specific overexpression of wild type or mutant Trpc6 in mice is sufficient to cause glomerular disease. *PLoS ONE*, *5*(9), 1–11. https://doi.org/10.1371/journal.pone.0012859

Kramer, A., Boenink, R., Stel, V. S., Santiuste De Pablos, C., Tomović, F., Golan, E., Kerschbaum, J., Seyahi, N., Ioanou, K., Beltrán, P., Zurriaga, O., Magaz, Á., Slon Roblero, M. F., Gjorgjievski, N., Garneata, L., Arribas, F., Galvão, A. A., Bell, S., Ots-Rosenberg, M., … Jager, K. J. (2021). The ERA-EDTA Registry Annual Report 2018: A summary. *Clinical Kidney Journal*, *14*(1), 107–123. https://doi.org/10.1093/ckj/sfaa271

Kreidberg, J. A. (2010). WT1 and kidney progenitor cells. *Organogenesis*, *6*(2), 61–70. https://doi.org/10.4161/org.6.2.11928

Kriz, W. (2003). The pathogenesis of “classic” focal segmental glomerulosclerosis - Lessons from rat models. *Nephrology Dialysis Transplantation*, *18*(SUPPL. 6), 39–

44. https://doi.org/10.1093/ndt/gfg1064

Kriz, W., & Kaissling, B. (2007). Structural Organization of the Mammalian Kidney. In *Seldin and Giebisch's The Kidney: Physiology & Pathophysiology 1-2* (Issue January). https://doi.org/10.1016/B978-012088488-9.50023-1

Kunert-Keil, C., Bisping, F., Krüger, J., & Brinkmeier, H. (2006). Tissue-specific expression of TRP channel genes in the mouse and its variation in three different mouse strains. *BMC Genomics*, *7*, 1–14. https://doi.org/10.1186/1471-2164-7-159

Kuure, S., Popsueva, A., Jakobson, M., Sainio, K., & Sariola, H. (2007). Glycogen synthase kinase-3 inactivation and stabilization of β-catenin induce nephron differentiation in isolated mouse and rat kidney mesenchymes. *Journal of the American Society of Nephrology*, *18*(4), 1130–1139. https://doi.org/10.1681/ASN.2006111206

Kuwahara, K., Wang, Y., McAnally, J., Richardson, J. A., Bassel-Duby, R., Hill, J. A., & Olson, E. N. (2006). TRPC6 fulfills a calcineurin signaling circuit during pathologic cardiac remodeling. *Journal of Clinical Investigation*, *116*(12), 3114–3126. https://doi.org/10.1172/JCI27702

Kwoh, C., Shannon, M. B., Miner, J. H., & Shaw, A. (2006). Pathogenesis of nonimmune glomeralopathies. *Annual Review of Pathology*, *1*, 349–374. https://doi.org/10.1146/annurev.pathol.1.110304.100119

Kwon, Y., Hofmann, T., & Montell, C. (2007). Integration of Phosphoinositide- and Calmodulin-Mediated Regulation of TRPC6. *Molecular Cell*, *25*(4), 491–503. https://doi.org/10.1016/j.molcel.2007.01.021

Lam, A. Q., Freedman, B. S., Morizane, R., Lerou, P. H., Valerius, M. T., & Bonventre, J. V. (2014). Rapid and efficient differentiation of human pluripotent stem cells into intermediate mesoderm that forms tubules expressing kidney proximal tubular markers. *Journal of the American Society of Nephrology*, *25*(6), 1211–1225. https://doi.org/10.1681/ASN.2013080831

Lazzeri, E., Angelotti, M. L., Peired, A., Conte, C., Marschner, J. A., Maggi, L., Mazzinghi, B., Lombardi, D., Melica, M. E., Nardi, S., Ronconi, E., Sisti, A., Antonelli, G., Becherucci, F., De Chiara, L., Guevara, R. R., Burger, A., Schaefer, B., Annunziato, F., … Romagnani, P. (2018). Endocycle-related tubular cell

hypertrophy and progenitor proliferation recover renal function after acute kidney injury. *Nature Communications*, *9*(1), 1–18. https://doi.org/10.1038/s41467-018-03753-4

Lee, J. M., Kronbichler, A., Shin, J. Il, & Oh, J. (2021). Current understandings in treating children with steroid-resistant nephrotic syndrome. *Pediatric Nephrology*, *36*(4), 747–761. https://doi.org/10.1007/s00467-020-04476-9

Lepage, P. K., Lussier, M. P., McDuff, F. O., Lavigne, P., & Boulay, G. (2009). The self-association of two N-terminal interaction domains plays an important role in the tetramerization of TRPC4. *Cell Calcium*, *45*(3), 251–259. https://doi.org/10.1016/j.ceca.2008.11.002

Li, Y., & Wingert, R. A. (2013). Regenerative medicine for the kidney: stem cell prospects & challenges. *Clinical and Translational Medicine*, *2*(1), 1–16. https://doi.org/10.1186/2001-1326-2-11

Liakopoulos, V., Huerta, A., Cohen, S., Pollak, M. R., Sirota, R. A., Superdock, K., & Appel, G. B. (2011). Familial collapsing focal segmental glomerulosclerosis. *Clinical Nephrology*, *75*(4), 362–368. https://doi.org/10.5414/CN106544

Lian, X., Zhang, J., Azarin, S. M., Zhu, K., Hazeltine, L. B., Bao, X., Hsiao, C., Kamp, T. J., & Palecek, S. P. (2013). Directed cardiomyocyte differentiation from human pluripotent stem cells by modulating Wnt/β-catenin signaling under fully defined conditions. *Nature Protocols*, *8*(1), 162–175. https://doi.org/10.1038/nprot.2012.150

Liao, M., Cao, E., Julius, D., & Cheng, Y. (2013). Structure of the TRPV1 ion channel determined by electron cryo-microscopy. *Nature*, *504*(7478), 107–112. https://doi.org/10.1038/nature12822

Lim, B. J., Yang, J. W., Do, W. S., & Fogo, A. B. (2016). Pathogenesis of focal segmental glomerulosclerosis. *Journal of Pathology and Translational Medicine*, *50*(6), 405–410. https://doi.org/10.4132/jptm.2016.09.21

Lin, B. L., Matera, D., Doerner, J. F., Zheng, N., Del Camino, D., Mishra, S., Bian, H., Zeveleva, S., Zhen, X., Blair, N. T., Chong, J. A., Hessler, D. P., Bedja, D., Zhu, G., Muller, G. K., Ranek, M. J., Pantages, L., McFarland, M., Netherton, M. R., … Pullen, S. S. (2019). In vivo selective inhibition of TRPC6 by antagonist BI 749327 ameliorates fibrosis and dysfunction in cardiac and renal disease. *Proceedings of*

the National Academy of Sciences of the United States of America, *116*(20), 10156–10161. https://doi.org/10.1073/pnas.1815354116

Linta, L., Stockmann, M., Boeckers, T. M., Kleger, A., & Liebau, S. (2012). The potential of iPS cells in synucleinopathy research. *Stem Cells International*, *2012*. https://doi.org/10.1155/2012/629230

Little, M., Georgas, K., Pennisi, D., & Wilkinson, L. (2010). Kidney development: Two tales of tubulogenesis. *Current Topics in Developmental Biology*, *90*(C), 193–229. https://doi.org/10.1016/S0070-2153(10)90005-7

Little, M. H. (2021). Returning to kidney development to deliver synthetic kidneys. *Developmental Biology*, *474*(September 2020), 22–36. https://doi.org/10.1016/j.ydbio.2020.12.009

Liu, Z., Yang, J., Zhang, X., Xu, P., Zhang, T., & Yang, Z. (2015). Developmental changes in the expression and function of TRPC6 channels related the F-actin organization during differentiation in podocytes. *Cell Calcium*, *58*(6), 541–548. https://doi.org/10.1016/j.ceca.2015.09.001

Loh, Y. H., Agarwal, S., Park, I. H., Urbach, A., Huo, H., Heffner, G. C., Kim, K., Miller, J. D., Ng, K., & Daley, G. Q. (2009). Generation of induced pluripotent stem cells from human blood. *Blood*, *113*(22), 5476–5479. https://doi.org/10.1182/blood-2009-02-204800

Macconi, D., Sangalli, F., Bonomelli, M., Conti, S., Condorelli, L., Gagliardini, E., Remuzzi, G., & Remuzzi, A. (2009). Podocyte repopulation contributes to regression of glomerular injury induced by ace inhibition. *American Journal of Pathology*, *174*(3), 797–807. https://doi.org/10.2353/ajpath.2009.080227

Mae, S. I., Shono, A., Shiota, F., Yasuno, T., Kajiwara, M., Gotoda-Nishimura, N., Arai, S., Sato-Otubo, A., Toyoda, T., Takahashi, K., Nakayama, N., Cowan, C. A., Aoi, T., Ogawa, S., McMahon, A. P., Yamanaka, S., & Osafune, K. (2013). Monitoring and robust induction of nephrogenic intermediate mesoderm from human pluripotent stem cells. *Nature Communications*, *4*. https://doi.org/10.1038/ncomms2378

Maehr, R., Chen, S., Snitow, M., Ludwig, T., Yagasaki, L., Goland, R., Leibel, R. L., & Melton, D. A. (2009). Generation of pluripotent stem cells from patients with type 1

diabetes. *Proceedings of the National Academy of Sciences of the United States of America*, *106*(37), 15768–15773. https://doi.org/10.1073/pnas.0906894106

Maier, T., Follmann, M., Hessler, G., Kleemann, H. W., Hachtel, S., Fuchs, B., Weissmann, N., Linz, W., Schmidt, T., Löhn, M., Schroeter, K., Wang, L., Rütten, H., & Strübing, C. (2015). Discovery and pharmacological characterization of a novel potent inhibitor of diacylglycerol-sensitive TRPC cation channels. *British Journal of Pharmacology*, *172*(14), 3650–3660. https://doi.org/10.1111/bph.13151

Majumdar, A., Vainio, S., Kispert, A., McMahon, J., & McMahon, A. P. (2003). Wnt11 and Ret/Gdnf pathways cooperate in regulating ureteric branching during metanephric kidney development. *Development*, *130*(14), 3175–3185. https://doi.org/10.1242/dev.00520

Mallipattu, S. K., & He, J. C. (2016). The podocyte as a direct target for treatment of glomerular disease? *American Journal of Physiology - Renal Physiology*, *311*(1), F46–F51. https://doi.org/10.1152/ajprenal.00184.2016

Maruyama, Y., Ogura, T., Mio, K., Kiyonaka, S., Kato, K., Mori, Y., & Sato, C. (2007). Three-dimensional reconstruction using transmission electron microscopy reveals a swollen, bell-shaped structure of transient receptor potential melastatin type 2 cation channel. *Journal of Biological Chemistry*, *282*(51), 36961–36970. https://doi.org/10.1074/jbc.M705694200

Maschmeyer, I., Lorenz, A. K., Schimek, K., Hasenberg, T., Ramme, A. P., Hübner, J., Lindner, M., Drewell, C., Bauer, S., Thomas, A., Sambo, N. S., Sonntag, F., Lauster, R., & Marx, U. (2015). A four-organ-chip for interconnected long-term co-culture of human intestine, liver, skin and kidney equivalents. *Lab on a Chip*, *15*(12), 2688–2699. https://doi.org/10.1039/c5lc00392j

Matejas, V., Hinkes, B., Alkandari, F., Al-Gazali, L., Annexstad, E., Aytac, M. B., Barrow, M., Bláhová, K., Bockenhauer, D., Cheong, H. Il, Maruniak-Chudek, I., Cochat, P., Dötsch, J., Gajjar, P., Hennekam, R. C., Janssen, F., Kagan, M., Kariminejad, A., Kemper, M. J., … Zenker, M. (2010). Mutations in the human laminin β2 (LAMB2) gene and the associated phenotypic spectrum. *Human Mutation*, *31*(9), 992–1002. https://doi.org/10.1002/humu.21304

Materne, E. M., Maschmeyer, I., Lorenz, A. K., Horland, R., Schimek, K. M. S., Busek,

M., Sonntag, F., Lauster, R., & Marx, U. (2015). The multi-organ chip - A microfluidic platform for long-term multi-tissue coculture. *Journal of Visualized Experiments*, *2015*(98), 1–11. https://doi.org/10.3791/52526

Matlin, K. S., & Caplan, M. J. (2008). Epithelial and Nonepithelial General Principles of Epithelial Epithelial Cell Structure and Polarity. In *Seldin and Geibisch'S the Kidney: Physiology and Pathophysiology* (Fourth Edi). Elsevier Inc. https://doi.org/10.1016/B978-0-12-088488-9.50004-8

Mauch, T. J., Yang, G., Wright, M., Smith, D., & Schoenwolf, G. C. (2000). Signals from trunk paraxial mesoderm induce pronephros formation in chick intermediate mesoderm. *Developmental Biology*, *220*(1), 62–75. https://doi.org/10.1006/dbio.2000.9623

MCGOVERN, V. J. (1964). Persistent Nephrotic Syndrome: a Renal Biopsy Study. *Australasian Annals of Medicine*, *13*, 306–312. https://doi.org/10.1111/imj.1964.13.4.306

McGrogan, A., Franssen, C. F. M., & De Vries, C. S. (2011). The incidence of primary glomerulonephritis worldwide: A systematic review of the literature. *Nephrology Dialysis Transplantation*, *26*(2), 414–430. https://doi.org/10.1093/ndt/gfq665

Miao, J., Pinto e Vairo, F., Hogan, M. C., Erickson, S. B., El Ters, M., Bentall, A. J., Kukla, A., Greene, E. L., Hernandez, L. H., Sethi, S., Lazaridis, K. N., Pichurin, P. N., Lisi, E., Prochnow, C. A., Zand, L., & Fervenza, F. C. (2021). Identification of Genetic Causes of Focal Segmental Glomerulosclerosis Increases With Proper Patient Selection. *Mayo Clinic Proceedings*, *96*(9), 2342–2353. https://doi.org/10.1016/j.mayocp.2021.01.037

Michael Jones, C., Dale, L., Hogan, B. L. M., Wright, C. V. E., & Smith, J. C. (1996). Bone morphogenetic protein-4 (BMP-4) acts during gastrula stages to cause ventralization of Xenopus embryos. *Development*, *122*(5), 1545–1554. https://doi.org/10.1242/dev.122.5.1545

Michaud, J. L. R., Chaisson, K. M., Parks, R. J., & Kennedy, C. R. J. (2006). FSGS-associated α-actinin-4 (K256E) impairs cytoskeletal dynamics in podocytes. *Kidney International*, *70*(6), 1054–1061. https://doi.org/10.1038/sj.ki.5001665

Mir, S., Yavascan, O., Berdeli, A., & Sozeri, B. (2012). TRPC6 gene variants in Turkish

children with steroid-resistant nephrotic syndrome. *Nephrology Dialysis Transplantation*, *27*(1), 205–209. https://doi.org/10.1093/ndt/gfr202

Miyoshi, T., Hiratsuka, K., Saiz, E. G., & Morizane, R. (2020). Kidney organoids in translational medicine: Disease modeling and regenerative medicine. *Developmental Dynamics*, *249*(1), 34–45. https://doi.org/10.1002/dvdy.22

Molinari, E., & Sayer, J. A. (2020). Disease modeling to understand the pathomechanisms of human genetic kidney disorders. *Clinical Journal of the American Society of Nephrology*, *15*(6), 855–872. https://doi.org/10.2215/CJN.08890719

Möller, C. C., Wei, C., Altintas, M. M., Li, J., Greka, A., Ohse, T., Pippin, J. W., Rastaldi, M. P., Wawersik, S., Schiavi, S., Henger, A., Kretzler, M., Shankland, S. J., & Reiser, J. (2007). Induction of TRPC6 channel in acquired forms of proteinuric kidney disease. *Journal of the American Society of Nephrology*, *18*(1), 29–36. https://doi.org/10.1681/ASN.2006091010

Montell, C. (2005). The TRP superfamily of cation channels. *Science's STKE : Signal Transduction Knowledge Environment*, *2005*(272). https://doi.org/10.1126/stke.2722005re3

Montell, C., Birnbaumer, L., & Flockerzi, V. (2002). The TRP channels, a remarkably functional family. *Cell*, *108*(5), 595–598. https://doi.org/10.1016/S0092-8674(02)00670-0

Morizane, R., & Bonventre, J. V. (2017). Generation of nephron progenitor cells and kidney organoids from human pluripotent stem cells. *Nature Protocols*, *12*(1), 195–207. https://doi.org/10.1038/nprot.2016.170

Morizane, R., Lam, A. Q., Freedman, B. S., Kishi, S., Valerius, M. T., & Bonventre, J. V. (2015). Nephron organoids derived from human pluripotent stem cells model kidney development and injury. *Nature Biotechnology*, *33*(11), 1193–1200. https://doi.org/10.1038/nbt.3392

Morrison, S. J., Shah, N. M., & Anderson, D. J. (2010). Stem cell biology. *In-Vitro Fertilization, Third Edition*, *88*, 93–108. https://doi.org/10.1017/CBO9780511984761.008

Moss, A. J., Shimizu, W., Wilde, A. A. M., Towbin, J. A., Zareba, W., Robinson, J. L., Qi, M., Vincent, G. M., Ackerman, M. J., Kaufman, E. S., Hofman, N., Seth, R., Kamakura, S., Miyamoto, Y., Goldenberg, I., Andrews, M. L., & McNitt, S. (2007). Clinical aspects of type-1 long-QT syndrome by location, coding type, and biophysical function of mutations involving the KCNQ1 gene. *Circulation*, *115*(19), 2481–2489. https://doi.org/10.1161/CIRCULATIONAHA.106.665406

Mottl, A. K., Lu, M., Fine, C. A., & Weck, K. E. (2013). A novel TRPC6 mutation in a family with podocytopathy and clinical variability. *BMC Nephrology*, *14*(1), 2–6. https://doi.org/10.1186/1471-2369-14-104

Mugford, J. W., Sipilä, P., McMahon, J. A., & McMahon, A. P. (2008). Osr1 expression demarcates a multi-potent population of intermediate mesoderm that undergoes progressive restriction to an Osr1-dependent nephron progenitor compartment within the mammalian kidney. *Developmental Biology*, *324*(1), 88–98. https://doi.org/10.1016/j.ydbio.2008.09.010

Mulder, J., Sharmin, S., Chow, T., Rodrigues, D. C., Hildebrandt, M. R., D'Cruz, R., Rogers, I., Ellis, J., & Rosenblum, N. D. (2020). Generation of infant- and pediatric-derived urinary induced pluripotent stem cells competent to form kidney organoids. *Pediatric Research*, *87*(4), 647–655. https://doi.org/10.1038/s41390-019-0618-y

Nagano, C., Yamamura, T., Horinouchi, T., Aoto, Y., Ishiko, S., Sakakibara, N., Shima, Y., Nakanishi, K., Nagase, H., Iijima, K., & Nozu, K. (2020). Comprehensive genetic diagnosis of Japanese patients with severe proteinuria. *Scientific Reports*, *10*(1), 1–10. https://doi.org/10.1038/s41598-019-57149-5

Naghavi, M., Abajobir, A. A., Abbafati, C., Abbas, K. M., Abd-Allah, F., Abera, S. F., Aboyans, V., Adetokunboh, O., Ärnlöv, J., Afshin, A., Agrawal, A., Kiadaliri, A. A., Ahmadi, A., Ahmed, M. B., Aichour, A. N., Aichour, I., Aichour, M. T. E., Aiyar, S., Al-Eyadhy, A., … Murray, C. J. L. (2017). Global, regional, and national age-sex specifc mortality for 264 causes of death, 1980-2016: A systematic analysis for the Global Burden of Disease Study 2016. *The Lancet*, *390*(10100), 1151–1210. https://doi.org/10.1016/S0140-6736(17)32152-9

Ngo, T. T. T., Rossbach, B., Sébastien, I., Neubauer, J. C., Kurtz, A., & Hariharan, K. (2022). Functional differentiation and scalable production of renal proximal tubular

epithelial cells from human pluripotent stem cells in a dynamic culture system. *Cell Proliferation*, *55*(3). https://doi.org/10.1111/cpr.13190

Nishikawa, M., Yanagawa, N., Kojima, N., Yuri, S., Hauser, P. V., Jo, O. D., & Yanagawa, N. (2012). Stepwise renal lineage differentiation of mouse embryonic stem cells tracing in vivo development. *Biochemical and Biophysical Research Communications*, *417*(2), 897–902. https://doi.org/10.1016/j.bbrc.2011.12.071

Obara-Ishihara, T., Kuhlman, J., Niswander, L., & Herzlinger, D. (1999). The surface ectoderm is essential for nephric duct formation in intermediate mesoderm. *Development*, *126*(6), 1103–1108. https://doi.org/10.1242/dev.126.6.1103

Obeidová, L., Reiterová, J., Lněnička, P., Štekrová, J., Šafránková, H., Kohoutová, M., & Tesař, V. (2012). TRPC6 gene variants in Czech adult patients with focal segmental glomerulosclerosis and minimal change disease. *Folia Biologica (Czech Republic)*, *58*(4), 173–176.

Ogino, D., Hashimoto, T., Hattori, M., Sugawara, N., Akioka, Y., Tamiya, G., Makino, S., Toyota, K., Mitsui, T., & Hayasaka, K. (2016). Analysis of the genes responsible for steroid-resistant nephrotic syndrome and/or focal segmental glomerulosclerosis in Japanese patients by whole-exome sequencing analysis. *Journal of Human Genetics*, *61*(2), 137–141. https://doi.org/10.1038/jhg.2015.122

OSHIMA, K. (1963). Kidney function. *[Sōgō Rinshō] Clinic All-Round*, *12*, 880–885. https://doi.org/10.1097/00000441-192201000-00001

Oyer, J. A., Chu, A., Brar, S., & Turker, M. S. (2009). Aberrant epigenetic silencing is triggered by a transient reduction in gene expression. *PLoS ONE*, *4*(3). https://doi.org/10.1371/journal.pone.0004832

Pankiewicz, R., Karlen, Y., Imhof, M. O., & Mermod, N. (2005). Reversal of the silencing of tetracycline-controlled genes requires the coordinate action of distinctly acting transcription factors. *Journal of Gene Medicine*, *7*(1), 117–132. https://doi.org/10.1002/jgm.644

Parameswaran, M., & Tam, P. P. L. (1995). Regionalisation of cell fate and morphogenetic movement of the mesoderm during mouse gastrulation. *Developmental Genetics*, *17*(1), 16–28. https://doi.org/10.1002/dvg.1020170104

Passweg, J. R., Baldomero, H., Bader, P., Bonini, C., Cesaro, S., Dreger, P., Duarte, R. F., Dufour, C., Kuball, J., Farge-Bancel, D., Gennery, A., Kroger, N., Lanza, F., Nagler, A., Sureda, A., & Mohty, M. (2016). Hematopoietic stem cell transplantation in Europe 2014: More than 40 000 transplants annually. *Bone Marrow Transplantation*, *51*(6), 786–792. https://doi.org/10.1038/bmt.2016.20

Pawlowski, M., Ortmann, D., Bertero, A., Tavares, J. M., Pedersen, R. A., Vallier, L., & Kotter, M. R. N. (2017a). Inducible and Deterministic Forward Programming of Human Pluripotent Stem Cells into Neurons, Skeletal Myocytes, and Oligodendrocytes. *Stem Cell Reports*, *8*(4), 803–812. https://doi.org/10.1016/j.stemcr.2017.02.016

Pawlowski, M., Ortmann, D., Bertero, A., Tavares, J. M., Pedersen, R. A., Vallier, L., & Kotter, M. R. N. (2017b). Inducible and Deterministic Forward Programming of Human Pluripotent Stem Cells into Neurons, Skeletal Myocytes, and Oligodendrocytessuccessful targeting. *Stem Cell Reports*, *8*(4), 803–812. https://doi.org/10.1016/j.stemcr.2017.02.016

Peired, A. J., Melica, M. E., Molli, A., Nardi, C., Romagnani, P., & Lasagni, L. (2021). Molecular mechanisms of renal progenitor regulation: How many pieces in the puzzle? *Cells*, *10*(1), 1–18. https://doi.org/10.3390/cells10010059

Pelletier, J., Bruening, W., Kashtan, C. E., Mauer, S. M., Manivel, J. C., Striegel, J. E., Houghton, D. C., Junien, C., Habib, R., Fouser, L., Fine, R. N., Silverman, B. L., Haber, D. A., & Housman, D. (1991). Germline mutations in the Wilms' tumor suppressor gene are associated with abnormal urogenital development in denys-drash syndrome. *Cell*, *67*(2), 437–447. https://doi.org/10.1016/0092-8674(91)90194-4

Picollet-D'hahan, N., Zuchowska, A., Lemeunier, I., & Le Gac, S. (2021). Multiorgan-on-a-Chip: A Systemic Approach To Model and Decipher Inter-Organ Communication. *Trends in Biotechnology*, *39*(8), 788–810. https://doi.org/10.1016/j.tibtech.2020.11.014

Raciti, D., Reggiani, L., Geffers, L., Jiang, Q., Bacchion, F., Subrizi, A. E., Clements, D., Tindal, C., Davidson, D. R., Kaissling, B., & Brändli, A. W. (2008). Organization of the pronephric kidney revealed by large-scale gene expression mapping. *Genome*

Biology, *9*(5). https://doi.org/10.1186/gb-2008-9-5-r84

Rahmoune, H., Thompson, P. W., Ward, J. M., Smith, C. D., Hong, G., & Brown, J. (2005). Glucose transporters in human renal proximal tubular cells isolated from the urine of patients with non-insulin-dependent diabetes. *Diabetes*, *54*(12), 3427–3434. https://doi.org/10.2337/diabetes.54.12.3427

Ramalho-Santos, M., & Willenbring, H. (2007). On the Origin of the Term “Stem Cell.” *Cell Stem Cell*, *1*(1), 35–38. https://doi.org/10.1016/j.stem.2007.05.013

Rand, U., Riedel, J., Hillebrand, U., Shin, D., Willenberg, S., Behme, S., Klawonn, F., Köster, M., Hauser, H., & Wirth, D. (2015). Single-cell analysis reveals heterogeneity in onset of transgene expression from synthetic tetracycline-dependent promoters. *Biotechnology Journal*, *10*(2), 323–331. https://doi.org/10.1002/biot.201400076

Randolph, L. N., Bao, X., Zhou, C., & Lian, X. (2017). An all-in-one, Tet-On 3G inducible PiggyBac system for human pluripotent stem cells and derivatives. *Scientific Reports*, *7*(1), 1–8. https://doi.org/10.1038/s41598-017-01684-6

Rashid, S. T., Corbineau, S., Hannan, N., Marciniak, S. J., Miranda, E., Alexander, G., Huang-Doran, I., Griffin, J., Ahrlund-Richter, L., Skepper, J., Semple, R., Weber, A., Lomas, D. A., & Vallier, L. (2010). Modeling inherited metabolic disorders of the liver using human induced pluripotent stem cells. *Journal of Clinical Investigation*, *120*(9), 3127–3136. https://doi.org/10.1172/JCI43122

Re’em-Kalma, Y., Lamb, T., & Frank, D. (1995). Competition between noggin and bone morphogenetic protein 4 activities may regulate dorsalization during Xenopus development. *Proceedings of the National Academy of Sciences of the United States of America*, *92*(26), 12141–12145. https://doi.org/10.1073/pnas.92.26.12141

Redondo, P. C., Jardin, I., Lopez, J. J., Salido, G. M., & Rosado, J. A. (2008). Intracellular Ca2+ store depletion induces the formation of macromolecular complexes involving hTRPC1, hTRPC6, the type II IP3 receptor and SERCA3 in human platelets. *Biochimica et Biophysica Acta - Molecular Cell Research*, *1783*(6), 1163–1176. https://doi.org/10.1016/j.bbamcr.2007.12.008

Reidy, K., & Kaskel, F. J. (2007). Pathophysiology of focal segmental glomerulosclerosis. *Pediatric Nephrology*, *22*(3), 350–354.

https://doi.org/10.1007/s00467-006-0357-2

Reiser, J., Polu, K. R., Möller, C. C., Kenlan, P., Altintas, M. M., Wei, C., Faul, C., Herbert, S., Villegas, I., Avila-casado, C., Mcgee, M., Sugimoto, H., Brown, D., Kalluri, R., Mundel, P., Paula, L., Clapham, D. E., Pollak, M. R., Instituto, U., & Medical, R. (2006). Required for Normal Renal Function. *Matrix*, *37*(7), 739–744.

Reiser, J., Polu, K. R., Möller, C. C., Kenlan, P., Altintas, M. M., Wei, C., Faul, C., Herbert, S., Villegas, I., Avila-Casado, C., McGee, M., Sugimoto, H., Brown, D., Kalluri, R., Mundel, P., Smith, P. L., Clapham, D. E., & Pollak, M. R. (2005). TRPC6 is a glomerular slit diaphragm-associated channel required for normal renal function. *Nature Genetics*, *37*(7), 739–744. https://doi.org/10.1038/ng1592

Reiser, J., & Sever, S. (2013). Podocyte biology and pathogenesis of kidney disease. *Annual Review of Medicine*, *64*, 357–366. https://doi.org/10.1146/annurev-med-050311-163340

Ren, X., Zhang, J., Gong, X., Niu, X., Zhang, X., Chen, P., & Zhang, X. (2010). Differentiation of murine embryonic stem cells toward renal lineages by conditioned medium from ureteric bud cells in vitro. *Acta Biochimica et Biophysica Sinica*, *42*(7), 464–471. https://doi.org/10.1093/abbs/gmq046

Riehle, M., Büscher, A. K., Gohlke, B. O., Kaßmann, M., Kolatsi-Joannou, M., Bräsen, J. H., Nagel, M., Becker, J. U., Winyard, P., Hoyer, P. F., Preissner, R., Krautwurst, D., Gollasch, M., Weber, S., & Harteneck, C. (2016). TRPC6 G757D loss-of-function mutation associates with FSGS. *Journal of the American Society of Nephrology*, *27*(9), 2771–2783. https://doi.org/10.1681/ASN.2015030318

Romagnani, P., Lasagni, L., & Remuzzi, G. (2013). Renal progenitors: An evolutionary conserved strategy for kidney regeneration. *Nature Reviews Nephrology*, *9*(3), 137–146. https://doi.org/10.1038/nrneph.2012.290

Rossbach, B., Hildebrand, L., El-Ahmad, L., Stachelscheid, H., Reinke, P., & Kurtz, A. (2016). Generation of a human induced pluripotent stem cell line from urinary cells of a healthy donor using an integration free vector. *Stem Cell Research*, *16*(2), 314–317. https://doi.org/10.1016/j.scr.2015.12.018

Ruggenenti, P., Perna, A., Gherardi, G., Garini, G., Zoccali, C., Salvadori, M., Scolari, F., Schena, F. P., & Remuzzi, G. (1999). Renoprotective properties of ACE-

inhibition in non-diabetic nephropathies with non-nephrotic proteinuria. *Lancet*, *354*(9176), 359–364. https://doi.org/10.1016/S0140-6736(98)10363-X

Ruotsalainen, V., Ljungberg, P., Wartiovaara, J., Lenkkeri, U., Kestila, M., Jalanko, H., Holmberg, C., & Tryggvason, K. (1999). Nephrin is specifically located at the slit diaphragm of glomerular podocytes. *Proceedings of the National Academy of Sciences of the United States of America*, *96*(14), 7962–7967. https://doi.org/10.1073/pnas.96.14.7962

Sadelain, M., Papapetrou, E. P., & Bushman, F. D. (2012). Safe harbours for the integration of new DNA in the human genome. *Nature Reviews Cancer*, *12*(1), 51–58. https://doi.org/10.1038/nrc3179

Sadowski, C. E., Lovric, S., Ashraf, S., Pabst, W. L., Gee, H. Y., Kohl, S., Engelmann, S., Vega-Warner, V., Fang, H., Halbritter, J., Somers, M. J., Tan, W., Shril, S., Fessi, I., Lifton, R. P., Bockenhauer, D., El-Desoky, S., Kari, J. A., Zenker, M., … Zolotnistskaya, A. (2015). A single-gene cause in 29.5% of cases of steroid-resistant nephrotic syndrome. *Journal of the American Society of Nephrology*, *26*(6), 1279–1289. https://doi.org/10.1681/ASN.2014050489

Sainio, K., Suvanto, P., Davies, J., Wartiovaara, J., Wartiovaara, K., Saarma, M., Arumäe, U., Meng, X., Lindahl, M., Pachnis, V., & Sariola, H. (1997). Glial-cell-line-derived neurotrophic factor is required for bud initiation from ureteric epithelium. *Development*, *124*(20), 4077–4087. https://doi.org/10.1242/dev.124.20.4077

Saleem, M. A. (2015). One hundred ways to kill a podocyte. *Nephrology Dialysis Transplantation*, *30*(8), 1266–1271. https://doi.org/10.1093/ndt/gfu363

Saliba, Y., Karam, R., Smayra, V., Aftimos, G., Abramowitz, J., Birnbaumer, L., & Farès, N. (2015). Evidence of a role for fibroblast transient receptor potential canonical 3 Ca2+ channel in renal fibrosis. *Journal of the American Society of Nephrology*, *26*(8), 1855–1876. https://doi.org/10.1681/ASN.2014010065

Sambharia, M., Rastogi, P., & Thomas, C. P. (2022). Monogenic focal segmental glomerulosclerosis: A conceptual framework for identification and management of a heterogeneous disease. *American Journal of Medical Genetics, Part C: Seminars in Medical Genetics*, *190*(3), 377–398. https://doi.org/10.1002/ajmg.c.31990

Santín, S., Ars, E., Rossetti, S., Salido, E., Silva, I., García-Maset, R., Giménez, I.,

Ruíz, P., Mendizábal, S., Nieto, J. L., Peña, A., Camacho, J. A., Fraga, G., Cobo, M. Á., Bernis, C., Ortiz, A., De Pablos, A. L., Sánchez-Moreno, A., Pintos, G., … Torra, R. (2009). TRPC6 mutational analysis in a large cohort of patients with focal segmental glomerulosclerosis. *Nephrology Dialysis Transplantation*, *24*(10), 3089–3096. https://doi.org/10.1093/ndt/gfp229

Saxon, L., & Sariola, H. (1987). Pediatric Nephrology Early organogenesis of the kidney. *Pediatr Nephrol*, *1*, 385–392.

Sayer, J. A., & Iqbal, Z. (2017). Case Report: Making a diagnosis of familial renal disease - clinical and patient perspectives. *F1000Research*, *6*(May), 1–10. https://doi.org/10.12688/f1000research.11316.1

Schaldecker, T., Kim, S., Tarabanis, C., Tian, D., Hakroush, S., Castonguay, P., Ahn, W., Wallentin, H., Heid, H., Hopkins, C. R., Lindsley, C. W., Riccio, A., Buvall, L., Weins, A., & Greka, A. (2013). Inhibition of the TRPC5 ion channel protects the kidney filter. *Journal of Clinical Investigation*, *123*(12), 5298–5309. https://doi.org/10.1172/JCI71165

Schell, C., & Huber, T. B. (2012). New players in the pathogenesis of focal segmental glomerulosclerosis. *Nephrology Dialysis Transplantation*, *27*(9), 3406–3412. https://doi.org/10.1093/ndt/gfs273

Schlöndorff, J., Del Camino, D., Carrasquillo, R., Lacey, V., & Pollak, M. R. (2009). TRPC6 mutations associated with focal segmental glomerulosclerosis cause constitutive activation of NFAT-dependent transcription. *American Journal of Physiology - Cell Physiology*, *296*(3), 558–569. https://doi.org/10.1152/ajpcell.00077.2008

Schultheiss, T. M., James, R. G., Listopadova, A., & Herzlinger, D. (2003). Formation of the Nephric Duct. *The Kidney: From Normal Development to Congenital Disease*, 51–60. https://doi.org/10.1016/B978-012722441-1/50006-3

Seely, J. C. (2017). A brief review of kidney development, maturation, developmental abnormalities, and drug toxicity: Juvenile animal relevancy. *Journal of Toxicologic Pathology*, *30*(2), 125–133. https://doi.org/10.1293/tox.2017-0006

Shabaka, A., Ribera, A. T., & Fernández-Juárez, G. (2020). Focal Segmental Glomerulosclerosis: State-of-the-Art and Clinical Perspective. *Nephron*, *144*(9),

413–427. https://doi.org/10.1159/000508099

Simpson, E., & Dazzi, F. (2019). Bone marrow transplantation 1957-2019. *Frontiers in Immunology*, *10*(JUN), 1–6. https://doi.org/10.3389/fimmu.2019.01246

Singer, S. D., Liu, Z., & Cox, K. D. (2012). Minimizing the unpredictability of transgene expression in plants: The role of genetic insulators. *Plant Cell Reports*, *31*(1), 13–25. https://doi.org/10.1007/s00299-011-1167-y

Sommer, C. A., Stadtfeld, M., Murphy, G. J., Hochedlinger, K., Kotton, D. N., & Mostoslavsky, G. (2009). Induced Pluripotent Stem Cell Generation Using a Single Lentiviral Stem Cell Cassette. *Stem Cells*, *27*(3), 543–549. https://doi.org/10.1634/stemcells.2008-1075

Song, B., Smink, A. M., Jones, C. V., Callaghan, J. M., Firth, S. D., Bernard, C. A., Laslett, A. L., Kerr, P. G., & Ricardo, S. D. (2012). The Directed Differentiation of Human iPS Cells into Kidney Podocytes. *PLoS ONE*, *7*(9), 1–9. https://doi.org/10.1371/journal.pone.0046453

Sottas, V., & Abriel, H. (2016). Negative-dominance phenomenon with genetic variants of the cardiac sodium channel Nav1.5. *Biochimica et Biophysica Acta - Molecular Cell Research*, *1863*(7), 1791–1798. https://doi.org/10.1016/j.bbamcr.2016.02.013

Soueid-Baumgarten, S., Yelin, R., Davila, E. K., & Schultheiss, T. M. (2014). Parallel waves of inductive signaling and mesenchyme maturation regulate differentiation of the chick mesonephros. *Developmental Biology*, *385*(1), 122–135. https://doi.org/10.1016/j.ydbio.2013.09.026

Stevens, P. E., & Levin, A. (2013). Evaluation and management of chronic kidney disease: Synopsis of the kidney disease: Improving global outcomes 2012 clinical practice guideline. *Annals of Internal Medicine*, *158*(11), 825–830. https://doi.org/10.7326/0003-4819-158-11-201306040-00007

Stokes, M. B., Valeri, A. M., Markowitz, G. S., & D'Agati, V. D. (2006). Cellular focal segmental glomerulosclerosis: Clinical and pathologic features. *Kidney International*, *70*(10), 1783–1792. https://doi.org/10.1038/sj.ki.5001903

Subramanian, B., Sun, H., Yan, P., Charoonratana, V. T., Higgs, H. N., Wang, F., Lai, K. M. V., Valenzuela, D. M., Brown, E. J., Schlöndorff, J. S., & Pollak, M. R. (2016).

Mice with mutant Inf2 show impaired podocyte and slit diaphragm integrity in response to protamine-induced kidney injury. *Kidney International*, *90*(2), 363–372. https://doi.org/10.1016/j.kint.2016.04.020

Sun, H., Perez-Gill, C., Schlöndorff, J. S., Subramanian, B., & Pollak, M. R. (2021). Dysregulated dynein-mediated trafficking of nephrin causes INF2-related podocytopathy. *Journal of the American Society of Nephrology*, *32*(2), 307–322. https://doi.org/10.1681/ASN.2020081109

Sun, Z. J., Ng, K. H., Liao, P., Zhang, Y., Ng, J. L., Liu, I. D., Tan, P. H., Chong, S. S. C., Chan, Y. H., Liu, J., Davila, S., Heng, C. K., Jordan, S. C., Soong, T. W., & Yap, H. K. (2015). Genetic interactions between TRPC6 and NPHS1 variants affect posttransplant risk of recurrent focal segmental glomerulosclerosis. *American Journal of Transplantation*, *15*(12), 3229–3238. https://doi.org/10.1111/ajt.13378

Taguchi, A., Kaku, Y., Ohmori, T., Sharmin, S., Ogawa, M., Sasaki, H., & Nishinakamura, R. (2014). Redefining the in vivo origin of metanephric nephron progenitors enables generation of complex kidney structures from pluripotent stem cells. *Cell Stem Cell*, *14*(1), 53–67. https://doi.org/10.1016/j.stem.2013.11.010

Takahashi, K., Tanabe, K., Ohnuki, M., Narita, M., Ichisaka, T., Tomoda, K., & Yamanaka, S. (2007). Induction of Pluripotent Stem Cells from Adult Human Fibroblasts by Defined Factors. *Cell*, *131*(5), 861–872. https://doi.org/10.1016/j.cell.2007.11.019

Takasato, M., Er, P. X., Becroft, M., Vanslambrouck, J. M., Stanley, E. G., Elefanty, A. G., & Little, M. H. (2014). Directing human embryonic stem cell differentiation towards a renal lineage generates a self-organizing kidney. *Nature Cell Biology*, *16*(1), 118–126. https://doi.org/10.1038/ncb2894

Takasato, M., & Little, M. H. (2015). The origin of the mammalian kidney: Implications for recreating the kidney in vitro. *Development (Cambridge)*, *142*(11), 1937–1947. https://doi.org/10.1242/dev.104802

Tam, P. P. L., & Beddington, R. S. P. (1987). The formation of mesodermal tissues in the mouse embryo during gastrulation and early organogenesis. *Development*, *99*(1), 109–126. https://doi.org/10.1242/dev.99.1.109

Tam, P. P. L., Parameswaran, M., Kinder, S. J., & Weinberger, R. P. (1997). The

allocation of epiblast cells to the embryonic heart and other mesodermal lineages: The role of ingression and tissue movement during gastrulation. *Development*, *124*(9), 1631–1642. https://doi.org/10.1242/dev.124.9.1631

Tan, W., Lovric, S., Ashraf, S., Rao, J., Schapiro, D., Airik, M., Shril, S., Gee, H. Y., Baum, M., Daouk, G., Ferguson, M. A., Rodig, N., Somers, M. J. G., Stein, D. R., Vivante, A., Warejko, J. K., Widmeier, E., & Hildebrandt, F. (2018). Analysis of 24 genes reveals a monogenic cause in 11.1% of cases with steroid-resistant nephrotic syndrome at a single center. *Pediatric Nephrology*, *33*(2), 305–314. https://doi.org/10.1007/s00467-017-3801-6

Tang, Q., Guo, W., Zheng, L., Wu, J. X., Liu, M., Zhou, X., Zhang, X., & Chen, L. (2018). Structure of the receptor-activated human TRPC6 and TRPC3 ion channels. *Cell Research*, *28*(7), 746–755. https://doi.org/10.1038/s41422-018-0038-2

Tesson, L., Usal, C., Meǫnoret, S., Leung, E., Niles, B. J., Remy, S., Santiago, Y., Vincent, A. I., Meng, X., Zhang, L., Gregory, P. D., Anegon, I., & Cost, G. J. (2011). Knockout rats generated by embryo microinjection of TALENs. *Nature Biotechnology*, *29*(8), 695–696. https://doi.org/10.1038/nbt.1940

Tian, D., Jacobo, S. M. P., Billing, D., Rozkalne, A., Gage, S. D., Anagnostou, T., Pavenstaedt, H., Hsu, H. H., Schlondorff, J., Ramos, A., & Greka, A. (2010). Antagonistic regulation of actin dynamics and cell motility by TRPC5 and TRPC6 channels (Science Signaling (2010)). *Science Signaling*, *3*(147), 1–14. https://doi.org/10.1126/scisignal.3147er11

Tian, X., Kim, J. J., Monkley, S. M., Gotoh, N., Nandez, R., Soda, K., Inoue, K., Balkin, D. M., Hassan, H., Son, S. H., Lee, Y., Moeckel, G., Calderwood, D. A., Holzman, L. B., Critchley, D. R., Zent, R., Reiser, J., & Ishibe, S. (2014). Podocyte-associated talin1 is critical for glomerular filtration barrier maintenance. *Journal of Clinical Investigation*, *124*(3), 1098–1113. https://doi.org/10.1172/JCI69778

Tonelli, M., Wiebe, N., Knoll, G., Bello, A., Browne, S., Jadhav, D., Klarenbach, S., & Gill, J. (2011). Systematic review: Kidney transplantation compared with dialysis in clinically relevant outcomes. *American Journal of Transplantation*, *11*(10), 2093–2109. https://doi.org/10.1111/j.1600-6143.2011.03686.x

Torisawa, Y. S., Spina, C. S., Mammoto, T., Mammoto, A., Weaver, J. C., Tat, T., Collins, J. J., & Ingber, D. E. (2014). Bone marrow-on-a-chip replicates hematopoietic niche physiology in vitro. *Nature Methods*, *11*(6), 663–669. https://doi.org/10.1038/nmeth.2938

Uusitalo, E., Rantanen, M., Kallionpää, R. A., Pöyhönen, M., Leppävirta, J., Ylä-Outinen, H., Riccardi, V. M., Pukkala, E., Pitkäniemi, J., Peltonen, S., & Peltonen, J. (2016). Distinctive cancer associations in patients with neurofibromatosis type 1. *Journal of Clinical Oncology*, *34*(17), 1978–1986. https://doi.org/10.1200/JCO.2015.65.3576

Van Rossum, D. B., Oberdick, D., Rbaibi, Y., Bhardwaj, G., Barrow, R. K., Nikolaidis, N., Snyder, S. H., Kiselyov, K., & Patterson, R. L. (2008). TRP_2, a lipid/trafficking domain that mediates diacylglycerol-induced vesicle fusion. *Journal of Biological Chemistry*, *283*(49), 34384–34392. https://doi.org/10.1074/jbc.M804707200

Varas, F., Stadtfeld, M., de Andres-Aguayo, L., Maherali, N., di Tullio, A., Pantano, L., Notredame, C., Hochedlinger, K., & Graf, T. (2009). Fibroblast-Derived Induced Pluripotent Stem Cells Show No Common Retroviral Vector Insertions. *Stem Cells*, *27*(2), 300–306. https://doi.org/10.1634/stemcells.2008-0696

Venkatachalam, K., & Montell, C. (2007). TRP channels. *Annual Review of Biochemistry*, *76*, 387–417. https://doi.org/10.1146/annurev.biochem.75.103004.142819

Verheijden, K. A. T., Sonneveld, R., Bakker-van Bebber, M., Wetzels, J. F. M., Van Der Vlag, J., & Nijenhuis, T. (2018). The calcium-dependent protease calpain-1 links TRPC6 activity to podocyte injury. *Journal of the American Society of Nephrology*, *29*(8), 2099–2109. https://doi.org/10.1681/ASN.2016111248

Vigneau, C., Polgar, K., Striker, G., Elliott, J., Hyink, D., Weber, O., Fehling, H. J., Keller, G., Burrow, C., & Wilson, P. (2007). Mouse embryonic stem cell-derived embryoid bodies generate progenitors that integrate long term into renal proximal tubules in vivo. *Journal of the American Society of Nephrology*, *18*(6), 1709–1720. https://doi.org/10.1681/ASN.2006101078

Vogetseder, A., Picard, N., Gaspert, A., Walch, M., Kaissling, B., & Le Hir, M. (2008). Proliferation capacity of the renal proximal tubule involves the bulk of differentiated

epithelial cells. *American Journal of Physiology - Cell Physiology*, *294*(1), 22–28. https://doi.org/10.1152/ajpcell.00227.2007

Wang, F., Zhang, Y., Mao, J., Yu, Z., Yi, Z., Yu, L., Sun, J., Wei, X., Ding, F., Zhang, H., Xiao, H., Yao, Y., Tan, W., Lovric, S., Ding, J., & Hildebrandt, F. (2017). Spectrum of mutations in Chinese children with steroid-resistant nephrotic syndrome. *Pediatric Nephrology*, *32*(7), 1181–1192. https://doi.org/10.1007/s00467-017-3590-y

Wang, H., Yang, H., Shivalila, C. S., Dawlaty, M. M., Cheng, A. W., Zhang, F., & Jaenisch, R. (2013). One-step generation of mice carrying mutations in multiple genes by CRISPR/cas-mediated genome engineering. *Cell*, *153*(4), 910–918. https://doi.org/10.1016/j.cell.2013.04.025

Wang, M., Chun, J., Genovese, G., Knob, A. U., Benjamin, A., Wilkins, M. S., Friedman, D. J., Appel, G. B., Lifton, R. P., Mane, S., & Pollak, M. R. (2019). Contributions of rare gene variants to familial and sporadic FSGS. *Journal of the American Society of Nephrology*, *30*(9), 1625–1640. https://doi.org/10.1681/ASN.2019020152

Weening, J. J., & Jennette, J. C. (2012). Historical milestones in renal pathology. *Virchows Archiv*, *461*(1), 3–11. https://doi.org/10.1007/s00428-012-1254-7

Winn, M. P., Conlon, P. J., Lynn, K. L., Farrington, M. K., Creazzo, T., Hawkins, A. F., Daskalakis, N., Kwan, S. Y., Ebersviller, S., Burchette, J. L., Pericak-Vance, M. A., Howell, D. N., Vance, J. M., & Rosenberg, P. B. (2005). Medicine: A mutation in the TRPC6 cation channel causes familial focal segmental glomerulosclerosis. *Science*, *308*(5729), 1801–1804. https://doi.org/10.1126/science.1106215

Woltjen, K., Michael, I. P., Mohseni, P., Desai, R., Mileikovsky, M., Hämäläinen, R., Cowling, R., Wang, W., Liu, P., Gertsenstein, M., Kaji, K., Sung, H. K., & Nagy, A. (2009). PiggyBac transposition reprograms fibroblasts to induced pluripotent stem cells. *Nature*, *458*(7239), 766–770. https://doi.org/10.1038/nature07863

Wu, Y. L., Xie, J., An, S. W., Oliver, N., Barrezueta, N. X., Lin, M. H., Birnbaumer, L., & Huang, C. L. (2017). Inhibition of TRPC6 channels ameliorates renal fibrosis and contributes to renal protection by soluble klotho. *Kidney International*, *91*(4), 830–841. https://doi.org/10.1016/j.kint.2016.09.039

Xia, Y., Nivet, E., Sancho-Martinez, I., Gallegos, T., Suzuki, K., Okamura, D., Wu, M. Z.,

Dubova, I., Esteban, C. R., Montserrat, N., Campistol, J. M., & Izpisua Belmonte, J. C. (2013). Directed Differentiation of Human Pluripotent Cells to Ureteric Bud Kidney Progenitor-Like Cells. *Nature Cell Biology*, *15*(12), 1507–1515. https://doi.org/10.1038/ncb2872

Yao, J., Le, T. C., Kos, C. H., Henderson, J. M., Allen, P. G., Denker, B. M., & Pollak, M. R. (2004). α-actinin-4-mediated FSGS: An inherited kidney disease caused by an aggregated and rapidly degraded cytoskeletal protein. *PLoS Biology*, *2*(6), 787–794. https://doi.org/10.1371/journal.pbio.0020167

Yatskievych, T. A., Ladd, A. N., & Antin, P. B. (1997). Induction of cardiac myogenesis in avian pregastrula epiblast: The role of the hypoblast and activin. *Development*, *124*(13), 2561–2570. https://doi.org/10.1242/dev.124.13.2561

Yue, Z., Xie, J., Yu, A. S., Stock, J., Du, J., & Yue, L. (2015). Role of trp channels in the cardiovascular system. *American Journal of Physiology - Heart and Circulatory Physiology*, *308*(3), H157–H182. https://doi.org/10.1152/ajpheart.00457.2014

Zeisberg, M., & Kalluri, R. (2008). Reversal of experimental renal fibrosis by BMP7 provides insights into novel therapeutic strategies for chronic kidney disease. *Pediatric Nephrology*, *23*(9), 1395–1398. https://doi.org/10.1007/s00467-008-0818-x

Zenker, M., Pierson, M., Jonveaux, P., & Reis, A. (2005). Demonstration of two novel LAMB2 mutations in the original Pierson syndrome family reported 42 years ago [5]. *American Journal of Medical Genetics*, *138 A*(1), 73–74. https://doi.org/10.1002/ajmg.a.30894

Zhang, Q., Ma, J., Xie, J., Wang, Z., Zhu, B., Hao, X., Yang, L., Ren, H., & Chen, N. (2013). Screening of ACTN4 and TRPC6 mutations in a chinese cohort of patients with adult-onset familial focal segmental glomerulosclerosis. *Contributions to Nephrology*, *181*, 91–100. https://doi.org/10.1159/000348471

Zheng, Z., Xu, Y., Krügel, U., Schaefer, M., Grune, T., Nürnberg, B., Köhler, M.-B., Gollasch, M., Tsvetkov, D., & Markó, L. (2022). In Vivo Inhibition of TRPC6 by SH045 Attenuates Renal Fibrosis in a New Zealand Obese (NZO) Mouse Model of Metabolic Syndrome. *International Journal of Molecular Sciences*, *23*(12), 6870. https://doi.org/10.3390/ijms23126870

Zhong, J., Yang, H. C., & Fogo, A. B. (2017). A perspective on chronic kidney disease progression. *American Journal of Physiology - Renal Physiology*, *312*(3), F375–F384. https://doi.org/10.1152/ajprenal.00266.2016

Zhou, T., Benda, C., Dunzinger, S., Huang, Y., Ho, J. C., Yang, J., Wang, Y., Zhang, Y., Zhuang, Q., Li, Y., Bao, X., Tse, H. F., Grillari, J., Grillari-Voglauer, R., Pei, D., & Esteban, M. A. (2012). Generation of human induced pluripotent stem cells from urine samples. *Nature Protocols*, *7*(12), 2080–2089. https://doi.org/10.1038/nprot.2012.115

Zhou, W., & Freed, C. R. (2009). Adenoviral gene delivery can reprogram human fibroblasts to induced pluripotent stem cells. *Stem Cells*, *27*(11), 2667–2674. https://doi.org/10.1002/stem.201

Zhou, Y., Castonguay, P., Sidhom, E. H., Clark, A. R., Dvela-Levitt, M., Kim, S., Sieber, J., Wieder, N., Jung, J. Y., Andreeva, S., Reichardt, J., Dubois, F., Hoffmann, S. C., Basgen, J. M., Montesinos, M. S., Weins, A., Johnson, A. C., Lander, E. S., Garrett, M. R., … Greka, A. (2017). A small-molecule inhibitor of TRPC5 ion channels suppresses progressive kidney disease in animal models. *Science*, *358*(6368), 1332–1336. https://doi.org/10.1126/science.aal4178

Zhu, B., Chen, N., Wang, Z. hui, Pan, X. xia, Ren, H., Zhang, W., & Wang, W. ming. (2009). Identification and functional analysis of a novel TRPC6 mutation associated with late onset familial focal segmental glomerulosclerosis in Chinese patients. *Mutation Research - Fundamental and Molecular Mechanisms of Mutagenesis*, *664*(1–2), 84–90. https://doi.org/10.1016/j.mrfmmm.2008.11.021

Zhu, M. X. (2005). Multiple roles of calmodulin and other Ca2+-binding proteins in the functional regulation of TRP channels. *Pflugers Archiv European Journal of Physiology*, *451*(1), 105–115. https://doi.org/10.1007/s00424-005-1427-1

STATUTORY DECLARATION

"I, Lilas Batool, by personally signing this document in lieu of an oath, hereby affirm that I prepared the submitted dissertation on the topic "Revealing the molecular nuances of TRPC6 in focal segmental glomerulosclerosis in an *in vitro* human podocyte model" or "Aufdeckung der molekularen Nuancen von TRPC6 bei der fokalen segmentalen Glomerulosklerose in einem *In-vitro*-Modell menschlicher Podozyten", independently and without the support of third parties, and that I used no other sources and aids than those stated.

All parts which are based on the publications or presentations of other authors, either in letter or in spirit, are specified as such in accordance with the citing guidelines. The sections on methodology (in particular regarding practical work, laboratory regulations, statistical processing) and results (in particular regarding figures, charts and tables) are exclusively my responsibility.

Furthermore, I declare that I have correctly marked all of the data, the analyses, and the conclusions generated from data obtained in collaboration with other persons, and that I have correctly marked my own contribution and the contributions of other persons (cf. declaration of contribution). I have correctly marked all texts or parts of texts that were generated in collaboration with other persons.

My contributions to any publications to this dissertation correspond to those stated in the below joint declaration made together with the supervisor. All publications created within the scope of the dissertation comply with the guidelines of the ICMJE (International Committee of Medical Journal Editors; www.icmje.org) on authorship. In addition, I declare that I shall comply with the regulations of Charité – Universitätsmedizin Berlin on ensuring good scientific practice.

I declare that I have not yet submitted this dissertation in identical or similar form to another Faculty.

The significance of this statutory declaration and the consequences of a false statutory declaration under criminal law (Sections 156, 161 of the German Criminal Code) are known to me."

_____

Date Doctoral Candidate Signature

Declaration of your own contribution to any publications

Lilas Batool contributed the following to the below listed publications:

Publication 1: Batool L, Raab C, Beez CM, Hariharan K, Kurtz A, Gollasch M, & Rossbach B. Generation of human induced pluripotent stem cell line (BCRTi006-A) from a patient with focal segmental glomerulosclerosis disease. *Stem Cell Res*. 2023;69(March)

Contribution: I am the first author of this publication. I have significantly contributed to the methodology, investigation, formal analysis, visualization, and writing the original draft. In figure 1, I contributed to reprogramming the urinary cells to induced pluripotent stem cells, characterized the pluripotency of the cells, checked for vector loss, and analyzed the differentiation potential of the cell line.

Publication 2: Batool L, Raab C, Beez CM, Kurtz A, Gollasch M, Rossbach B. Generation of human induced pluripotent stem cell line (BCRTi007-A) from urinary cells of a patient with autosomal dominant polycystic kidney disease. *Stem Cell Res*. 2023;69(March)

Contribution: I am the first author of this publication. I have significantly contributed to the methodology, investigation, formal analysis, visualization, and writing the original draft. In figure 1, I contributed to reprogramming the urinary cells to induced pluripotent stem cells, characterized the pluripotency of the cells, checked for vector loss, and analyzed the differentiation potential of the cell line.

Publication 3: Batool L, Storozhuk O, Raab C, Beez CM, Selig M, Harder A, Kurtz A. Generation of two human induced pluripotent stem cell lines from a patient with Neurofibromatosis type 1 (NF1) and pathogenic NF1 gene variant c . 1466 A > G BCRTi011-A as well as a first-degree healthy relative. *Stem Cell Res*. 2023;71(August)

Contribution: I am the first author of this publication. I have significantly contributed to the methodology, investigation, formal analysis, visualization, and writing the original draft. In figure 1, I contributed to reprogramming the urinary cells to induced pluripotent stem cells, characterized the pluripotency of the cells, checked for vector loss, and analyzed the differentiation potential of the cell line.

Publication 4: Batool L, Hariharan K, Xu Y, Kaßmann M, Tsvetkov D, Gohlke OB,

Kaden S, Gossen M, Nürnberg, Kurtz, Gollasch M. An inactivating human TRPC6 channel mutation without focal segmental glomerulosclerosis. Cellular and Molecular Life Sciences. 2023; (August)

Contribution: I am the first author of this publication. I have significantly contributed to the methodology, investigation, formal analysis, visualization, and writing the original draft. In Figure 1, I contributed to the construction of the plasmids and performed transfection. Figure 4, 5, and 8 was created on the basis of my statistical evaluation.

_____

Signature, date and stamp of first supervising university professor / lecturer

_____

Signature of doctoral candidate

CURRICULUM VITAE

[My curriculum vitae does not appear in the electronic version of my paper for reasons of data protection]

[My curriculum vitae does not appear in the electronic version of my paper for reasons of data protection]

[My curriculum vitae does not appear in the electronic version of my paper for reasons of data protection]

LIST OF PUBLICATION

Batool, L., Hariharan, K., Xu, Y., Kaßmann M., Tsvetkov D., Gohlke BO., Kaden S., Gossen M., Nürnberg B., Kurtz A., Gollasch M. An inactivating human TRPC6 channel mutation without focal segmental glomerulosclerosis. *Cellular and Molecular Life Sciences*, 1–16. https://doi.org/10.1007/s00018-023-04901-w

Batool L., Storozhuk O., Raab C., Beez CM., Selig M., Harder A., Kurtz A. Generation of two human induced pluripotent stem cell lines from a patient with Neurofibromatosis type 1 (NF1) and pathogenic NF1 gene variant c . 1466 A > G BCRTi011-A as well as a first-degree healthy relative. *Stem Cell Res*. 2023;71(August):103184. doi:10.1016/j.scr.2023.103184

Batool L., Raab C., Beez CM., Hariharan K., Kurtz A., Gollasch M., Rossbach B. Generation of human induced pluripotent stem cell line (BCRTi006-A) from a patient with focal segmental glomerulosclerosis disease. *Stem Cell Research*, *69*(March), 103070. https://doi.org/10.1016/j.scr.2023.103070

Batool L., Raab C., Beez CM., Kurtz A., Gollasch M., Rossbach B. Generation of human induced pluripotent stem cell line (BCRTi007-A) from urinary cells of a patient with autosomal dominant polycystic kidney disease. *Stem Cell Res*. 2023;69(March):103071. doi:10.1016/j.scr.2023.103071

ACKNOWLEDGEMENT

I would like to express my sincere gratitude and appreciation to my supervisors, friends, and family who have supported and helped me throughout the completion of this thesis. First and foremost, I am extremely grateful to my supervisor Prof. Andreas Kurtz, for giving me the opportunity to work in his lab. Your guidance, encouragement, and valuable insights have helped me to complete this thesis.

My deep gratitude goes to Dr. Maik Gollasch and Dr. Manfred Gossen for providing me with immense knowledge to anchor me in this niche and for challenging me to think critically and analytically. Their teaching has not only broadened my understanding but also motivated me to pursue higher goals. I would like to thank Prof. Petra Reinke for her dedication and support in supervising me.

A special mention goes to Dr. Krithika Hariharan with whom I enjoyed numerous discussions and troubleshooting during the course of my project. I am very grateful to you for your support and guidance; you have definitely changed my way of thinking and persuaded me to become a better researcher.

I would also like to thank the Charité University of Medicine Berlin and Berlin Brandenburg School for Regenerative Therapies for giving me the opportunity to pursue my Ph.D. at the BIH Center for Regenerative Therapies. I would like to thank Dr. Sabine Bartosch and Bianca Kühl for their support and resourcefulness in providing an academic environment where graduate students could learn and interact with each other. I would like to take this opportunity to thank the Einstein Foundation for funding me to complete the last phase of my Ph.D.

A cheerful and supportive environment is always what one looks for in friends and colleagues. I would like to thank Dr. Bella Rossbach, Ghazaleh Zarinrad, Dania Hamo, Thi Thanh Thao Ngo, TingTing Zhong, Hanieh Moradian, Valeria Fernandez Vallone, Constanze Raab, Regina, Dr. Mario Kaßmann, and Dr. Nancy Mah for their help, conversations, and supportive advice. I have greatly benefited from the company of Dr. Christien Madlen Beez, a great friend who has been a great source of inspiration in completing my thesis. I would like to thank Kristin Fischer, Valeria Fernandez Vallone and Janine Cernoch from the BIH Core Unit Pluripotent Stem Cells and Organoids (CUSCO) for their support on this project.

Last but not least, I would be remiss if I did not mention the support of my father and sister, who have always been a source of boundless optimism. Their belief in me has kept my spirits and motivation high throughout these years.

CERTIFICATE OF THE ACCREDITED STATISTICIAN

CHARITÉ

CharitéCentrum für Human- und Gesundheitswissenschaften

Charité | Campus Charité Mitte | 10117 Berlin

Institut für Biometrie und klinische Epidemiologie (IBikE)

Direktor: Prof. Dr. Frank Konietschke

Postanschrift:
Charitéplatz 1 | 10117 Berlin
Besucheranschrift:
Reinhardtstr. 58 | 10117 Berlin

Tel. +49 (0)30 450 562171
frank.konietschke@charite.de
https://biometrie.charite.de/

Name, Vorname: Batool, Lilas
Emailadresse: lilas.batool@charite.de
Matrikelnummer: [redacted]
PromotionsbetreuerIn: Dr. Andreas Kurtz
Promotionsinstitution / Klinik: BIH Center for Regenerative Therapies at Charité Universitaetsmedizin Berlin

Bescheinigung

Hiermit bescheinige ich, dass Frau Lilas Batool innerhalb der Service Unit Biometrie des Instituts für Biometrie und klinische Epidemiologie (iBikE) bei mir eine statistische Beratung zu einem Promotionsvorhaben wahrgenommen hat. Folgende Beratungstermine wurden wahrgenommen:

- 28.08.2023

Folgende wesentliche Ratschläge hinsichtlich einer sinnvollen Auswertung und Interpretation der Daten wurden während der Beratung erteilt:

- ANOVA und ihre Annahmen.
- Biologische und technische Replikate.

Diese Bescheinigung garantiert nicht die richtige Umsetzung der in der Beratung gemachten Vorschläge, die korrekte Durchführung der empfohlenen statistischen Verfahren und die richtige Darstellung und Interpretation der Ergebnisse. Die Verantwortung hierfür obliegt allein dem Promovierenden. Das Institut für Biometrie und klinische Epidemiologie übernimmt hierfür keine Haftung.

Datum:	Name des Beraters\ der Beraterin:
28.08.2023	Camilo J. Hernandez-Toro

Camilo Jose Hernandez Toro

Digital unterschrieben von Camilo Jose Hernandez Toro
Datum: 2023.08.28 11:11:01 +02'00'

CHARITÉ
UNIVERSITÄTSMEDIZIN BERLIN
Institut für Biometrie und Klinische Epidemiologie
Campus Charité Mitte
Charitéplatz 1 | D-10117 Berlin
Sitz: Reinhardtstr. 58

Unterschrift BeraterIn, Institutsstempel